Western Cape Government

FOR YOU

Agriculture

CLIMATE SYSTEM ANALYSIS GROUP

CSAG

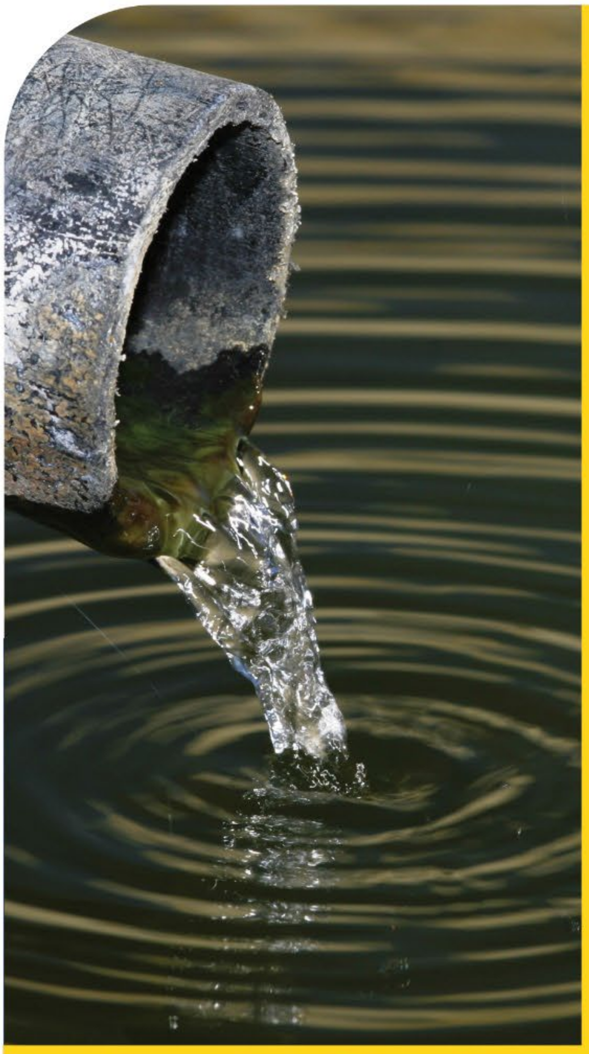

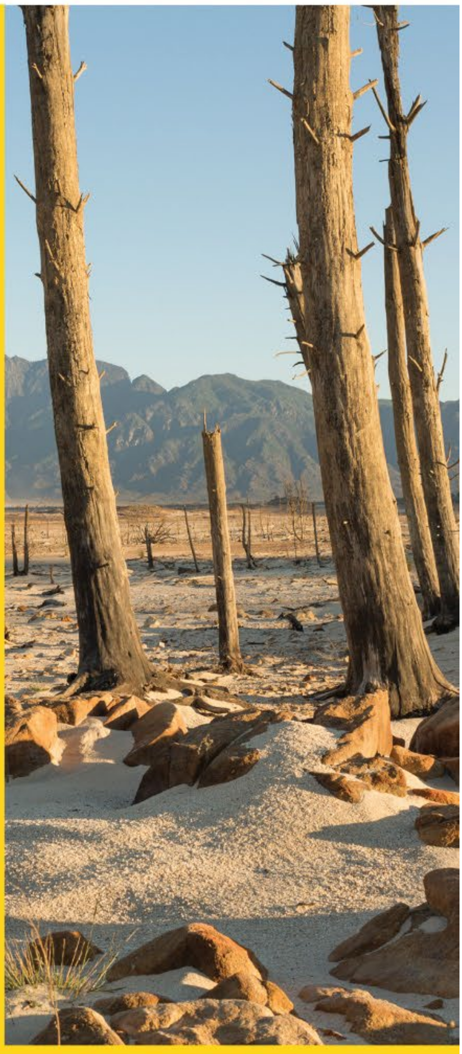

SmartAgri: Updated Climate Change Trends and Projections for the Western Cape

SmartAgri:
Updated Climate Change Trends and Projections for the Western Cape

2022

Compiled by Christopher Jack
Data management, analysis and written contributions by Lisa van Aardenne, Piotr Wolski, Izidine Pinto, Kwesi Quagraine and Pierre Kloppers

Climate System Analysis Group (CSAG)
Address and e-mail below:
CSAG, Environmental and Geographical Science, University of Cape Town
Private Bag X3, Rondebosch, 7701, South Africa
Tel: +27 (0) 21 650 2784
Email: climate@csag.uct.ac.za

Hyperlink to the Status Quo Review:
https://www.greenagri.org.za/assets/documents-/SmartAgri/Briefs-/Smart-Agri-Status-Quo-Review-2016.pdf

Acknowledgements
We acknowledge the World Climate Research Programme, which, through its Working Group on Coupled Modelling, coordinated and promoted CMIP5 and CMIP6. We thank the climate modelling groups for producing and making available their model output, the Earth System Grid Federation (ESGF) for archiving the data and providing access and the multiple funding agencies who support CMIP5, CMIP6 and ESGF.
We acknowledge the World Climate Research Programme's Working Group on Regional Climate and the Working Group on Coupled Modelling, former coordinating body of CORDEX and responsible panel for CMIP5. We also thank the climate modelling groups for producing and making available their model output. We also acknowledge the Earth System Grid Federation infrastructure, an international effort led by the U.S. Department of Energy's Program for Climate Model Diagnosis and Intercomparison, the European Network for Earth System Modelling and other partners in the Global Organisation for Earth System Science Portals (GO-ESSP).

QR Code for DOA website

ISBN number on back page

Table of contents

Executive summary

The updated analysis of historical observed and future projected climate over the Western Cape SmartAgri zones presented in this report provides strong evidence that the climate of the region is shifting and will continue to shift into the future. The region is characterised by strong climatic gradients and widely varying mean temperature and rainfall magnitudes driven by both the complex topography as well as the adjacent ocean. As a whole, the region has experienced significant increases in temperature across all zones and all seasons over the past century, with more rapid warming over the past 30 years.

The Cape Town "Day Zero" drought (Wolski, 2018) brought climate change into sharp focus for the province, though it must be noted that many other parts of the province experienced significant and impactful drought that failed to gain the same level of attention in the media. The role of climate change in contributing to increasingly frequent and intense droughts has been strongly determined through the analysis of the drought. There is now increased urgency to develop plans and move plans into action, to prepare for further climate shifts across the province.

While the message of climate change is now well established by the evidence presented in the previous assessment, and confirmed by the assessment presented in this report, we must acknowledge that some uncertainty and complexity remain, especially with regard to changes in rainfall. The Western Cape region encompasses a number of somewhat independent climate zones (Wolski et al. 2021). These can be seen in the observed climate trends analysed in Section 5 (e.g. Figure 15), as well as in the cited literature.

Future projected changes in rainfall indices also show some variation across the province so that, while reductions in rainfall are strongly dominant, it is possible that different patterns of change may unfold. Different dynamics are involved in producing changes in summer rainfall over the northern/eastern parts of the province versus the southern regions and the western regions. The range of possible shifts are unpacked further through the archetype analysis in Section 6. The clear message is that reductions in rainfall should be anticipated across the region, but some subregions may experience much stronger reductions than other subregions.

Some uncertainty around projected changes in rainfall continues to play a factor in decision-making. However, the analysis of projected changes in water balance (Standardised Precipitation Evaporation Index, SPEI) and Potential Evapotranspiration (PET) in Section 6 shows very clearly that increases in temperature, involving very little uncertainty, strongly dominate any uncertainty in rainfall changes. A clear message of increasing water deficit frequency as well as increasing frequency and intensity of drought conditions emerges. This is the key message for agriculture across the province.

1. Introduction

The report constitutes a review and update of the climate information (Status Quo Review[1]) that formed the basis for the SmartAgri Plan[2]. The updates entail integration of more analytical variety as well as more recent datasets that have become available since the previous report[1]. Inclusion of more recent literature has drawn heavily from academic analysis of the "Day Zero" drought event. The sections below reference the original Status Quo Review sections; however, some sections have been combined into a single section as this provides a more cohesive narrative.

SmartAgri Zones

The analysis is based on the original 23 SmartAgri Zones (Figure 1). These zones represent reasonably homogeneous climate and agricultural regions. Like any zonation, they represent various compromises, but do provide a useful spatial disaggregation for the region. In the section on Climate Projections (Section 6), these 23 zones are also aggregated into six clustered zones in order to consolidate some of the presented evidence.

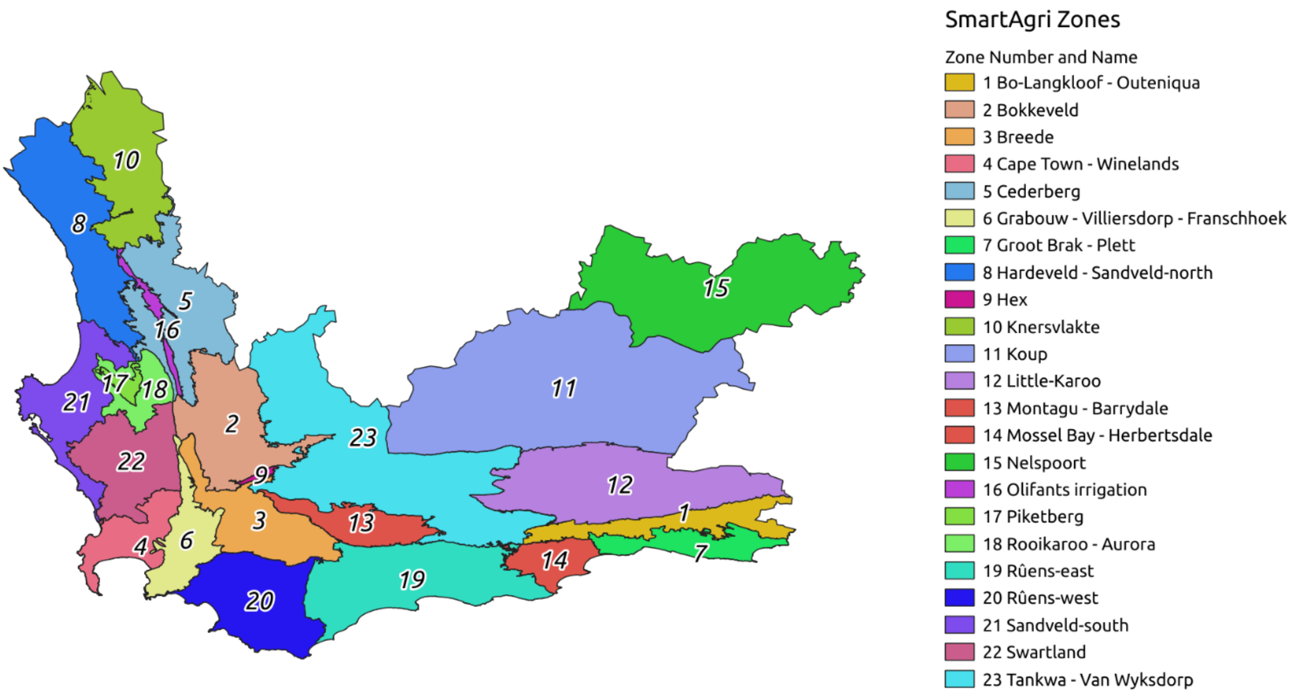

Figure 1: The 23 primary SmartAgri zones used for the majority of the analysis

[1] Status Quo Review of Climate Change and the Agriculture Sector of the Western Cape Province (2016). https://www.greenagri.org.za/assets/documents-/SmartAgri/Briefs-/Smart-Agri-Status-Quo-Review-2016.pdf

[2] Climate Change Response Strategy and Implementation Plan for the Agricultural Sector of the Western Cape province (2016). http://www.greenagri.org.za/smartagri-2/smartagri-plan/

2. Western Cape climate processes

Update to Section 4.2 in the SmartAgri Status Quo[1] Review.

Winter rainfall region

Classically, we consider winter rainfall to mean rainfall that occurs during the core winter period of June-August (JJA); however, substantial amounts of rainfall occur due to the same mechanisms outside of this core season. It is, therefore, important to consider rainfall during the autumn, March-May (MAM), and spring, September-November (SON), periods as part of the winter rainfall season. Importantly, some trends and projected future rainfall changes occur predominantly during these “shoulder” seasons (spring and autumn).

Figure 2 illustrates the seasonal total rainfall across the province and the SmartAgri Zones. The core winter season map (JJA) clearly shows the focus of the winter rainfall over the high topography of the Grabouw-Villiersdorp-Franschhoek zone in the south-west of the province. However, winter rainfall occurs throughout much of the province, extending both north towards the Cederberg zone and east towards the south coast region.

Extended winter (including autumn and spring) rainfall is predominantly linked to cold fronts associated with mid-latitude cyclones. These systems are responsible for most of the region’s extended winter season (March to November) rainfall; 89% of the total winter half-year rainfall is frontal or post-frontal (Burls et al., 2019). Other winter rainfall is produced by cut-off lows (COLs) (Favre et al., 2013) and west coast troughs (Tyson and Preston-Whyte, 2000).

The region’s rainfall is also affected by other hemispheric phenomena such as the expansion of the Hadley cell (Burls et al., 2019), and the position of subtropical and polar jets. These phenomena share some co-variability with the Southern Annular Mode (SAM) (Reason and Rouault, 2005) although the relationships are weak. Rainfall in the region also potentially responds to some extent to sea surface temperature (SST) anomalies in the south-east Atlantic Ocean. This includes the Agulhas Current retroflection region, which may drive intensification of low-pressure systems, leading to strengthening and moistening of fronts as they make landfall over the Western Cape (Reason and Jagadheesha, 2005). However, the relationships are again weak and often do not hold up to subsequent analysis with longer time series. Unlike the summer rainfall regions to the north, the relationship between the winter rainfall region’s rainfall and ENSO is generally weak and inconsistent through time (Philippon et al. 2012).

Out of the above, the SAM appears to be the main and the most consistent dynamic process affecting rainfall variability in the winter rainfall region. The mechanisms behind that relationship involve shifts and weakening in the subtropical jet, as well as changes in the low-level moisture flux, convergence, and relative vorticity over the region (Reason and Rouault, 2005). Note, however, that while in the post-1950 period the SAM displays a long-term trend, the Cape Town region’s rainfall does not (Wolski et al. 2021).

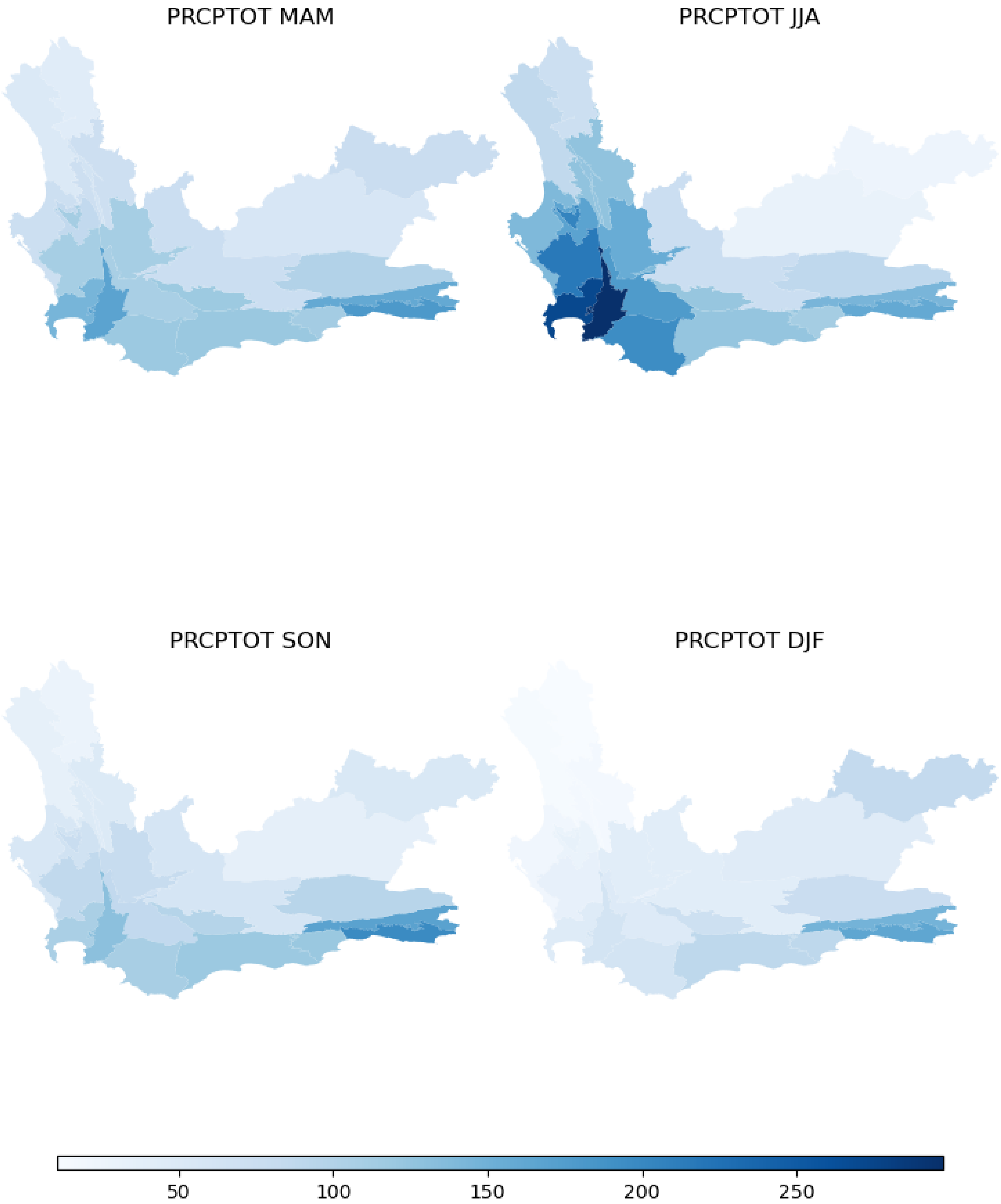

Figure 2: Mean total seasonal rainfall [in mm/season] across the SmartAgri zones. Values are derived from the CHIRPS high resolution merged rainfall product (see Section 5) extending from 1983 - 2020.

The SAM varies with a characteristic decorrelation time of ~2 weeks, but its low frequency variability is influenced by greenhouse gases (GHGs) (Fyfe et al., 2012), stratospheric ozone (Arblaster et al., 2011, Thomson et al., 2011) and El Niño-Southern Oscillation (ENSO) (Lim et al., 2016). However, the influence of ENSO on SAM manifests mostly in the austral summer and hence there is limited, if any, influence on the Western Cape rainfall.

The influence of GHGs on SAM is similar in nature to that resulting from the depletion of ozone in the Antarctic, with the historical trend in SAM relating mostly to ozone depletion. The ongoing ozone recovery compensates for GHG increase, but the GHG increase is projected to dominate after 2045 (Barnes et al., 2014).

In 2018, a multi-year drought triggered a water-supply crisis in Cape Town and its environs with a potential consequence of a shutdown of supply to its 3.4 million residents. The day when such shutdown would happen was termed “Day Zero”. That water crisis, and associated significant water supply restrictions, caused significant economic and social impacts in the city and its region. The drought has received considerable attention from climate and water researchers worldwide. It became one of the case studies illustrating regional and local impacts of climate change presented in the Intergovernmental Panel on Climate Change (IPCC) 6th Assessment Report of 2021 (Doblas-Reyes et al., 2021). Due to the apparent singularity of that event and its significance in the context of this report, that event is covered extensively in a dedicated section.

Summer rainfall region

Only the far north-east of the province experiences dominantly summer rainfall. Variability in this region is expected to be subject to the same drivers of interannual variability as that in the broader summer rainfall region of South Africa, in that a weak relationship between ENSO and rainfall anomalies has been identified (Hart et al., 2013). In particular, summer rainfall within the summer rainfall region and the all-year rainfall region as well, is partly associated with the occurrence of tropical-temperate-troughs (TTT), dynamic linkages between the mid-latitude westerlies and the tropics. TTTs have been associated with as much as 50% of rainfall in early summer in the summer and all-year rainfall regions, although the north-east of the Western Cape province lies on the border of this TTT influence (Hart et al., 2013).

All-year rainfall region

The far eastern coastal zones (Groot Brak - Plett and Bo-Langkloof - Outeniqua) are part of the broader all-year rainfall region extending along the southern coast of South Africa. In this region, rainfall is generated by weather systems characteristic of both the winter and summer rainfall regimes of South Africa during their respective seasons. Similar to the winter rainfall region, rainfall heterogeneity in the all-year rainfall region is also affected by local topography and meso-scale processes such as the interaction of the Agulhas Current with regional circulation (Rouault et al., 2002).

Jury and Levey (1993) suggested that COLs and ridging high pressure systems play a part in driving the interannual rainfall variability. They implied that the frequency of these systems is lower during dry years. Weldon and Reason (2014) showed that the occurrence of COLs in this region is associated with ENSO. Mature phase La Niña years are usually wet and accompanied by a higher frequency of COLs from late spring to early autumn. However, the relationship between COL frequency and ENSO is not systematic.

Dry years characterised by a lower frequency of COLs might occur during neutral and positive ENSO years. A negative correlation is also observed between wet-day frequency and the Niño 3.4 index in December and January (Weldon and Reason 2014), corresponding to the known association between ENSO and rainfall over the summer rainfall region of South Africa (Landman and Beraki, 2012). The relationship between DJF and SON seasonal rainfall and ENSO (negative correlation implying dry anomalies during El Niño years) is confirmed in the analyses by Engelbrecht and Landman (2016). In addition to the above, Engelbrecht and Landman (2016) reveal a statistically significantly positive correlation between SAM and all-year zone rainfall in DJF and MAM. That association corresponds to the relationship between ENSO and SAM, although the latter manifests strongly only in Nov-Feb (L’Heureux and Thompson, 2006).

Climate change and the Western Cape

Update to Section 4.3 in the SmartAgri Status Quo[1] Review.

This section presents a short and general overview of understanding of the role of anthropogenic climate in the climate of the Western Cape, both in the historical period and in the future, based on literature. Dedicated analyses of data at the SmartAgri zones level are presented in Sections 5 and 6.

This section also includes a detailed analysis of the Cape Town "Day Zero" drought, as much of the associated dynamics are relevant to the broader province.

Historical trends

It is clear that global mean surface temperature (GMST) has been increasing in the past. The average over the decade 2006-2015 was 0.87°C [with 95% confidence interval between 0.75°C and 0.99°C] higher than the average over the 1850–1900 period (IPCC, 2018). Average temperatures in the Western Cape region have increased at 1.2 times the global average and the change in temperature has been larger than natural variability (Pinto et al., in review). Hot extremes have increased and cold extremes have decreased over the period of 1931-2005 (Kruger and Nxumalo, 2017).

Historical rainfall trends are less consistent. In their studies of the 2015-2017 drought, Sousa et al. (2018) and Mahlalela et al. (2019) revealed a strong drying trend, particularly in the post-1979 period. An earlier country-scale study of rainfall trends, however, concluded that in the Cape Town region, 1960-2010 "trends in rainfall indices are generally not significant and show little spatial consistency" (McKellar et al., 2014). Kruger and Nxumalo (2017) confirmed this for the 1921-2015 period. Wolski et al. (2021) performed a rigorous analysis of rainfall trends in station data over the western two thirds of the province, the area dominated by the "Day Zero" drought. They revealed that over the most recent period (1981-2017) there has been a drying trend in a majority of stations, although mostly not statistically significant. However, during the 1981-2014 period (i.e. prior to the drought), only a few stations had statistically significant drying and a large number of stations in the region experienced an increase in rainfall (Figure 3). These results suggest that the predominant tendency towards decreasing rainfall noted by Sousa et al. (2018) and Mahlalela et al. (2019) emerged only due to the very low rainfall of the 2015-2017 drought (Figure 3). Longer-term trends in the period prior to the 2015-2017 drought are generally weak, with direction varying between individual locations and do not support a message of consistent historical drying (Figure 4).

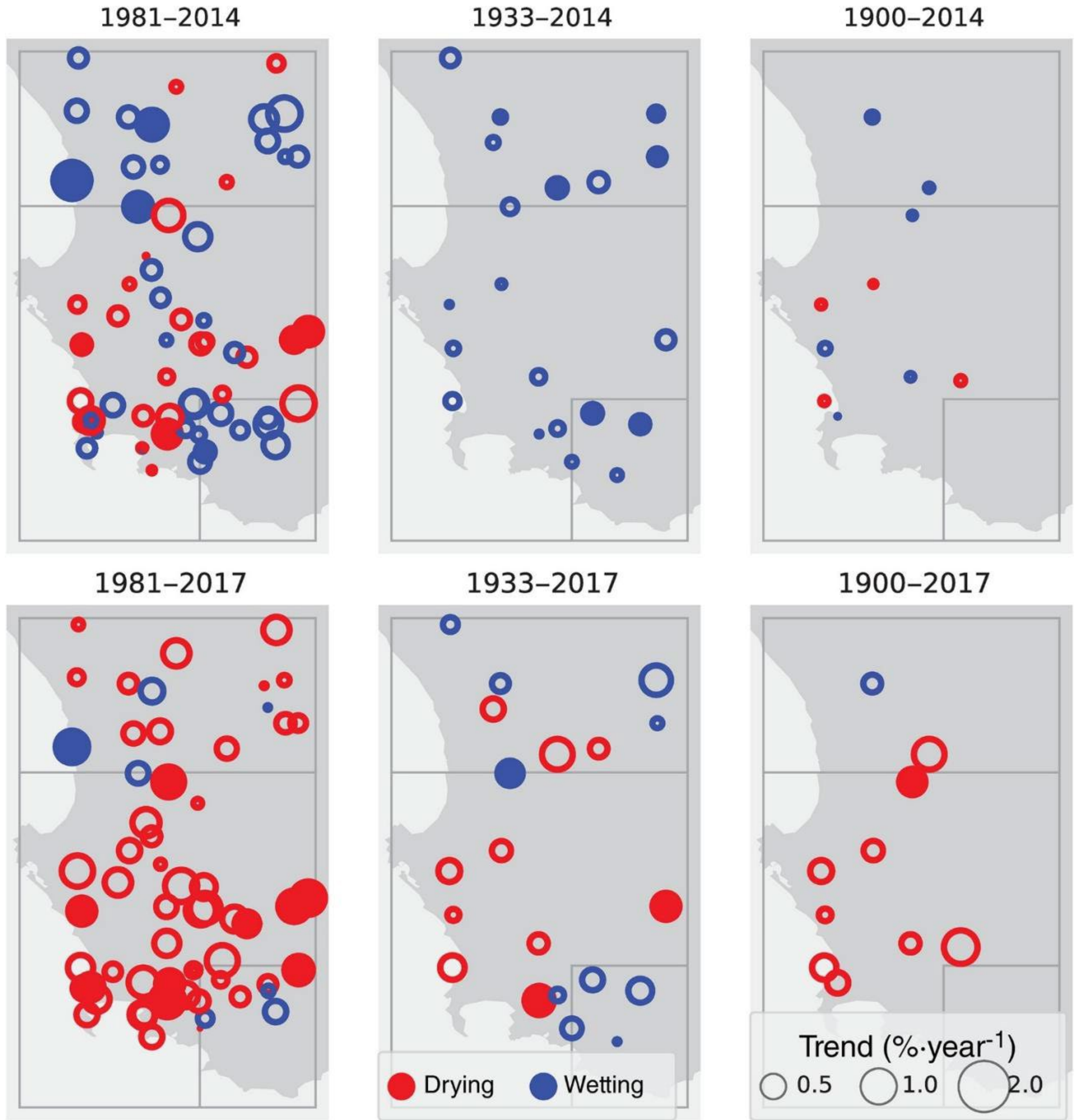

Figure 3: Maps of trends in total annual rainfall at individual gauges in period-specific datasets. Filled symbols show a trend significant at the 5% level. (From Wolski et al., 2021)

Trends on the seasonal timescale in the period prior to the 2015-2017 drought appear to be stronger and relatively coherent in space (Figure 4). Over the 1981-2014 period, there was a trend towards wetting during the core winter (June-August) period over the region, with strong signals in the Knersvlakte, Cederberg and Hardeveld SmartAgri Zones. During summer (December-February), a trend towards wetting was observed over the southern part of the Northern Cape. During autumn (March-April), significant drying was seen in almost all the stations. A drying trend was observed over the northern parts and a wetting trend over the southern parts of the Western Cape during September-November (Figure 4 and Wolski et al., 2021).

The recent drying trend identified in the winter rainfall region in MAM is likely associated with changes in large-scale drivers, in this case SAM and the expansion of the Hadley cell, which in turn affect the positioning of the westerlies, fronts and jet streams (Sousa et al., 2018; Burls et al., 2019; Mahlalela et al., 2019). These processes and relationships are described in more detail in Section 3 devoted to the "Day Zero" drought.

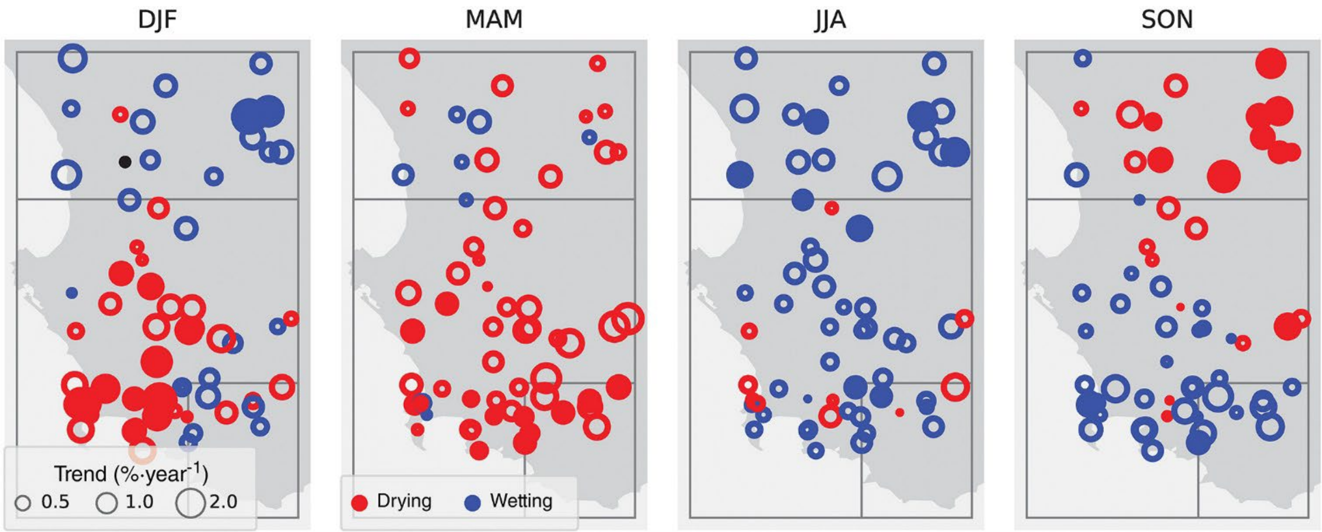

Figure 4: Trends in seasonal rainfall totals at individual gauges in the recent period (1981-2014, excluding the 2015-2017 drought). Filled symbols show a trend significant at the 5% level. (From Wolski et al., 2021)

Future climate projections

With increases in global warming levels, the region is expected to experience upward trends in hot extremes and downward trends in cold extremes (Mbokodo et al., 2020; Seneviratne and Hauser, 2020; Vogel et al., 2020).

Projections from climate models suggest a further drying associated with the Hadley cell expansion, positive phases of SAM and a poleward shift of the westerlies over the coming decades (Lim et al., 2016; Pinto et al., 2016, 2018; Maúre et al., 2018; Seager et al., 2019; Almazroui et al., 2020; Naik and Abiodun, 2020; Ukkola et al., 2020).

Detailed analysis of future projected changes are detailed in Section 6 below.

Cape Town "Day Zero" 2015-2017 drought

In this section, an overview of the literature is presented addressing the characterisation, drivers and role of anthropogenic climate change in the 2015-2017 drought, drawing heavily from the overview included in the IPCC AR6 report (Doblas-Reyes et al., 2021). By the nature and implications of the drought, the majority of research focused on the conditions in the winter rainfall region rather than on the entire Western Cape province. Consequently, so does this section.

In terms of meteorological drought underlying the "Day Zero" water crisis — an evaluation of the relative role of rainfall and temperature signal gives a strong indication that a multi-year rainfall anomaly was the primary driver of that water deficit (Otto et al., 2018). It is thus not surprising that most of the research and analyses of the climatic drivers of the 2015-2017 drought focused on the rainfall anomaly. The 2015–2017 drought had strong low-rainfall anomalies in the shoulder seasons (March to May and September to November, though weaker in the latter – Figure 5), and average rainfall in June and July (Sousa et al., 2018; Mahlalela et al., 2019). The anomaly resulted from fewer rainfall events and lower average intensity of events (Oudoulami et al., 2020, Burls et al., 2019).

Spatial distributions of anomalies have not been analysed in detail in the available literature. Botai et al. (2017) analysed station-level anomalies for major stations in the entire Western

Cape Province, but only for the 2017 rainy season. The majority of studies focused only on the anomalies in the core of the winter rainfall region, i.e. the City of Cape Town and its immediate environs, including the mountainous catchments draining to the Cape Town water supply system dams. Wolski et al. (2021) analysed stations in the winter rainfall region only, but revealed that the drought-period anomalies were spatially varied, suggesting that the three-year anomaly was largest in the mountains in the vicinity of the Western Cape Water Supply System (WCWSS) dams, but considerably weaker in the northern and eastern parts of that region. The strong and systematic heterogeneity of the drought is also supported by recent analyses by Conradie et al. (2022).

Although the 2015–2017 drought was unprecedented in the historical record, the Cape Town region has experienced other droughts of substantial magnitude, notably in the 1930s, 1970s and more recently from 2000–2003. Long term (> 90 years) rainfall trends are mixed in sign, location-dependent and weak (Kruger and Nxumalo, 2017; Wolski et al., 2021, see also Section 5 on historical trends in this report). Mid-term (~50 years) trends are similarly mixed in sign (MacKellar et al., 2014). Rainfall is mostly decreasing in the post-1981 period, particularly in DJF and MAM. Rainfall trends of similar magnitude and duration to the post-1981 trend accompanied previous strong droughts in the region (Wolski et al., 2021).

The main drivers of rainfall and climate variability in the winter rainfall region are described in Section 2. Recent work towards an improved understanding of the drivers of the 2015-2017 Cape Town drought have pointed to hemispheric processes of poleward displacement of the mid-latitude westerlies and expansion of the subtropical high pressure systems, which are linked to anthropogenic climate change, as the primary factors underlying that event (Sousa et al., 2018; Mahlalela et al., 2019; Burls et al., 2019; Otto et al., 2018). They are also responsible for the recent (post-1981) rainfall trends, particularly in MAM.

Sousa et al. (2018) showed that the seasonal rainfall anomalies were driven by a poleward shift of the Southern Hemisphere moisture corridor delivering moisture from the sub-tropical south-western Atlantic to the mid-latitude systems. This was associated with a displacement of the jet-stream and the South Atlantic mid-latitude storm-track. They also demonstrated that the post-1980 decreasing rainfall is consistent with an expansion of the semi-permanent South Atlantic high pressure and reflects the prevalence of the positive phase of the SAM.

Burls et al. (2019) found no robust regional trend in the number of fronts reaching south-western Africa over the last 40 years, but detected a decrease in the duration of rainfall events associated with cold fronts. That decrease takes the form of fewer events during days after the passing of the cold front over the region (so-called post-frontal rainfall). As a mechanism behind that effect, they showed that the poleward expansion of the Hadley Circulation Cell, and hence increased sea-level pressure along the poleward flank of the South Atlantic high pressure system, suppresses conditions promoting orographic precipitation. This, in particular, reduces the onshore and up-slope winds that promote orographic uplift.

Mahlalela et al. (2019) showed that the dry conditions during the early winter months (April-May), as experienced during the 2015-2017 drought, tend to be associated with a weaker subtropical jet, less moisture flowing into the domain and a more stable atmosphere.

Abba Omar and Abiodun (2020) analysed variability and the nature of COLs — an atmospheric system responsible for ~11% of the Cape Town region's rainfall. The formation of COLs over a region depends on the strength of the westerlies and position of the jets in the region (Favre et al., 2013) and thus likely responds to the same drivers that were suggested to be responsible for the 2015-2017 drought. However, Abba Omar and Abiodun

(2020) showed that COLs contributed an unusually large amount of rainfall in 2015 and 2016, alleviating the drought, and that a stronger rainfall anomaly in 2017 was associated with fewer COL events. These year-to-year differences in COL occurrence suggest that the COLs were not affected by the hemispheric processes that affect the frontal rainfall and imply differences between the dynamics of the 2015-2016 and 2017 drought years. These differences have not been critically evaluated in the existing literature.

It is now generally accepted that the global climate is changing and that this is largely due to anthropogenic impacts. Otto et al. (2018) attributed a three-fold increase in probability of the observed rainfall deficit during this drought to anthropogenic climate change. The study was concerned with rainfall deficit only and did not consider evaporation anomalies. The study was done using a state-of-the-art attribution approach based on analysis of multi-model, multi-method data.

Another formal attribution study, Kam et al. (2021), analysed the role of anthropogenic climate change on the duration of the 2015-2019 drought using CMIP6[3] experiments. Their study revealed that there is no clear increase in probability of long-duration droughts that could be attributed to anthropogenic climate change. Importantly, this result is not in contradiction to the result of the Otto et al. (2018) study, as these two studies consider two different aspects of the drought – severity and duration.

In summary, there is a prevailing narrative that the 2015-2017 rainfall anomalies recorded in the winter rainfall region of the Western Cape were a result of hemispheric processes of expansion of the tropics and associated reduction of moisture supply from the sub-tropical Atlantic, as well as with the poleward shift of mid-latitude storm track and cyclonic systems and the associated key circulation process, the SAM. These processes likely manifest through reduction of the frequency of rain days associated with the cold fronts passing over the region. The process-rainfall relationships are supported by the correspondence of the post-1979 trends (Figure 7).

There is also consistency in rainfall projections with the projections of rainfall drivers and with the general understanding of the influence of global warming on the circulation dynamics and rainfall patterns in the region as outlined above.

Notably, however, some CMIP5[4] and CMIP6 GCMs simulate increases in rainfall in the post-1979 period associated with positive trend in SAM, which is in contradiction to that narrative (Figure 7). Additionally, there is less support for the precipitation-hemispherical processes relationship in historical, longer-term CMIP5 and CMIP6 simulations and reanalyses. When the observational record is extended back further to times when the anthropogenic greenhouse forcing was weaker, there is no strong association between the SAM and Cape Town droughts in terms of overall pattern and trends (Figures 6 and 7). These suggest that other than the anthropogenic climate change-related, hemispheric processes might be responsible for drought conditions over the winter rainfall region of the Western Cape.

As a consequence, the IPCC AR6 chapter 10.6.2 concludes with a statement of a reduced confidence that these process changes produced the 2015-2017 drought. Also, although there is a high agreement between various datasets as to the expectation of a future drier climate for Cape Town, a high confidence could not be attached to that expectation.

[3] The Coupled Model Intercomparison Project. The 6th iteration of the CMIP experiment was developed in preparation for the IPCC 6th assessment report published in 2021 and 2022.
[4] The 5th iteration of the CMIP experiment.
[5] https://www.ipcc.ch/report/ar6/wg1/downloads/report/IPCC_AR6_WGI_Chapter10.pdf

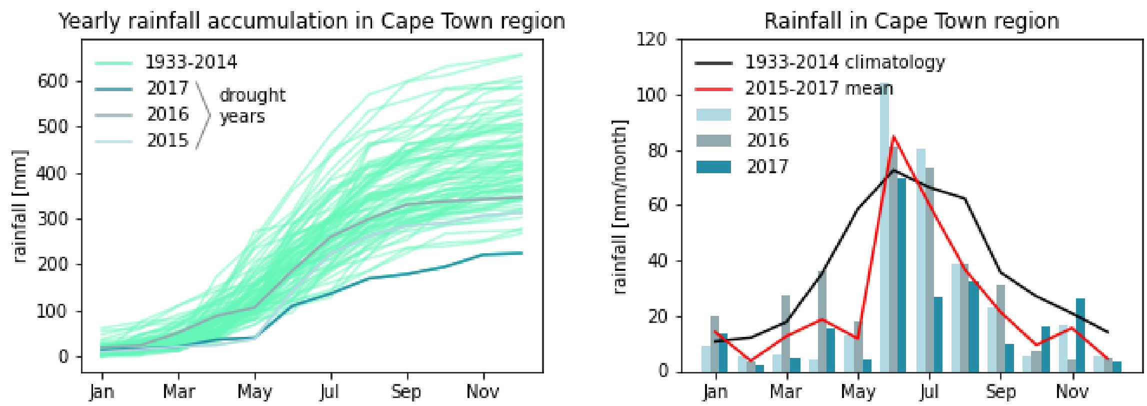

Figure 5: Anomalies of the accumulated daily rainfall (left) and monthly rainfall total (right) in the drought period (Figure replicated from Doblas-Reyes et al., 2021)

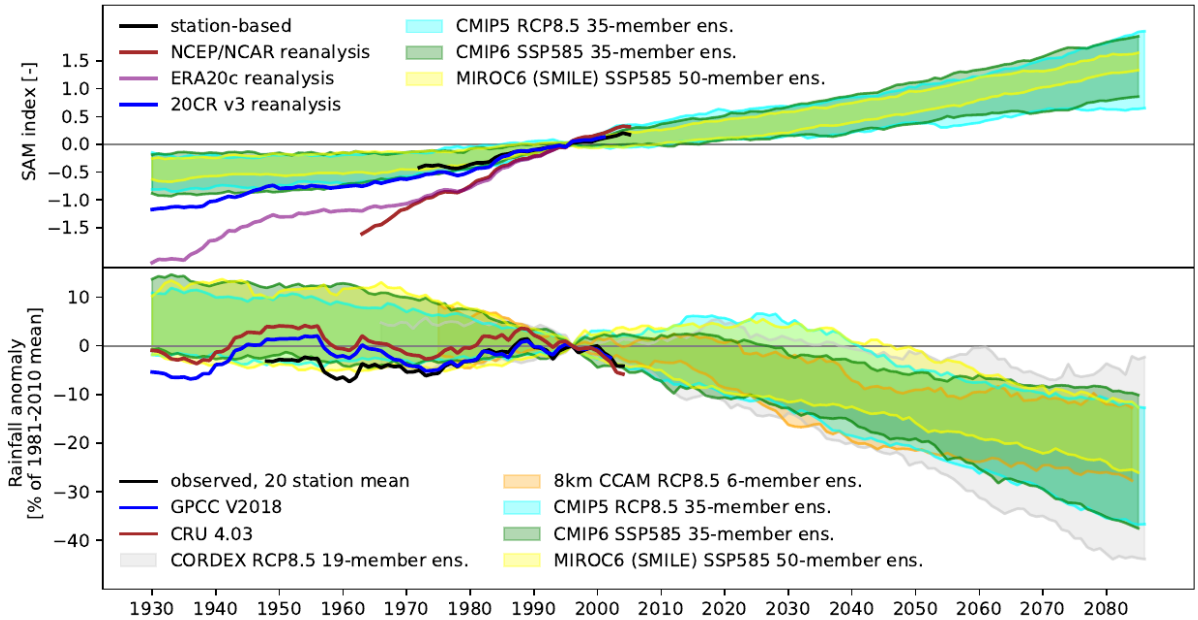

Figure 6: SAM and rainfall anomalies in model-simulated, observed and reanalysis data. All data presented as 30-year running means. Anomalies calculated with respect to 1981-2010 period. Shaded area represents central 95 percentile of range of each of the ensembles. (Figure replicated from Doblas-Reyes et al., 2021)

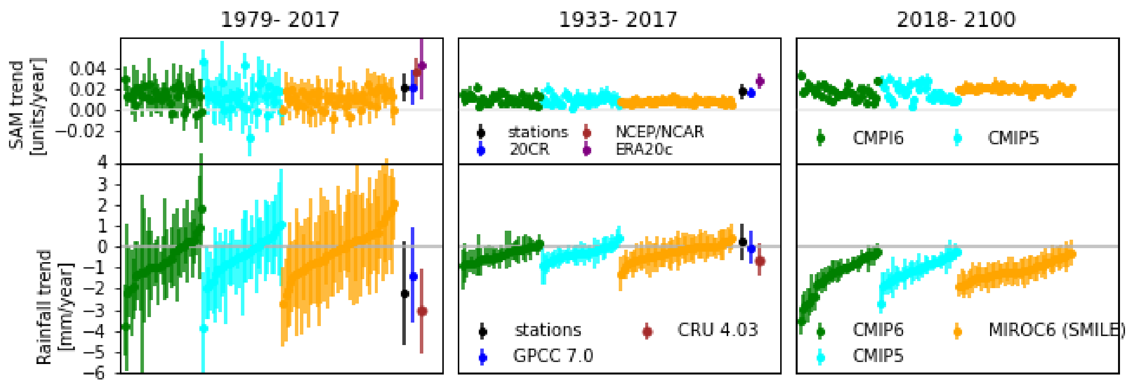

Figure 7: SAM and rainfall trends (with 95% confidence interval) in model-simulated, observed and reanalysis data. Trends calculated using Theil-Sen approach; confidence intervals calculated using block bootstrapping to account for autocorrelation in data. (Figure replicated from Doblas-Reyes et al., 2021)

4. Climate indices

In order to provide analysis and information of relevance to a wide range of stakeholders, though with a strong focus on agriculture, a wide suite of standard climate indices has been calculated for both historical observations (mean conditions and trends) as well as future projections. These indices are largely based on the widely adopted indices of the Expert Team for Climate Change Detection. Monitoring and Indices (ETCCDMI) as documented here: http://etccdi.pacificclimate.org/list_27_indices.shtml.

Table 1 details the indices that have been used in the subsequent analyses, including some related to evaporation and drought that are not part of the ETCCDMI suite. The results for some of these indices are available in a digital appendix (see Appendix A) and are available on request.

Table 1: Indices used in analyses presented in this report

Variable	index	Description	units
Temperature indices	TG	mean daily mean temperature	deg C
	TX	mean daily maximum temperature	deg C
	TXx	maximum daily maximum temperature	deg C
	SU30	frequency of daily maximum temperature above 30 deg C	days
	TN	mean daily minimum temperature	deg C
	TNn	minimum daily minimum temperature	deg C
	FD	frequency of daily minimum temperature below 0 deg C	days
	TR20	frequency of daily minimum temperature above 20 deg C	days
Rainfall indices	CDD	maximum number of consecutive dry days	days
	CWD	maximum number of consecutive wet days	days
	PRCPTOT	total accumulated precipitation	mm
	R10mm	number of days with pr > 10 mm	days
	R20mm	number of days with pr > 20 mm	days
	RR1	number of days with pr > 1 mm	days
	RX1day	maximum 1 day rainfall total	mm
	RX5day	maximum 5 day rainfall total	mm
	SDII	simple daily intensity index	mm
Evaporation and drought indices	PET	Potential evapotranspiration	mm/day
	SPI	Standardised Precipitation Index	
	SPEI	Standardised Precipitation Evaporation Index	

5. Observations and trends

Combined update to sections 4.4 (observations), 4.5 (trends) and 4.6 (extremes) in the SmartAgri Status Quo[1] Review. Note that the 2015-2017 "Day Zero" drought is described in detail in Section 3.

This section describes the suite of observational data products that have been used to analyse observed mean climate conditions across the SmartAgri Zones, as well as analysis of mean climatological conditions and historical trends of a number of key climate indices (see Section 4).

Datasets

Challenges with obtaining reliable station observations have resulted in the selection of alternative datasets for historical analysis of climatology and trends. These alternative datasets have been carefully assessed both within the context of the Western Cape region, for this update, as well as more broadly. The alternative datasets are merged/reanalysis products integrating station observations with satellite proxy data, and, in the case of reanalysis, dynamical atmospheric and land surface models. The following quasi observed datasets have been used:

CRU TS-4.05

The University of East Anglia Climate Research Unit monthly global observed dataset is one of the most used datasets for historical climate analysis globally. It incorporates a large number of observed stations. The most recent iteration (Harris et al., 2020) includes improvements to ensure reliability for trend analysis. As the product only provides monthly values for some rainfall and temperature related variables, daily timescale indices such as short-term extremes are not available. A varying number of primary stations are integrated for the Western Cape region through the 1900 to present period of coverage. Consideration of the number of stations is important for interpretation of the analysis results.

CHIRPS

The Climate Hazards Group InfraRed Precipitation with Station data (CHIRPS) rainfall dataset (Funk et al., 2015) has emerged as one of the most reliable high resolution daily time scale rainfall proxy datasets globally and has been assessed in a number of contexts across southern Africa and found to be very reliable. The one advantage of this update is that availability of daily time scale rainfall estimates at 0.05° (~5 km) spatial resolution means that the strong spatial variability of rainfall across the Western Cape can be well represented (see comparison in the digital appendix). One uncertainty with CHIRPS rainfall over the Western Cape appears to be the long-term trend, which does not agree well with primary station observations.

GPCC

The Global Precipitation Climatology Centre daily rainfall product (Schamm et al., 2014) is also a widely used estimate of both daily and monthly rainfall on a regular global grid. GPCC daily is based on a very large ensemble of daily rainfall observations from global weather stations and is interpolated to a 0.5° horizontal grid using a variation on the Kriging algorithm. It is regularly updated to include recent observations. The current version extends to the end of 2020.

ECMWF ERA5-Land

The European Centre for Medium range Weather Forecasts (ECMWF) ECMWF Reanalysis version 5 (Hersbach et al., 2020) is the latest high resolution atmospheric reanalysis from ECMWF. It represents the state of the art in observational assimilation coupled to dynamical modelling. The ERA5-Land product (Muñoz-Sabater et al., 2021) is based on the ERA5 reanalysis but includes a dynamic land surface model in order to derive higher resolution (~10 km) land surface parameters, including evaporation and potential evaporation. While it is based on a reanalysis and is relatively new, ERA5-Land is demonstrating very good performance in representing regional climate history. See comparisons in the digital appendix.

Temperature indices climatology and trends

Two datasets for temperature related climatology and trends were analysed. The CRU TS4.05 dataset extends back to 1900 and is based on primary station records, but with only a small number of stations contributing to the dataset pre-1960. Because CRU is a monthly product it is not possible to calculate most daily indices. These have been calculated using the ERA5-Land product.

The CRU figures are shown in Figures 8 and 9, while the ERA5-Land figures are provided separately in digital format (see Appendix A).

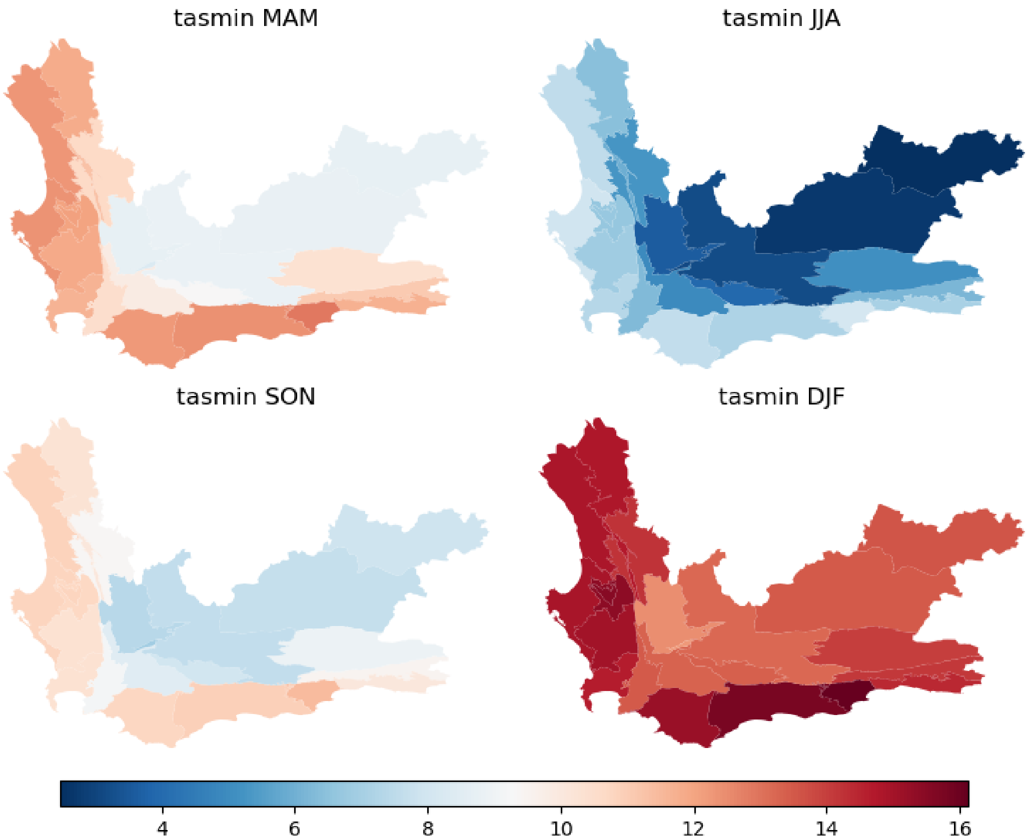

Figure 8: Mean seasonal daily minimum temperature (°C) across SmartAgri zones based on the CRU TS4.05 dataset from 1902-2020.

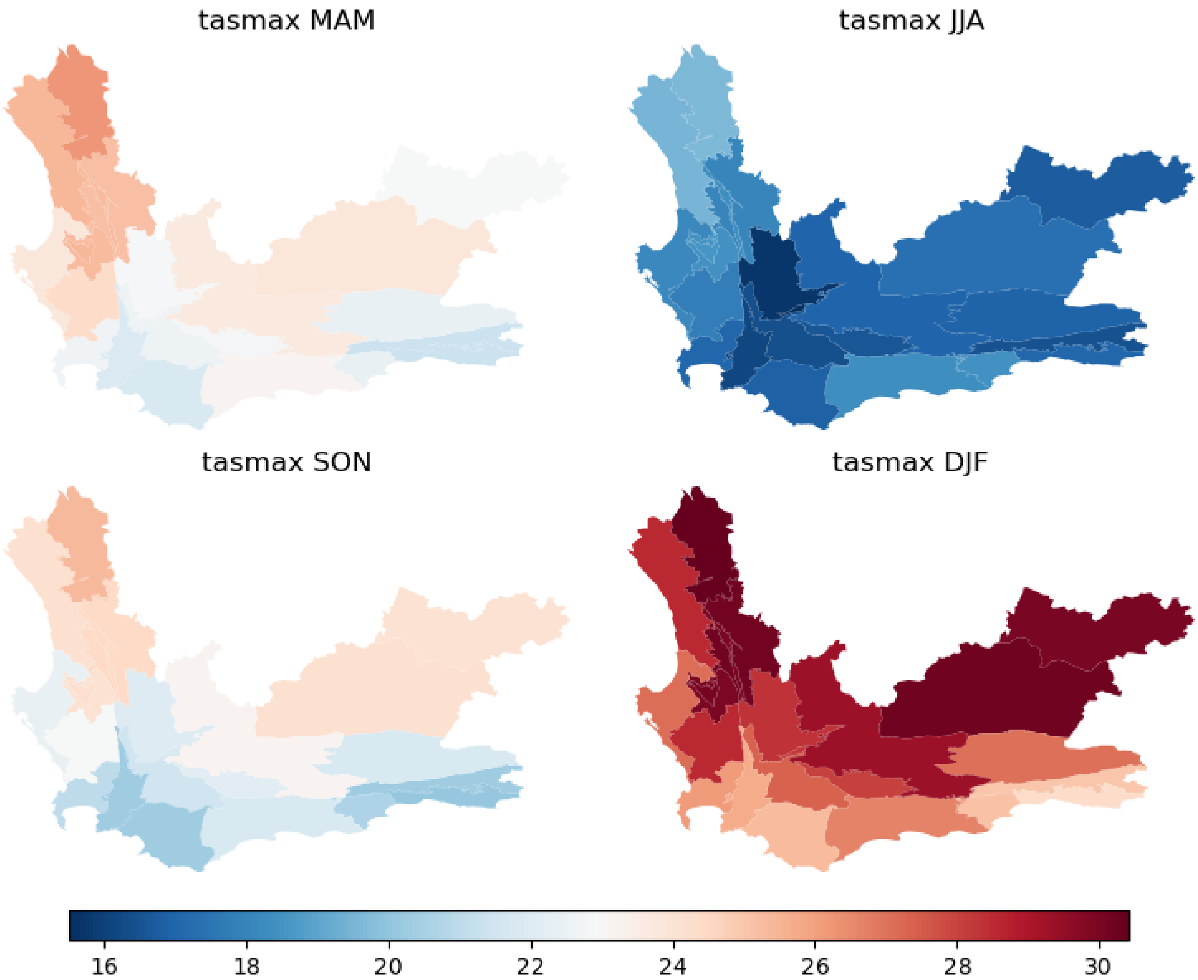

Figure 9: Mean seasonal daily maximum temperature (°C) across SmartAgri zones based on the CRU TS4.05 dataset from 1902-2020.

Figures 8 and 9 illustrate spatial patterns in the seasonal mean of maximum and minimum daily temperatures. The overall spatial pattern reflects the coastal-to-inland gradient, with minimum temperature lower inland than on the coast and maximum temperature higher inland than on the coast.

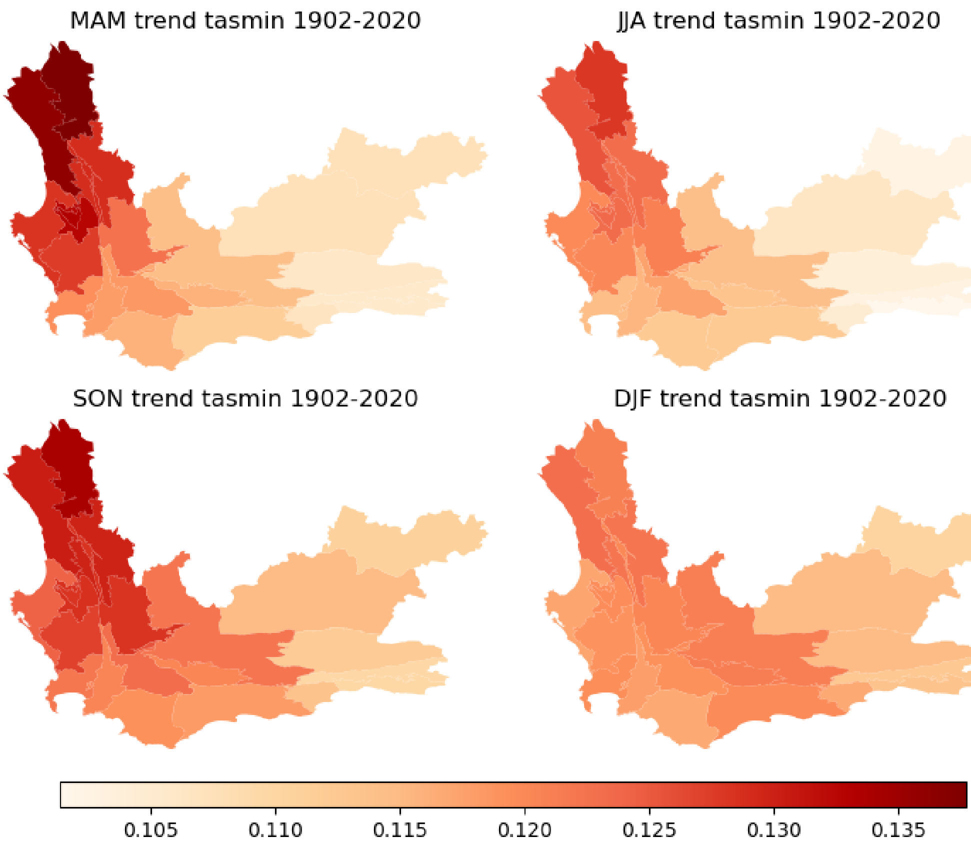

Figure 10: Mean seasonal daily minimum temperature trends (°C/decade) across SmartAgri zones based on the CRU TS4.05 dataset from 1902-2020.

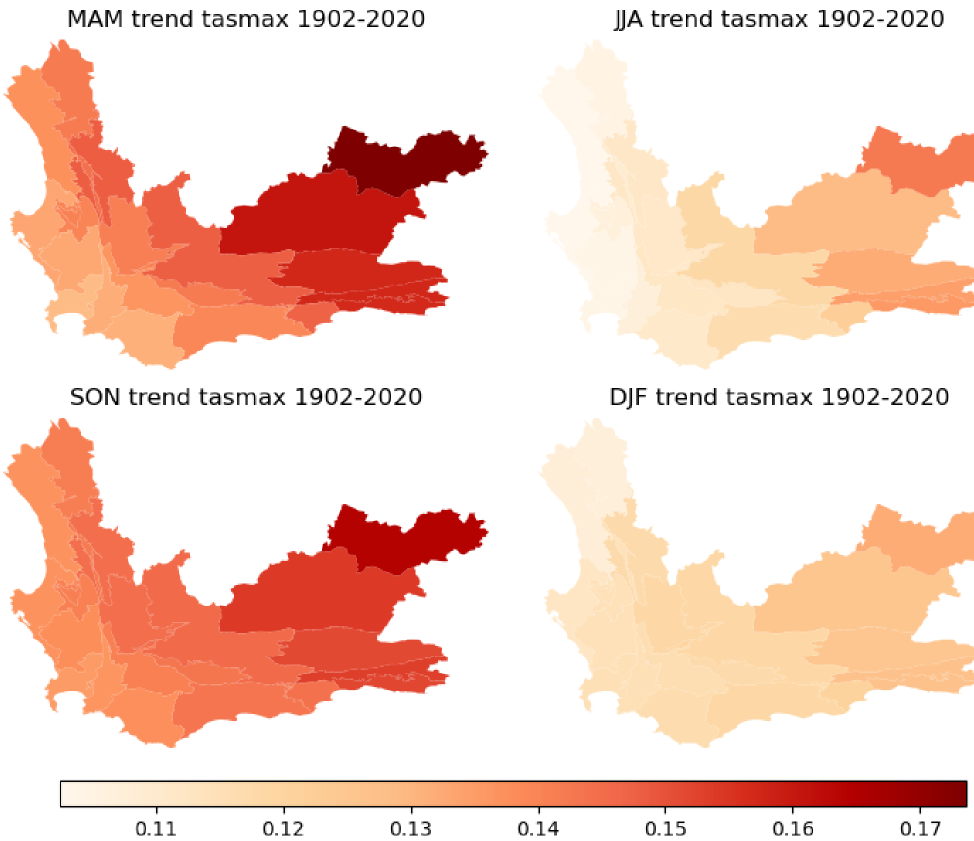

Figure 11: Mean seasonal daily maximum temperature trends (°C/decade) across SmartAgri zones based on the CRU TS4.05 dataset from 1902-2020.

Century scale temperature trends, presented in Figures 10 and 11, indicate that temperatures have consistently increased over the past century at a rate close to the global mean of around 0.1°C/decade. Trends in daily maximum temperature are the highest during the shoulder seasons of autumn (MAM) and spring (SON), with slightly weaker trends during the mid-winter (JJA) and mid-summer (DJF). This is in line with a common theme of stronger climate change signal during the shoulder seasons (Burls et al., 2018).

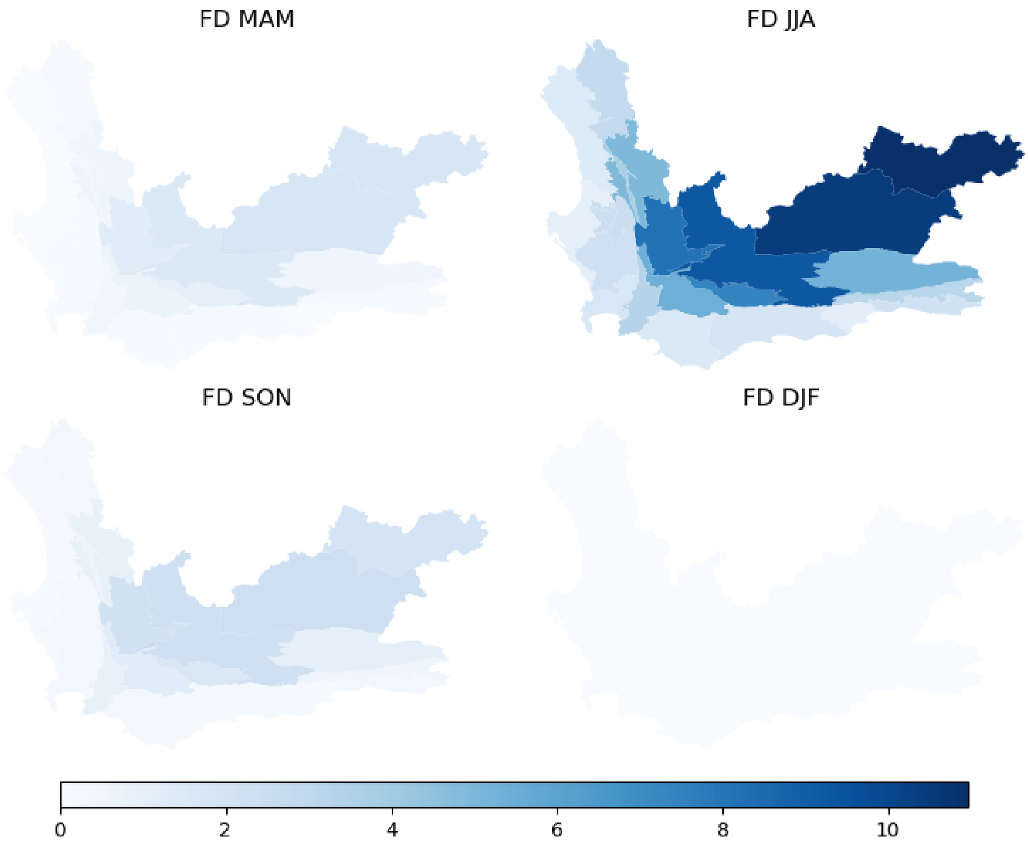

Figure 12: Seasonal average number of frost days (Tmin < 0°C) over the SmartAgri zones based on the CRU TS4.05 observations over the period 1902-2020. Summer (DJF) has zero frost days on average.

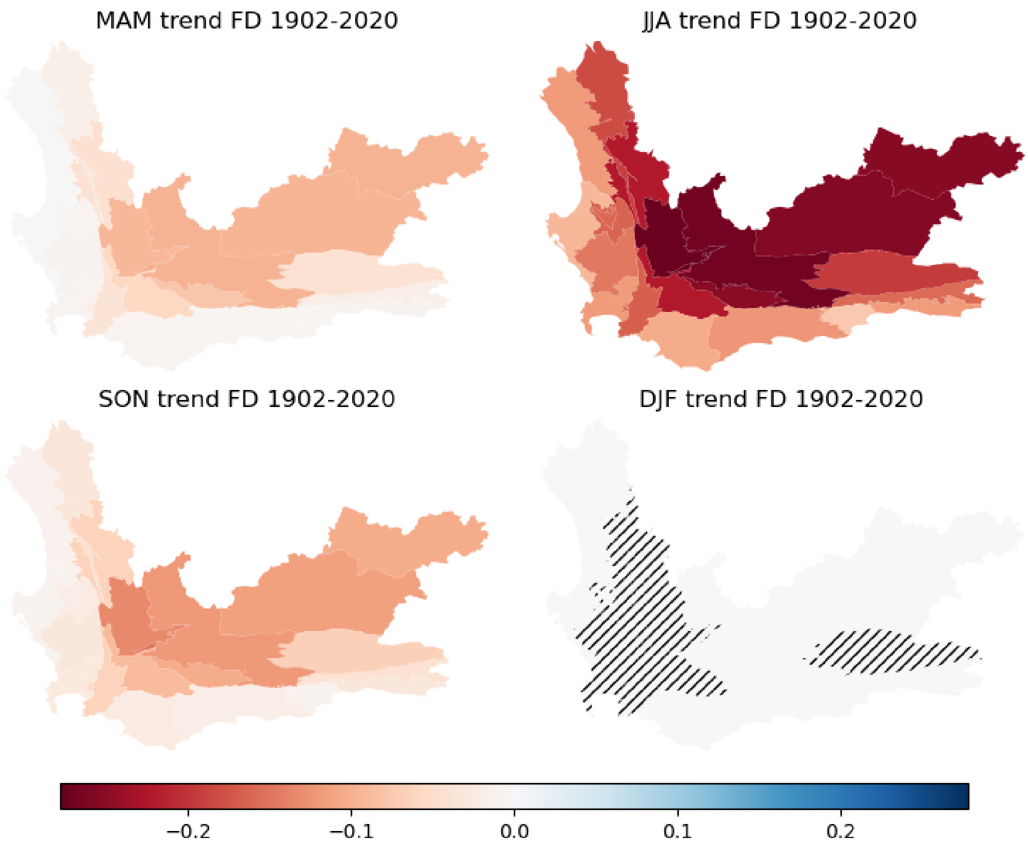

Figure 13: Seasonal trend in the average number of frost days (Tmin < 0°C) expressed as change in frost days/decade over the SmartAgri zones based on the CRU TS4.05 observations over the period 1902-2020. Diagonal hashing indicates trends that are not statistically significant with a p-value threshold of 0.05.

Maps of mean seasonal frost days in Figure 12 illustrate the dominance of frost days in the higher altitude interior zones during JJA, while the strongest absolute trends in frost days also occur in the same zones (Figure 13). With downward trends in frost days of as high as -0.3 days/decade over the century, this is equivalent to a reduction in frost days of as many as 3 days per season or, in some zones, a 30% reduction in frost days.

Precipitation indices climatology and trends

Precipitation climatology and trend indices have been calculated using CRU, GPCC, and CHIRPS. As CHIRPS provides the highest spatial resolution these results are presented here. CRU provides only monthly values and so the daily indices cannot be calculated. GPCC provides daily values for similar period to CHIRPS but at a lower spatial resolution. Both CRU and GPCC figures are made available for comparison in the digital appendix.

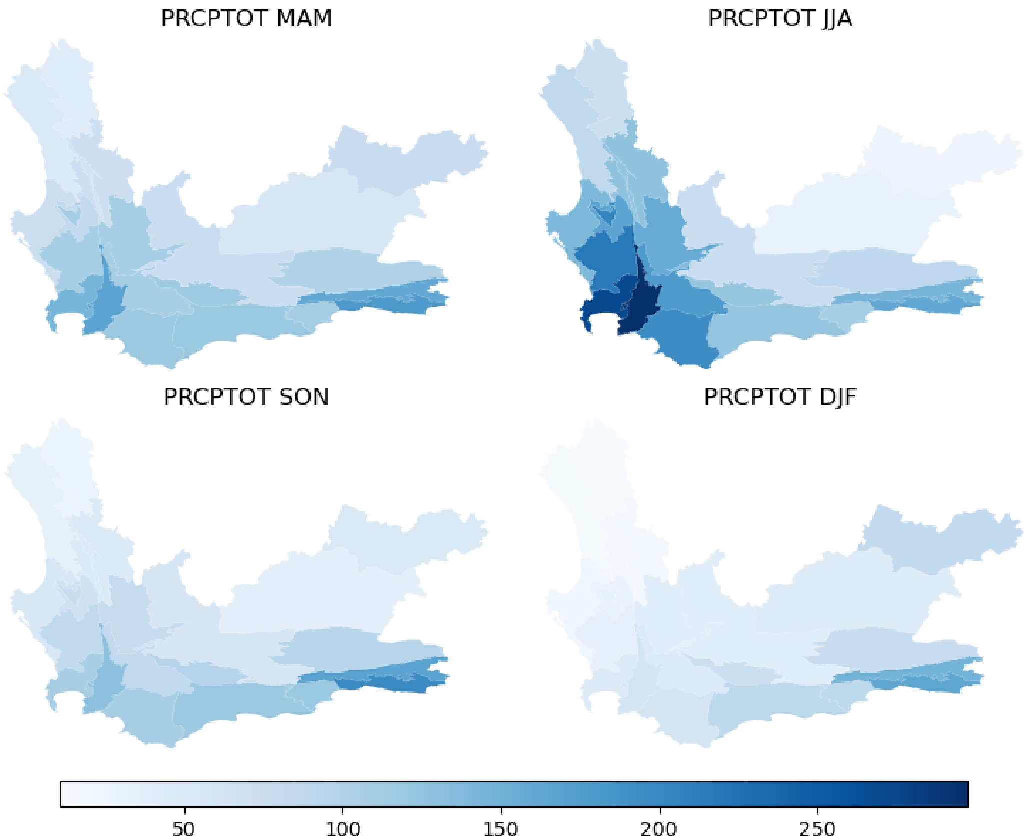

Figure 14: Seasonal total rainfall (mm) over the SmartAgri zones based on the CHG CHIRPS merged rainfall product over the period 1982-2020.

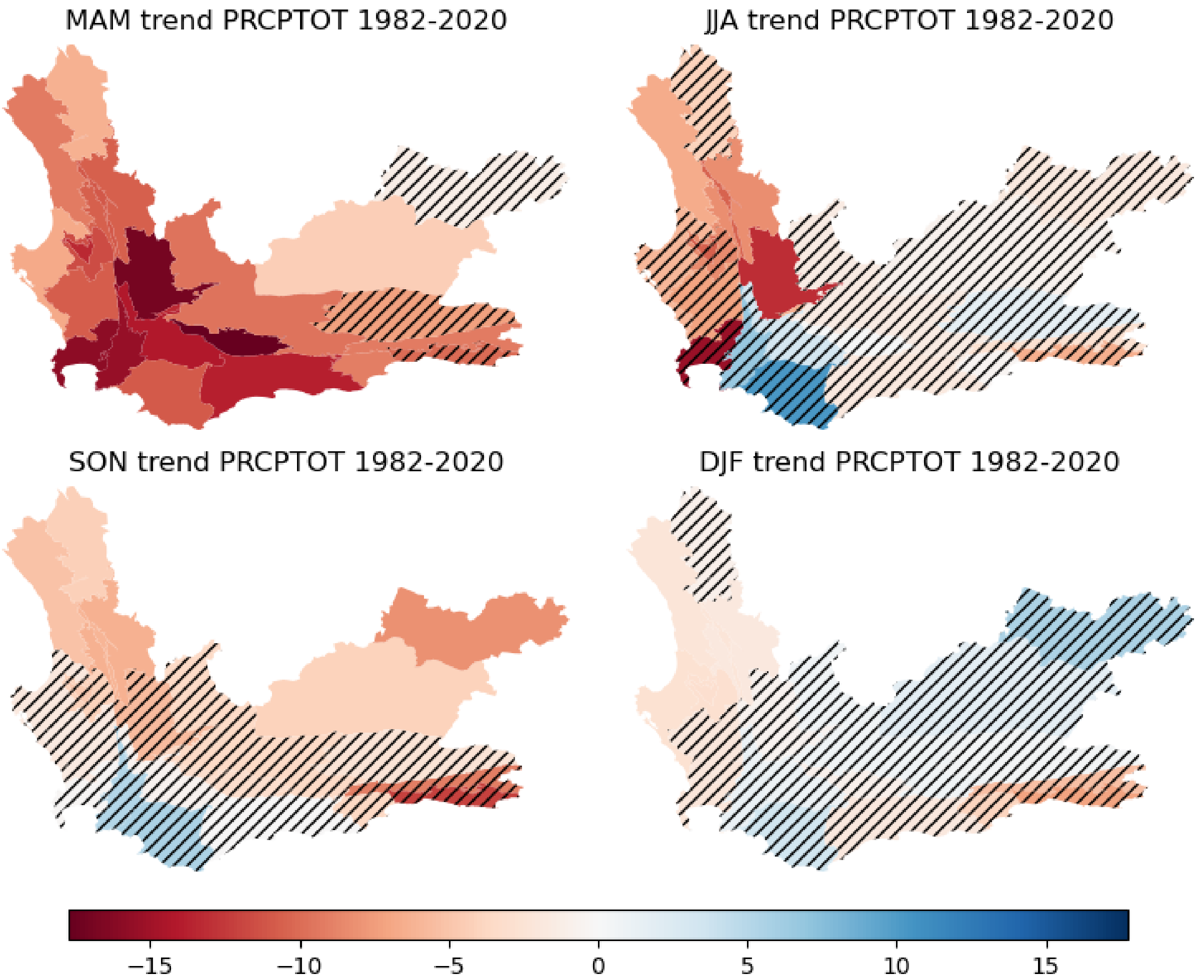

Figure 15: Trend in seasonal total rainfall (mm/decade) over the SmartAgri zones based on the CHG CHIRPS merged rainfall product over the period 1982-2020. Diagonal hashing indicates trends that are not statistically significant with a p-value threshold of 0.05.

Figure 14 clearly illustrates the dominance of winter rainfall over the province with summer rainfall occurring mainly in the far north-eastern zones. The all-year rainfall zones along the eastern coast also stand out as distinct from the rest of the province across all seasons. Absolute trends in rainfall (Figure 15) are strongest during the autumn season. Trends in core winter rainfall are quite mixed and demonstrate a dipole from the north-west towards the south-east. The Rûens-west zone, in particular, stands out strongly as behaving differently to most of the other zones, with stronger, while still not statistically significant, increases in rainfall than other zones. Drying in autumn is consistent with the processes identified that led to the “Day Zero” drought event and other analyses of climate change in the region (Burls et al., 2019, see also Section 3).

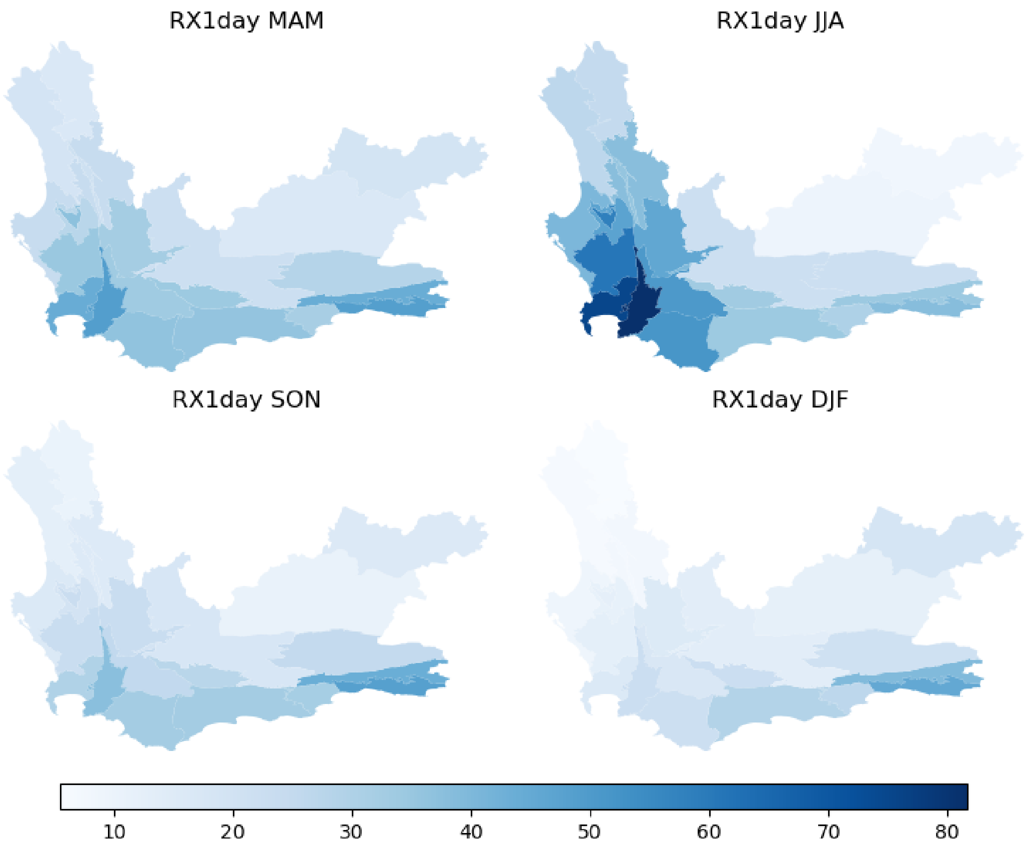

Figure 16: Seasonal maximum 1 day rainfall (mm) over the SmartAgri zones based on the CHG CHIRPS merged rainfall product over the period 1983-2020.

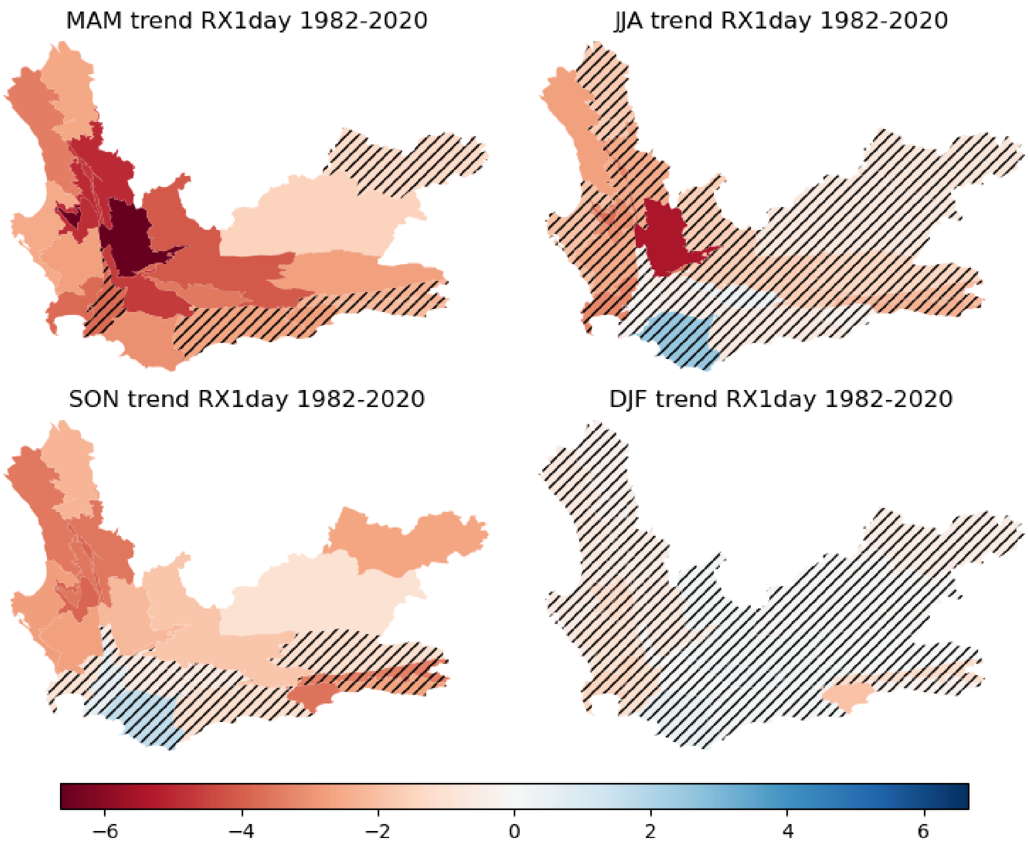

Figure 17: Trend in season maximum 1 day rainfall (mm/decade) over the SmartAgri zones based on the CHG CHIRPS merged rainfall product over the period 1983-2020. Diagonal hashing indicates trends that are not statistically significant with a p-value threshold of 0.05.

Figure 16 shows that the climatology of intense rainfall events (period maximum 1 day rainfall amount) follows very closely the mean precipitation climatology in spatial pattern, i.e. high rainfall intensity occurs in the overall wetter locations. No other patterns emerge, and in particular, there is no noticeable difference in intense rainfall between the different climatological sub-regions: summer rainfall regions dominated by convective rainfall events do not experience more intense rainfall, on a daily timescale, than regions more influenced by frontal rainfall. However, sub-daily rainfall intensities (e.g. maximum 1 hour rainfall), which are not possible to analyse using any of the datasets available for this report, may differ between convective and frontal rainfall regimes.

Figure 17 similarly shows that trends in intense daily rainfall largely follow both the spatial pattern and the seasonal variations of total rainfall, with strongest decreasing trends occurring in autumn (MAM) and some non-significant increase in intense daily rainfall in the Rûens-west during mid-winter (JJA) and spring (SON).

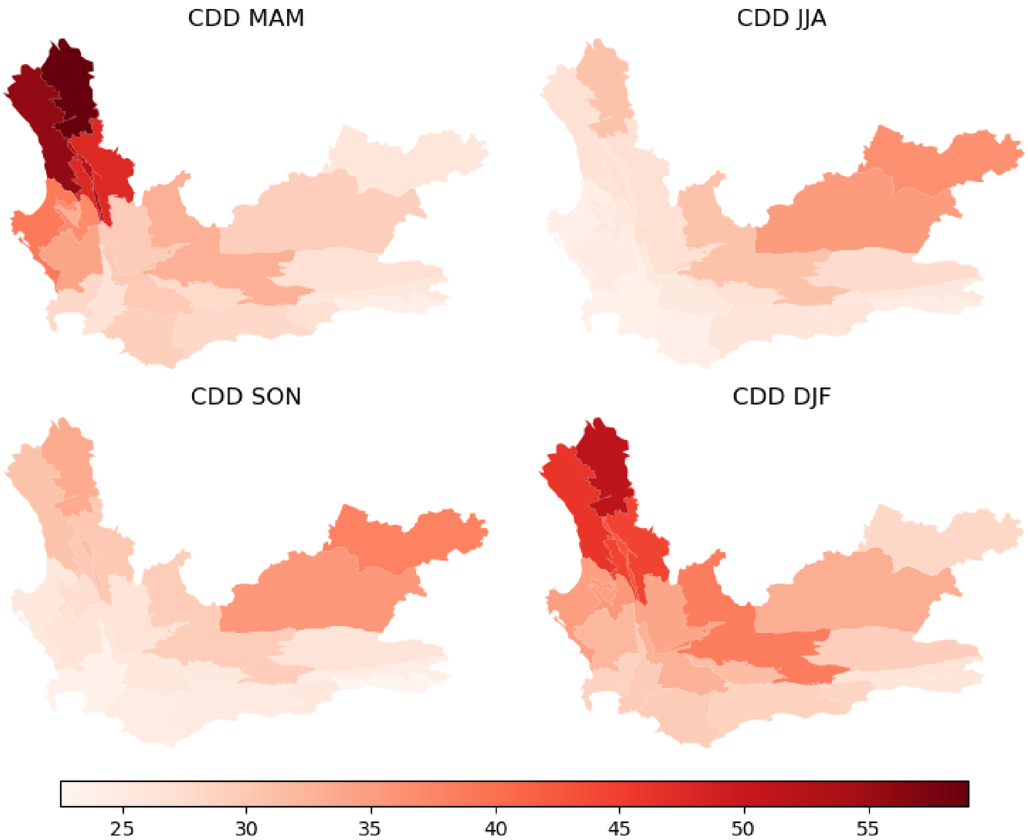

Figure 18: Seasonal mean of the maximum consecutive dry days over the SmartAgri zones based on the CHG CHIRPS merged rainfall product over the period 1983-2020.

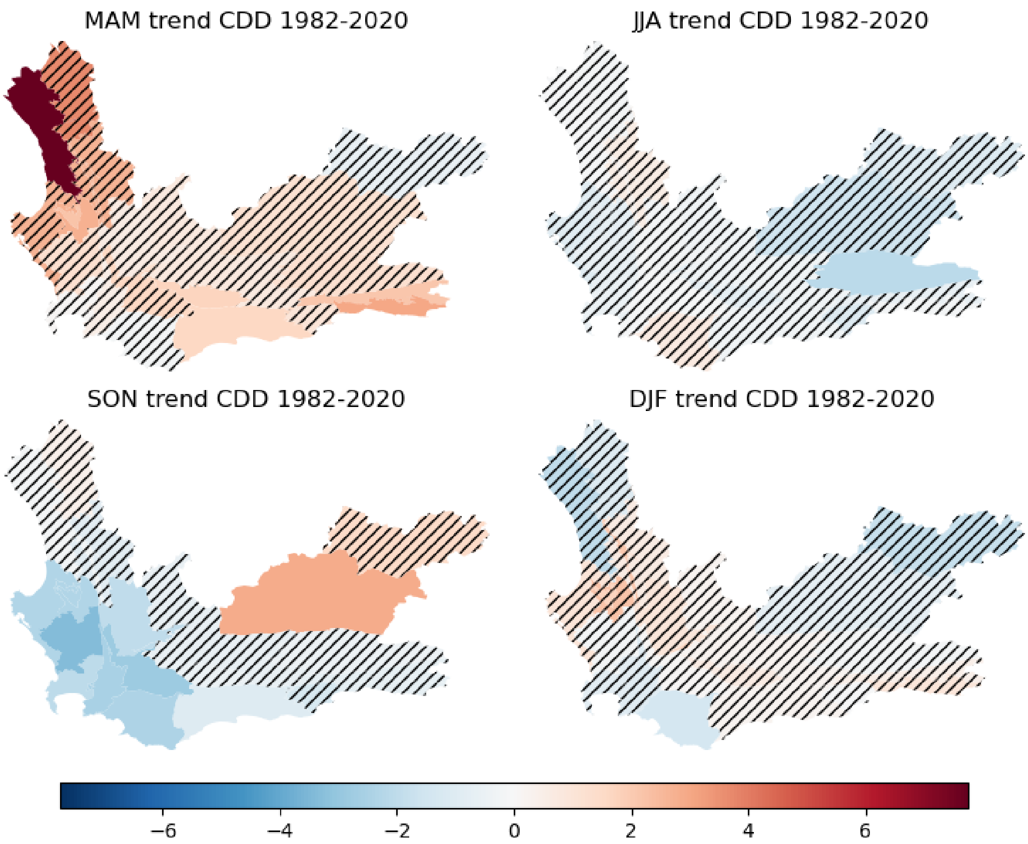

Figure 19: Trend in season maximum consecutive dry days (days/decade) over the SmartAgri zones based on the CHG CHIRPS merged rainfall product over the period 1983-2020. Diagonal hashing indicates trends that are not statistically significant with a p-value threshold of 0.05.

Figure 18 shows the climatology of seasonal maximum consecutive dry days across the region. This clearly illustrates that the northern zones experience by the far the largest dry spells during autumn (MAM) with some dry spells exceeding 55 days. The shorter dry spells in these regions during summer (DJF) is likely a result of localised convective events associated with summer rainfall dynamics rather than frontal rainfall.

Trends in consecutive dry days, shown in Figure 19, indicate very weak trends for most seasons and most regions, except for strong increases in the north-west coastal region during autumn. This is likely a result of a southern shift in cold fronts and their northward extent, which would be the cause of important autumn rainfall events in this region. Some regions show a reduction in dry spells during spring which is not aligned very strongly with a reduction in total rainfall during this season, suggesting a shift towards more frequent but less intense rainfall.

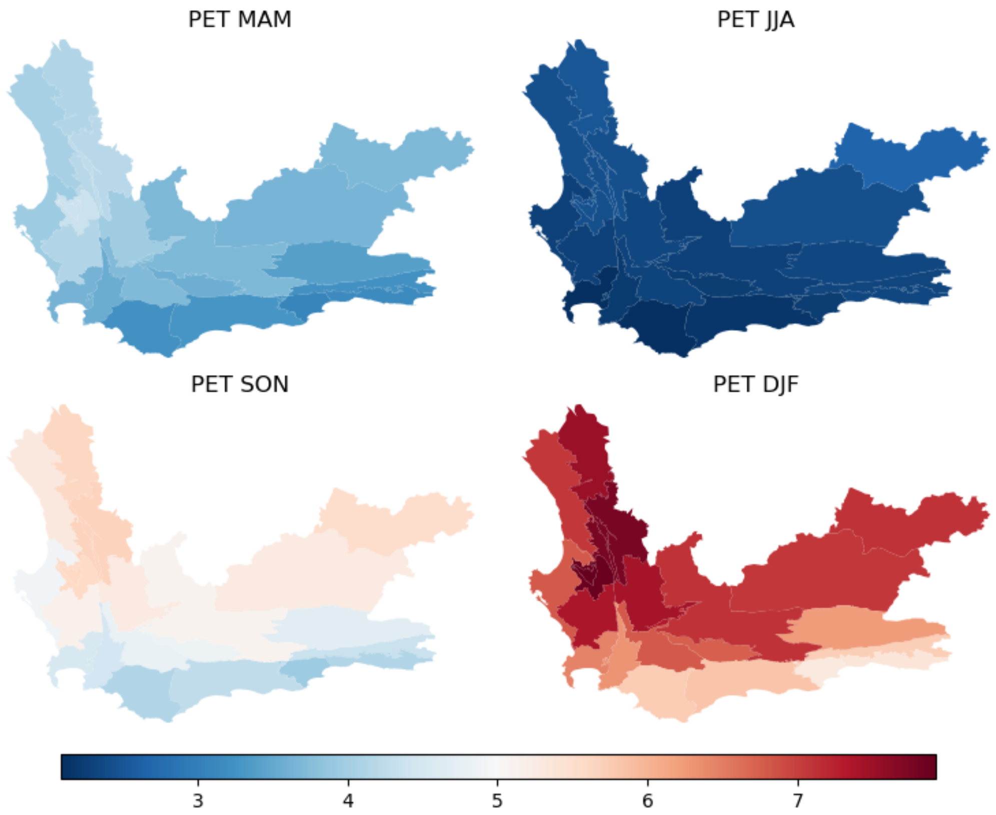

Figure 20: Seasonal mean Potential Evapotranspiration (PET, mm/day) across the SmartAgri zones based on the CRU TS4.05 product. CRU PET is calculated using the Penman-Monteith method.

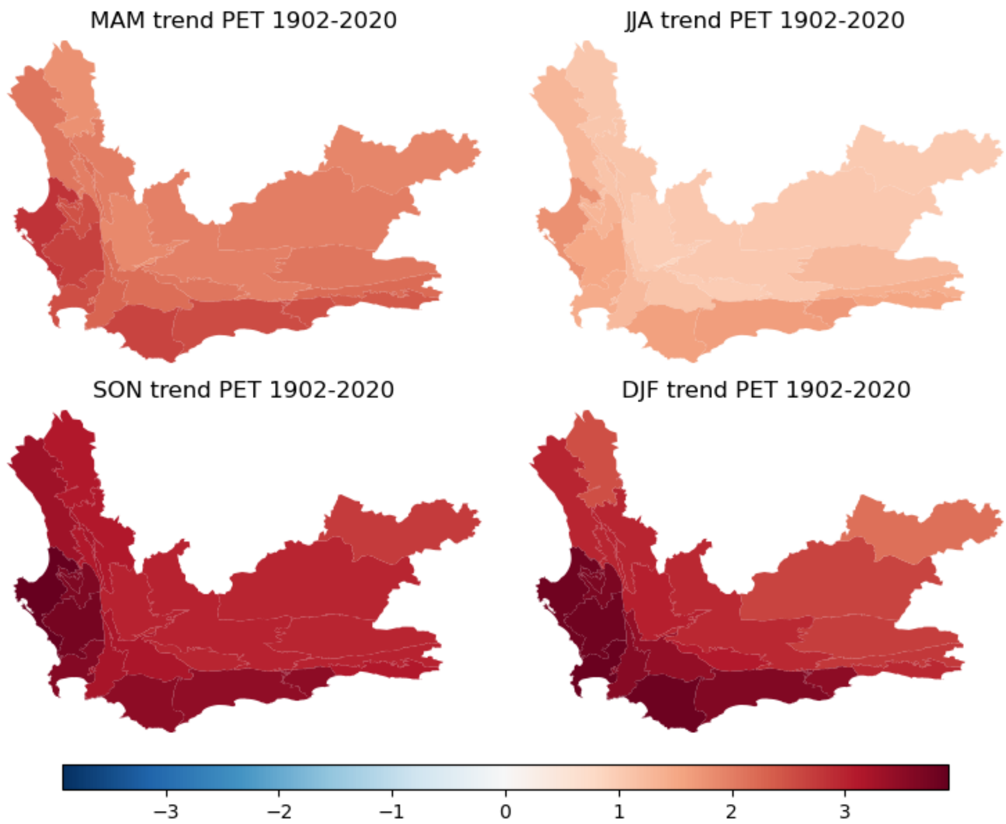

Figure 21: Trend in seasonal mean Potential Evapotranspiration (PET, mm/day) across the SmartAgri zones based on the CRU TS4.05 product over the period 1902-2020. CRU PET is calculated using the Penman-Monteith method.

Figures 20 and 21 show the distribution, both spatially and through the seasons, of mean seasonal Potential Evapotranspiration (PET) and its long-term trend. In this case PET is a variable provided by the CRU TS4.05 data product and is calculated using the Penman-Monteith method that includes estimates of solar radiation and atmospheric humidity. The next section includes future projections of PET based on the simpler Hargreaves approach.

PET is clearly strongest during the core summer months and to some extent during spring (SON) in the far northern zones. It is important to note that PET is the *potential* evapotranspiration and assumes unlimited moisture availability. In many seasons and zones, evapotranspiration would be limited by soil moisture and so actual evaporation is likely higher during spring than mid-summer in many zones.

Trends in PET are consistently positive across all zones in all seasons following the consistent driving positive trend in temperature.

Other daily rainfall indices are available in the digital appendix (see Appendix A).

Summary

Temperature trends

- Temperature trends are very consistent across all zones. Historical trends are on the order of 0.1°C/decade, which is in line with global rates.
- Daily maximum trends are slightly larger in the inland (north/east) zones, in line with continental patterns of higher inland temperature trends.
- Daily minimum trends are slightly larger closer to the coast and to the north, which likely reflects shifts in humidity and cloudiness (not analysed here).

Rainfall trends

- Rainfall trends are more mixed and, for many zones, not statistically significant ($p < 0.05$).
- Autumn (March-May) exhibits the most dominant statistically significant trends with largest negative trends in some of the interior zones such as the Bokkeveld.
- The core winter season (June-August) exhibits a mix of drying and increasing trends but only the Bokkeveld, Cederberg and Hardeveld zones stand out as having a significant trend, with the Bokkeveld exhibiting very strong drying trends.
- Spring (September-November) exhibits relatively weak and insignificant trends, except for some interior and northern-eastern zones which are more dominated by summer rainfall dynamics. These trends suggest a trend towards a later start to the summer rainfall dynamics.
- Core summer (December-February) trends are largely weak and insignificant, except for the zones from the Cederberg through to the Sandveld/Hardeveld along the west coast.
- Trends in wet days largely follow the same pattern as trends in total rainfall.
- Trends in consecutive dry days are largely insignificant, except for a negative trend during the September-November period.

Evaporation trends

- Trends in PET are consistently significantly positive, driven by consistently positive and significant temperature trends.
- Trends in PET are highest in the most southern and the most western zones, while being strongest in spring (September-November) and summer (December-February).

6. Climate change projections

Update to section 4.7 in the SmartAgri Status Quo[1] Review.

The approach taken to climate change projections in this analysis is based on the multiple lines of evidence framing well documented in the IPCC AR6: Chapter 10 (Doblas-Reyes et al., 2021). The multiple lines of evidence approach does not assume that any singular source of climate projections is superior, but rather aims to look across multiple model ensembles and downscaling and identify common agreement as well as aspects of disagreement.

For this analysis three model ensembles were analysed:

CMIP5

The 5th iteration of the Coupled Model Intercomparison Project (CMIP5, Taylor et al., 2012) was the primary basis of the climate projections analysed under the IPCC 5th assessment report. The CMIP5 experiment utilised Representative Concentration Pathways (RCP, Van Vuuren et al., 2011) to describe different future socio-economic scenarios and their associated emissions related scenarios (greenhouse gases, aerosols and land use change). Included here is RCP 4.5, which represents a "middle of the road" scenario with fairly strong mitigation action culminating in an increase in 4.5 W/m^2 in equivalent radiative forcing by 2100, as well as RCP 8.5, which represents a very negative scenario with very little mitigation of emissions into the future. While RCP 8.5 is a very pessimistic and arguably unlikely scenario, it is useful to analyse as it produces clearer climate change signals that are easier to discriminate from background variability. As a means of exploring possible directions of change in variables it is therefore useful, even if the magnitude of changes is unlikely.

CMIP6

The 6th iteration of the CMIP experiment (CMIP6 Eyring et al., 2016) was developed in preparation for the IPCC 6th assessment report. While deploying a different approach to future emissions scenarios called Shared Socioeconomic Pathways (SSPs, O'Neill et al., 2014), the experiment designers did choose to align the SSPs with the CMIP5 RCPs in terms of radiative forcing. This means that largely equivalent scenarios across CMIP5 and CMIP6 could be analysed. In this case, SSP5 8.5 and SSP2 4.5 were analysed as roughly equivalent to RCP 8.5 and RCP 4.5.

The CMIP6 ensemble includes much improved Atmosphere Ocean Global Climate Models (AOGCM) with, in some cases, improved spatial resolution, as well as many other improvements in relevant sub-processes such as land use, vegetation and ocean modelling.

Projected changes derived from CMIP6 do not vary significantly to those derived from CMIP5 over the southern African region (e.g. Almazroui et al., 2020), though CMIP6 on average projects stronger temperature increases globally and there are some differences in regional patterns of rainfall change.

CORDEX

The Coordinated Regional Downscaling Experiment (CORDEX, Giorgi et al., 2009) is a globally coordinated project with the objective of dynamically (and statistically) downscaling the CMIP model ensembles, as well as further develop regional downscaling. The original CORDEX activity focused on dynamical downscaling of the CMIP5 climate projections across multiple regions across the globe. CORDEX Africa developed dynamical downscaling of CMIP5 across the entire African continent at a grid resolution of around 0.44° horizontally (45-50km). CORDEX Africa has been extensively analysed and used to develop climate impacts assessments across all regions of Africa. The higher spatial resolution of the participating dynamic downscaling models enables the CORDEX ensemble to represent regions of complex topography more realistically (Dosio et al., 2019). Hence it is applied to the Western Cape in the understanding that the models will provide an improved representation of the impact of the regional topography on the climate and change in the climate.

Plume plots

An effective approach to visualising multiple climate ensembles is the plume plot. Plume plots provide a visualisation of the range of projections resulting from multiple models as members of ensembles, from historical periods into future periods. Multiple model ensembles can be overlaid and agreements and disagreements easily identified.

Combined SmartAgri Zones

To obtain a workable number of plume plots, it was decided to cluster the original SmartAgri Zones based on some measure of climatic similarity. Various approaches and numbers of clusters were explored and finally the inter-annual variability of annual rainfall was used as the clustering variable. Thus the Zones with the most similar inter-annual variability were clustered together. Agglomerative clustering was applied and resulted in six clusters (see Figure 22). Both more clusters and fewer clusters were explored. More clusters did not offer significant advantage as many zones, such as the central Montagu through to van Wyksdorp cluster, remained as a single cluster. Fewer clusters agglomerated zones that are known to have distinct climates. As the purpose of the clustering is purely to explore the level of agreement across multiple climate model ensembles, rather than provide detailed spatial information, it was decided to retain six clustered zones.

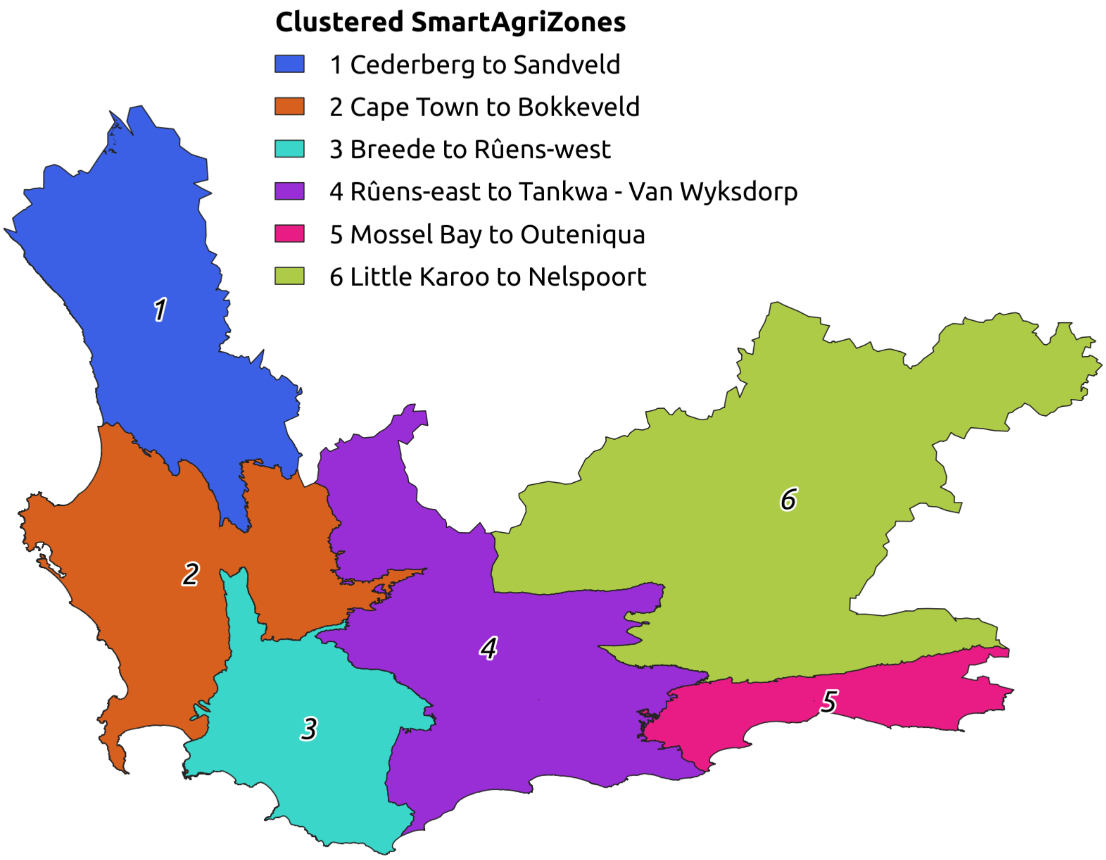

Figure 22: Clustered SmartAgri zones based on similarity of inter-annual total rainfall variability.

Multi-ensemble plume plots

Figure 23 presents plume plots for each of the six clustered zones for annual mean temperature as a primary indicator of climate change across the region. All clustered zones exhibit very similar behaviour, with the strongest projected changes occurring in the Cederberg to Sandveld and the Little Karoo to Nelspoort zones. Here, only the CORDEX, CMIP5 and CMIP6 projections for the RCP 4.5/SSP2 4.5 scenarios are included, which are closest to current emissions trajectories. It can be seen that both ensembles agree very well, with the strongest differences occurring in the Cederberg to Sandveld zone where the CMIP5 ensemble projects stronger temperature increases and in the Little Karoo to Nelspoort zone where CMIP6 projects the strongest changes. The number of models included in each ensemble varies by variable as different models archived slightly different sets of variables.

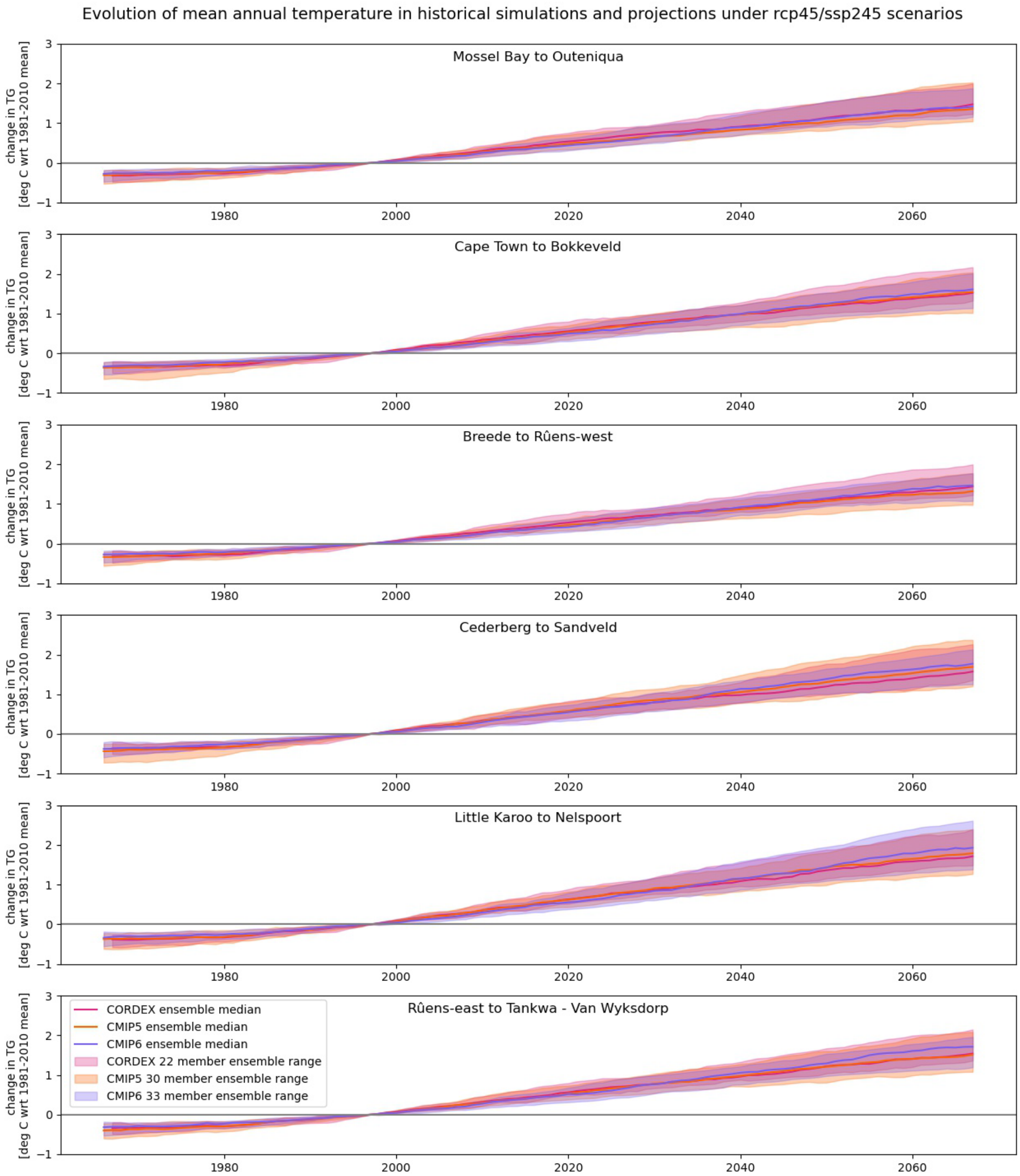

Figure 23: Plume plots of annual mean temperature change across CMIP5, CMIP6 and CORDEX ensembles and the clustered SmartAgri zones for the RCP 4.5 and SSP2 4.5 scenarios.

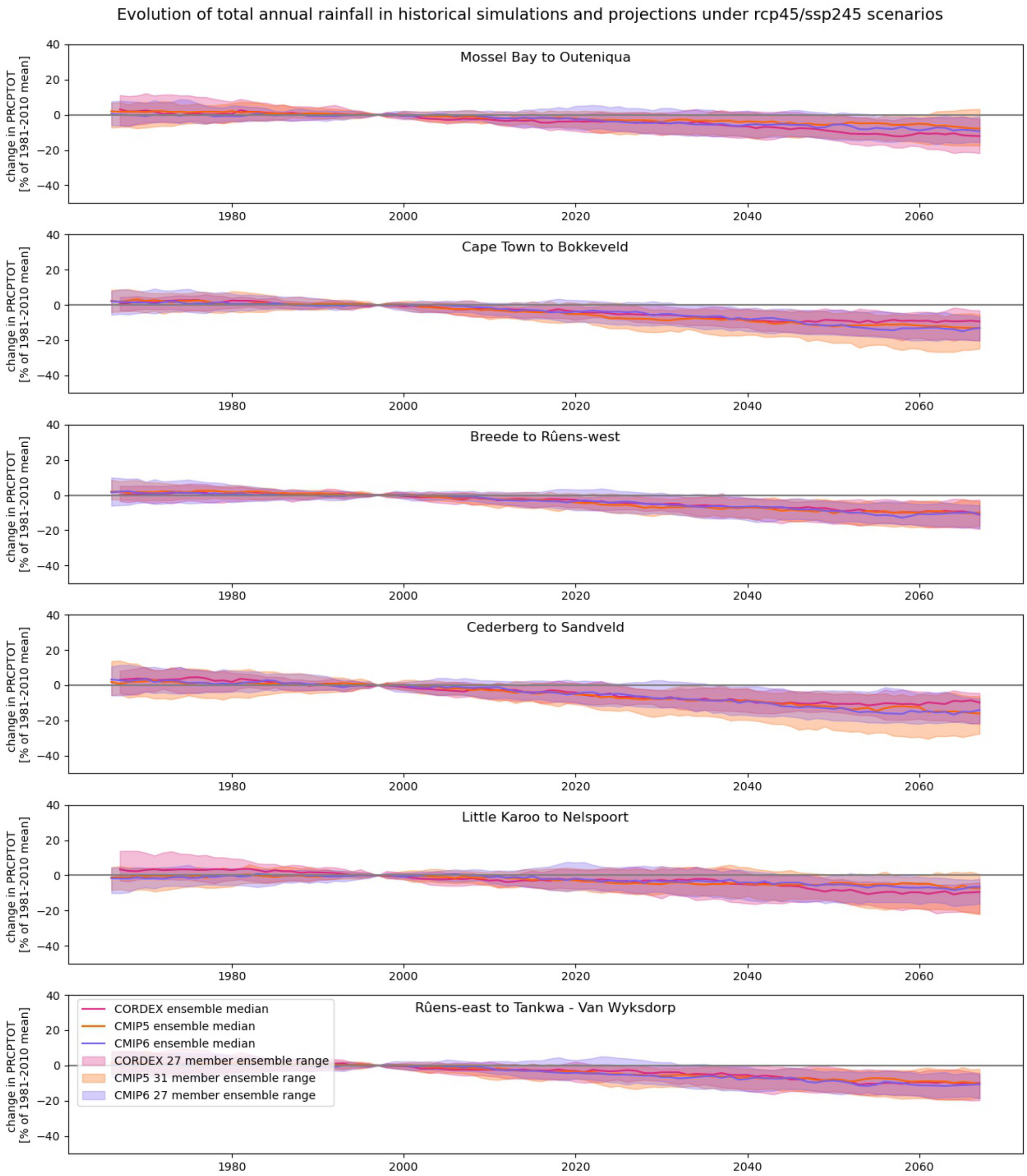

Figure 24: Plume plots of annual mean rainfall change (%) across CMIP5, CMIP6 and CORDEX ensembles and the clustered SmartAgri zones for the RCP 4.5 and SSP2 4.5 scenarios.

Figure 24 presents plume plots for total annual rainfall change. There is relatively good agreement across the CMIP5 and CMIP6 ensembles in projected change in core winter (JJA) rainfall. The CMIP6 ensemble tends to produce weaker drying across most clustered zones, especially the Rûens-east to Tankwa-Van Wyksdorp zones, with the older CMIP5 ensemble indicating stronger drying across the zones. There is however a broadly consistent message of decreasing rainfall across all regions and hence across the whole province.

Based on the analysis above, and the supporting plume plots in the digital appendix, it was decided to focus the further analysis on the most recent projections based on the CMIP6 ensemble.

Projected anomaly maps and archetypes

In this section, projected anomaly maps based only on CMIP6 are presented. The full suite of CORDEX and CMIP5 maps are available in the digital appendix (see Appendix A). It should be noted that the projected changes do not vary significantly across the different ensembles except the broad differences noted above (CMIP6 has a reduced magnitude of drying). The projected anomalies for all members of the ensemble in each map are presented. However, the ensemble members, and hence the submaps in each plot, are ordered by the spatially averaged projected change in order to help identify high, middle and low scenarios for each index.

Projected changes in temperature indices

Figures 25-28 represent projected changes in temperature related indices: mean annual temperature, average maximum daily temperature in the hot (DJF) season, average minimum daily temperature in the cold (JJA) season and very hot days (number of days with air temperature exceeding 30°C). The projections are based on the CMIP6 ensemble and the SSP2 4.5 "middle of the road" scenario for the 2030-2060 period.

The spatial patterns of change in mean annual temperature shown in Figure 25 are fairly consistent across all models, even while the magnitude of changes varies from less than 0.8°C average warming through to as high as 1.6°C warming. The strongest warming occurs in the interior summer rainfall regions which aligns with much other literature pointing towards strongest increases further away from the moderating influence of the oceans.

Increases in the maximum temperatures in the hot season (Figure 26) and minimum temperatures in the cold season (Figure 27) show spatial patterns that are similar to those of average temperatures, although the range of values of the increases are slightly different: maximum temperatures increase by about 0.1-0.2°C stronger and minimum temperatures by about 0.1-0.2°C weaker than the mean annual temperature.

Interestingly, some models do not demonstrate significant changes in very hot days (number of days with maximum daily temperature exceeding 30°C, Figure 28) *despite* increases in average temperatures. This is likely due to compensating increases in rainfall and moderated warming during some periods of the year.

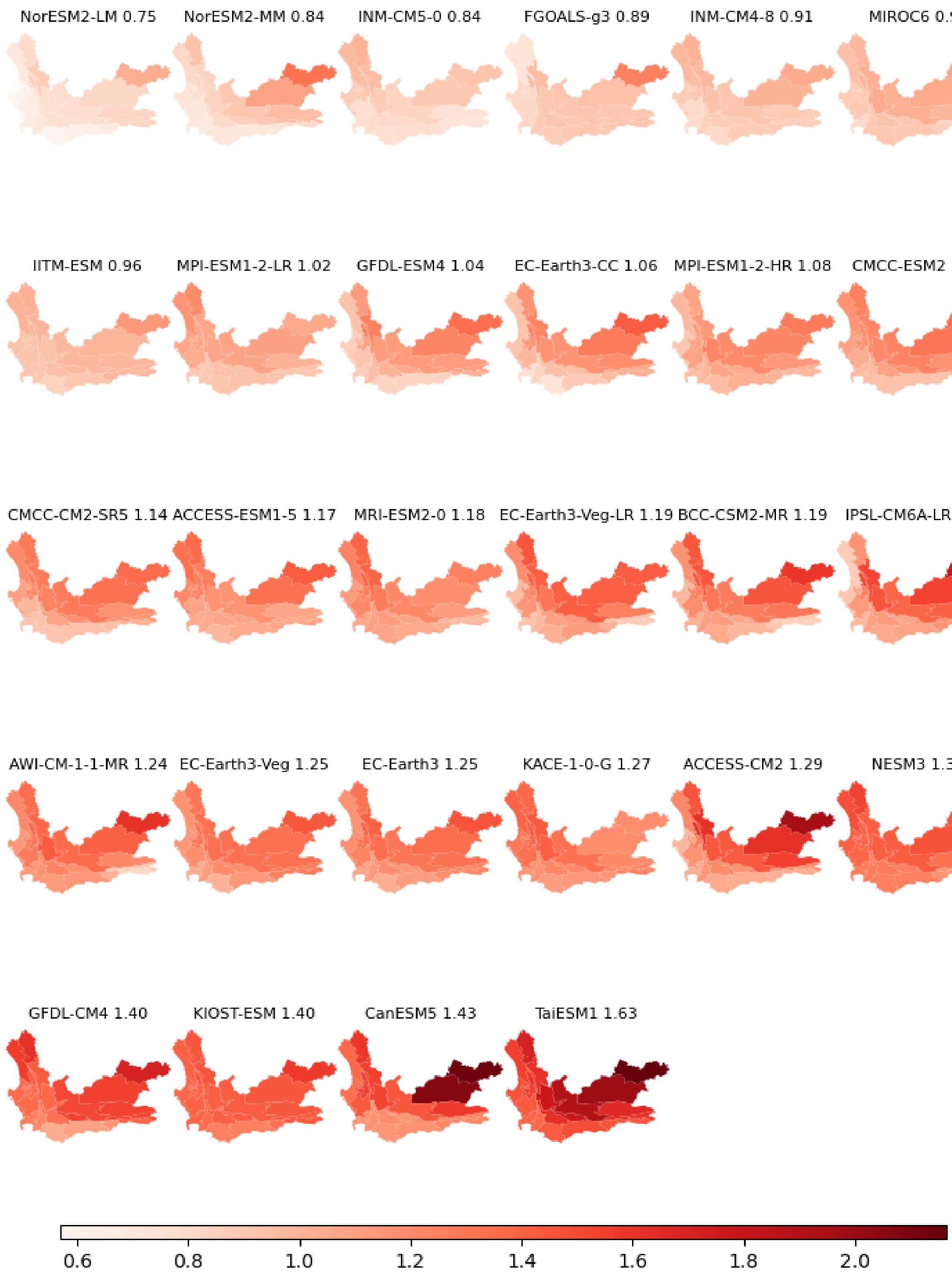

Figure 25: Projected changes in mean annual daily average temperature (°C) across the SmartAgri zones derived from the CMIP6 model ensemble SSP2 4.5 pathway experiment for the period 2030-2060. Figure titles are the name of the model and the area average change in temperature (°C). Diagonal hashing indicates trends that are not statistically significant with a p-value threshold of 0.05.

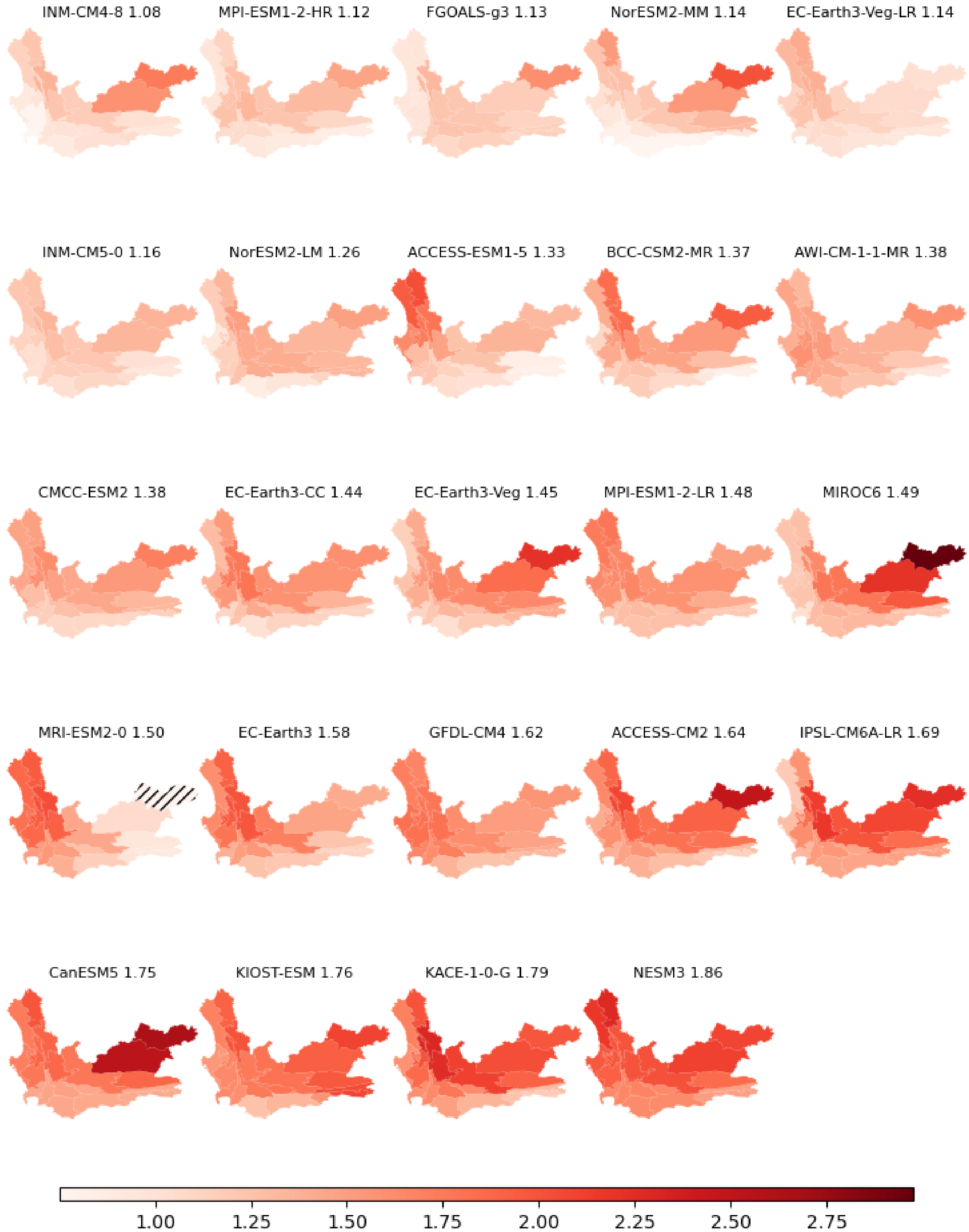

Figure 26: Projected changes in seasonal mean of maximum daily temperature in DJF (°C) across the SmartAgri zones derived from the CMIP6 model ensemble SSP2 4.5 pathway experiment for the period 2030-2060. Figure titles are the name of the model and the area average change in temperature (°C). Diagonal hashing indicates trends that are not statistically significant with a p-value threshold of 0.05.

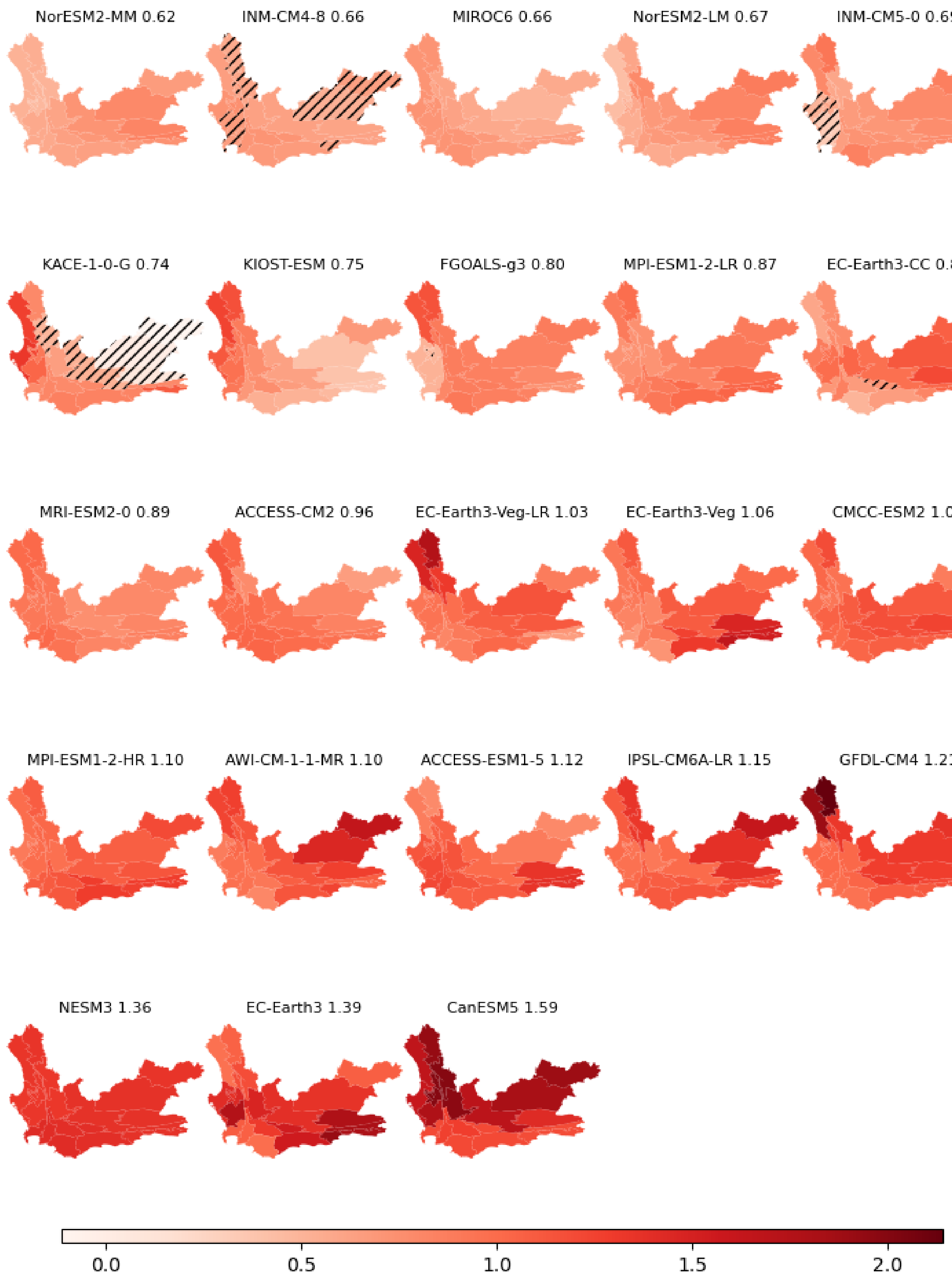

Figure 27: Projected changes in seasonal mean of minimum daily temperature in JJA (°C) across the SmartAgri zones derived from the CMIP6 model ensemble SSP2 4.5 pathway experiment for the period 2030-2060. Figure titles are the name of the model and the area average change in temperature (°C). Diagonal hashing indicates trends that are not statistically significant with a p-value threshold of 0.05.

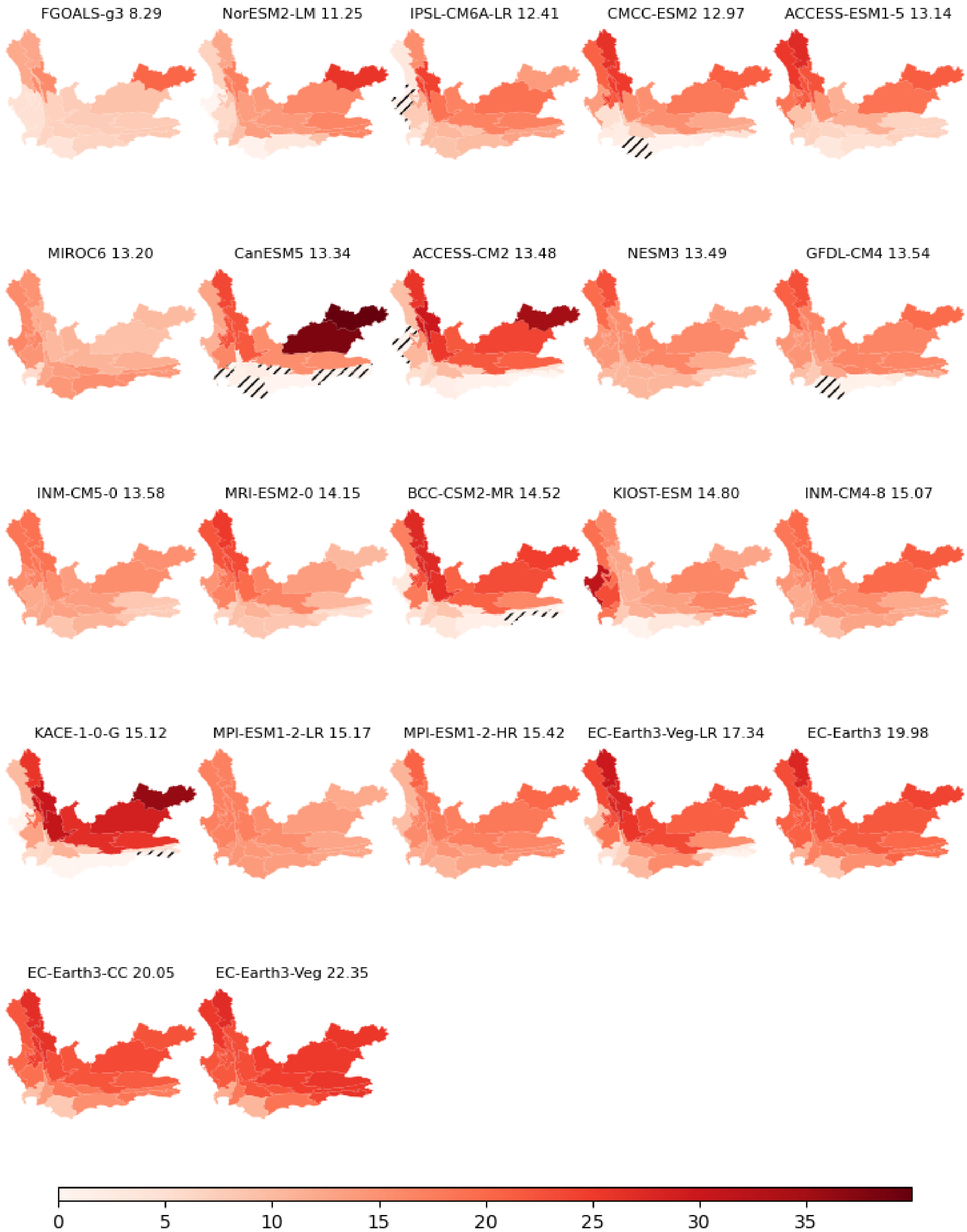

Figure 28: Projected changes in days/year with maximum temperature exceeding 30°C (days) across the SmartAgri zones derived from the CMIP6 model ensemble SSP2 4.5 pathway experiment for the period 2030-2060. Figure titles are the name of the model and the area average change in days. Diagonal hashing indicates trends that are not statistically significant with a p-value threshold of 0.05.

Projected changes in rainfall indices

Figures 30-35 represent projected changes in precipitation related indices (total rainfall, maximum 1 day rainfall, consecutive dry days) based on the CMIP6 ensemble and the SSP2 4.5 “middle of the road” scenario for the 2030-2060 period. Figures 30-32 show the core summer period (DJF), and Figures 33-35 show the autumn period (MAM). Projections for the remaining seasons (JJA and SON) are included in the digital appendices.

Changes in summer (DJF) rainfall

The projected changes vary in magnitude and pattern across the ensemble. For the core summer rainfall (DJF), the strongest decreases are as expected in the north-east summer rainfall regions, with one particular model demonstrating strong increases in summer rainfall for this zone (Figure 30). This can be unpacked further in the plume plot (Figure 29) where it is seen that all of the CMIP5, CMIP6 and CORDEX ensembles include the possibility of increasing summer rainfall over the Nelspoort zone.

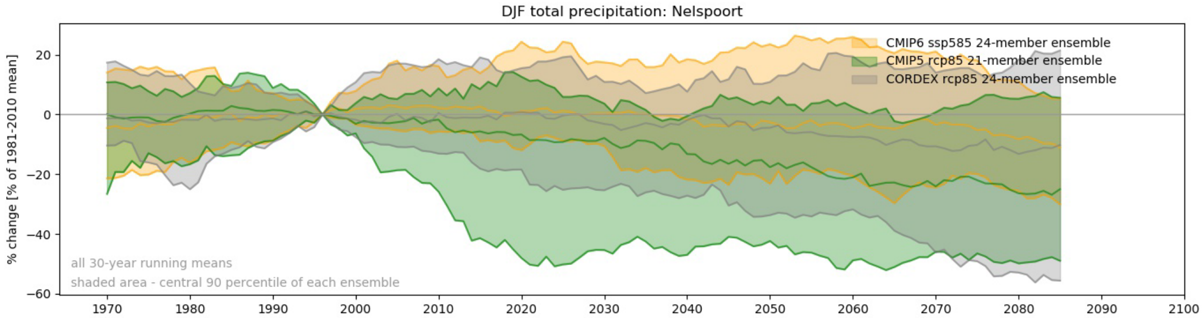

Figure 29: Plume plot of CMIP5, CMIP6 and CORDEX projections of total seasonal summer rainfall DJF for the Nelspoort SmartAgri zone illustrating the uncertainty in magnitude and direction of change of rainfall in this zone.

Changes in intense 1 day rainfall (Figure 31) are largely not significant across the region, except for the interior north-eastern zones, where some models project significant increases in intensity of 1 day rainfall. Increases in extreme rainfall are anticipated generally under climate change, but do depend on the overall change in rainfall in a particular region. Regions experiencing a reduction in total rainfall may in some cases also experience increases in extreme rainfall, but often decreasing rainfall is also associated with decreasing rainfall intensity. It must be noted that dynamical models do tend to under-estimate the magnitude of changes in extreme rainfall. Recent experiments with very high resolution models that explicitly simulate convective dynamics have demonstrated that much stronger increases in convective rainfall should be anticipated across many areas of Africa (Kendon et al., 2019). However, for the Western Cape these increases remain weak.

Projected changes in consecutive dry days (Figure 32) span both increases and decreases, similarly to other rainfall indices. The changes are in general weak and mostly not statistically significant, although several models project statistically significant increases – mostly in the summer rainfall region (north-eastern part of the Western Cape).

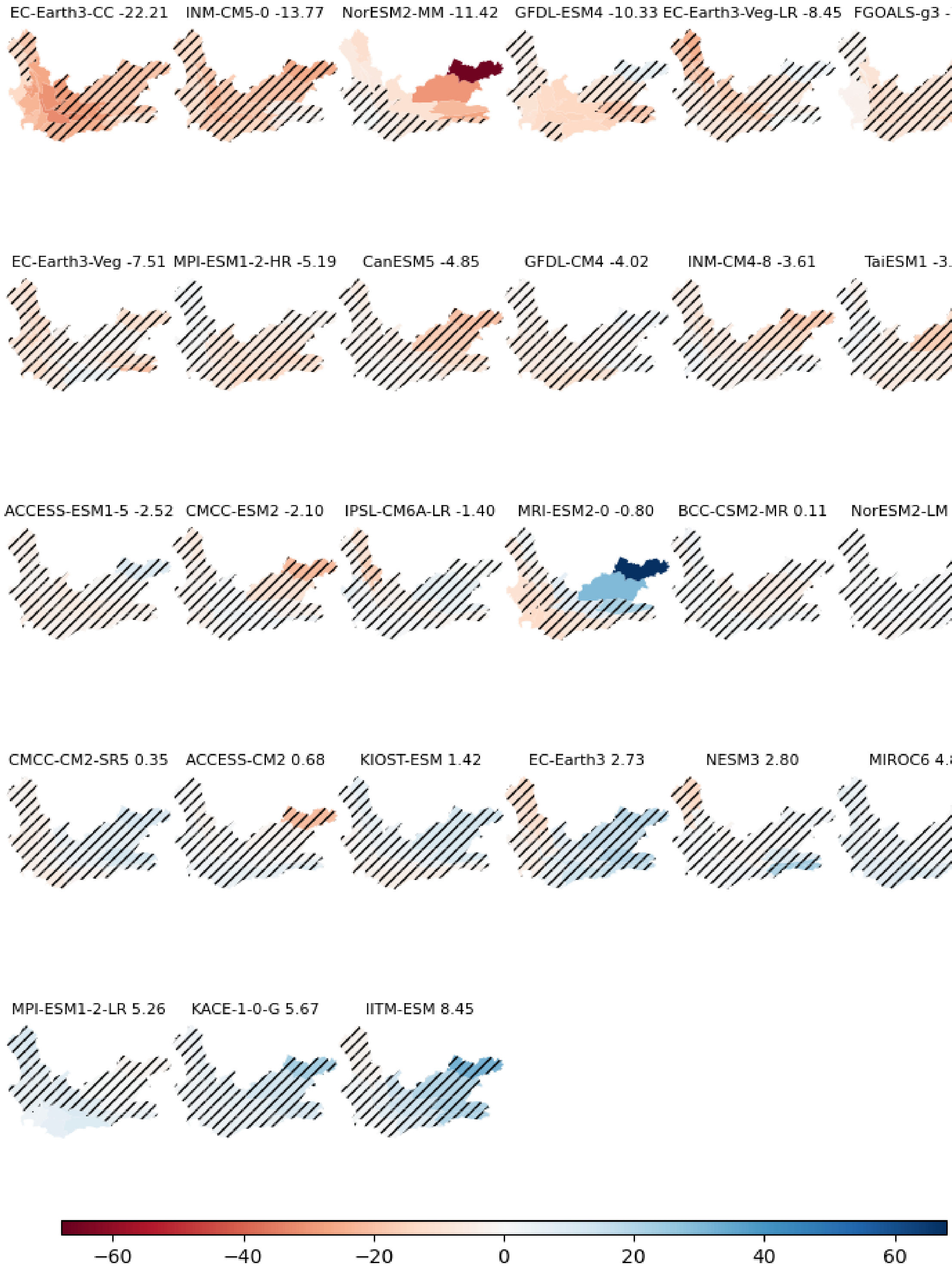

Figure 30: Projected changes in seasonal summer (DJF) total rainfall (mm) across the SmartAgri zones derived from the CMIP6 model ensemble SSP2 4.5 pathway experiment for the period 2030-2060. Figure titles are the name of the model and the area average change in rainfall (mm). Diagonal hashing indicates trends that are not statistically significant with a p-value threshold of 0.05.

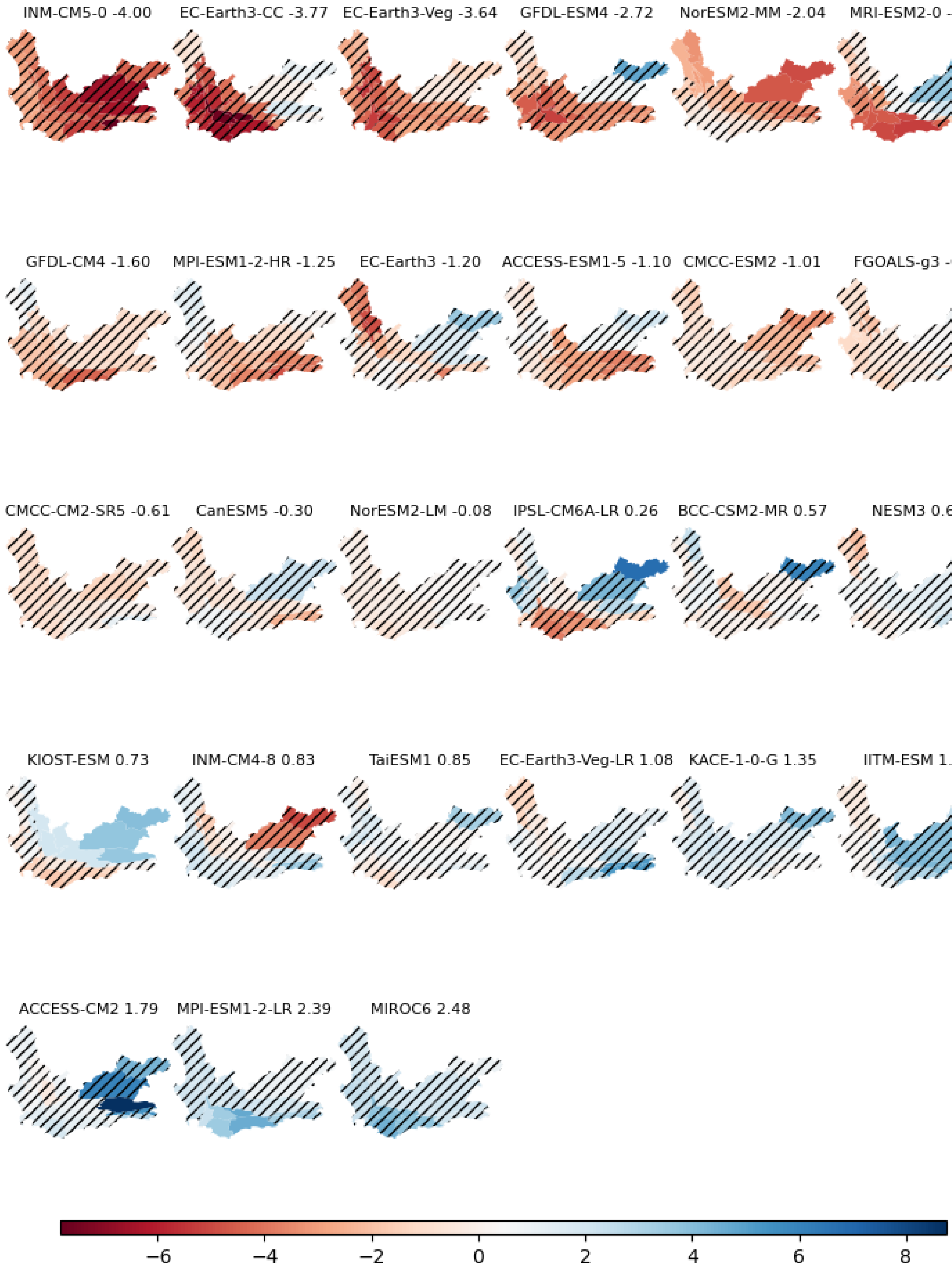

Figure 31: Projected changes in maximum 1 day daily rainfall (mm) for the DJF season across the SmartAgri zones derived from the CMIP6 model ensemble SSP2 4.5 pathway experiment for the period 2030-2060. Figure titles are the name of the model and the area average change in rainfall (mm). Diagonal hashing indicates trends that are not statistically significant with a p-value threshold of 0.05.

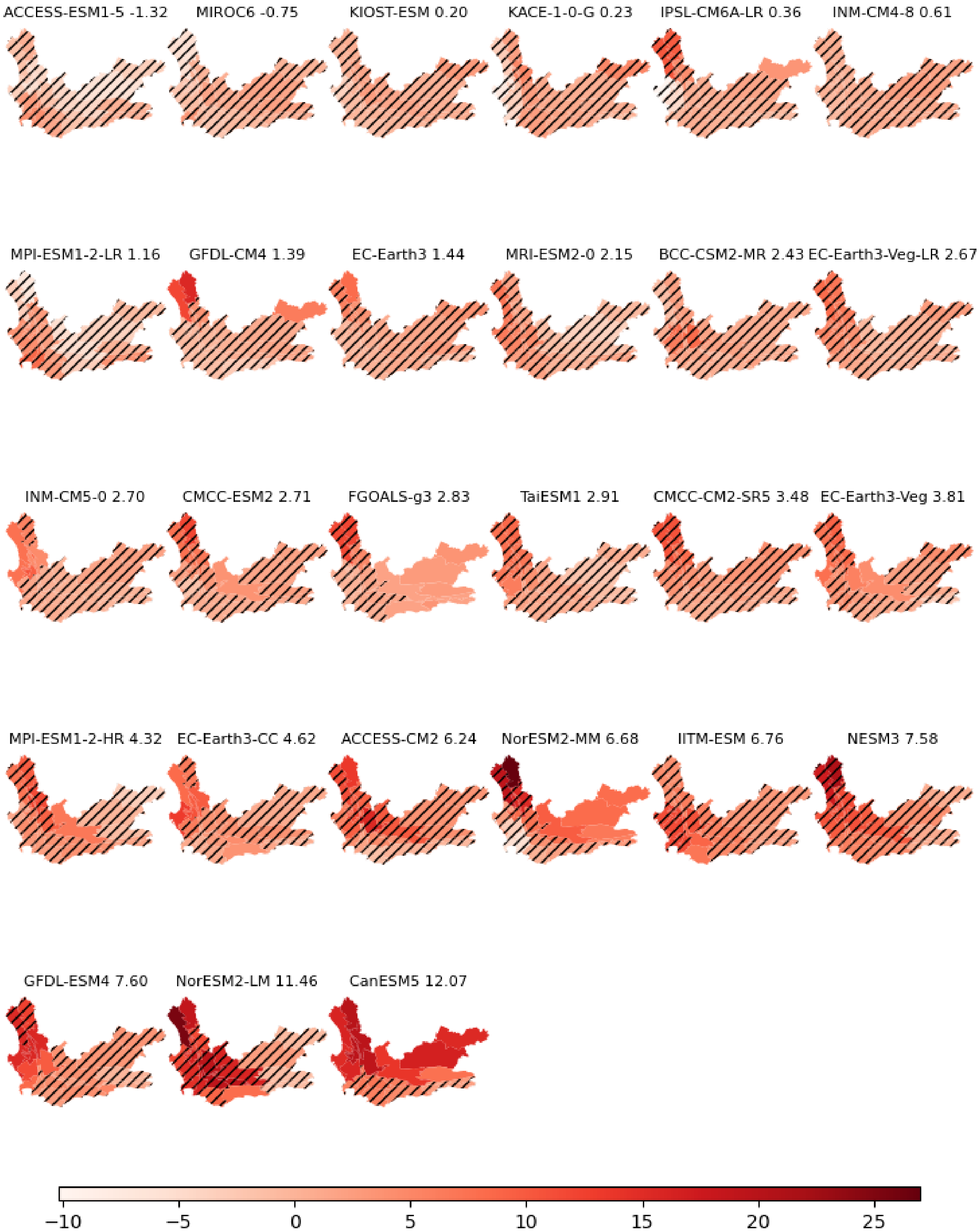

Figure 32: Projected changes in maximum consecutive dry days for the core summer season DJF, across the SmartAgri zones derived from the CMIP6 model ensemble SSP2 4.5 pathway experiment for the period 2030-2060. Figure titles are the name of the model and the area average change in days. Diagonal hashing indicates trends that are not statistically significant with a p-value threshold of 0.05.

Changes in autumn (MAM) rainfall
The projected changes in autumn rainfall (Figure 33) range from very strong drying across all zones, but with a stronger decrease in the southern coastal zones, through to insignificant increases in rainfall.

Projected changes in extreme 1 day rainfall are largely insignificant across the zones, with some models showing significant positive or negative changes in particular zones (Figure 34). It is difficult to unpack these changes in more detail given the datasets available, but it can likely be concluded that this model ensemble is not projecting systematic significant changes in extreme daily rainfall events.

Similarly projected changes in consecutive dry days, an index of importance to many agricultural activities, do not show much consistent significant changes, though a few models project increases in consecutive dry days in several zones, but without much spatial consistency (Figure 35).

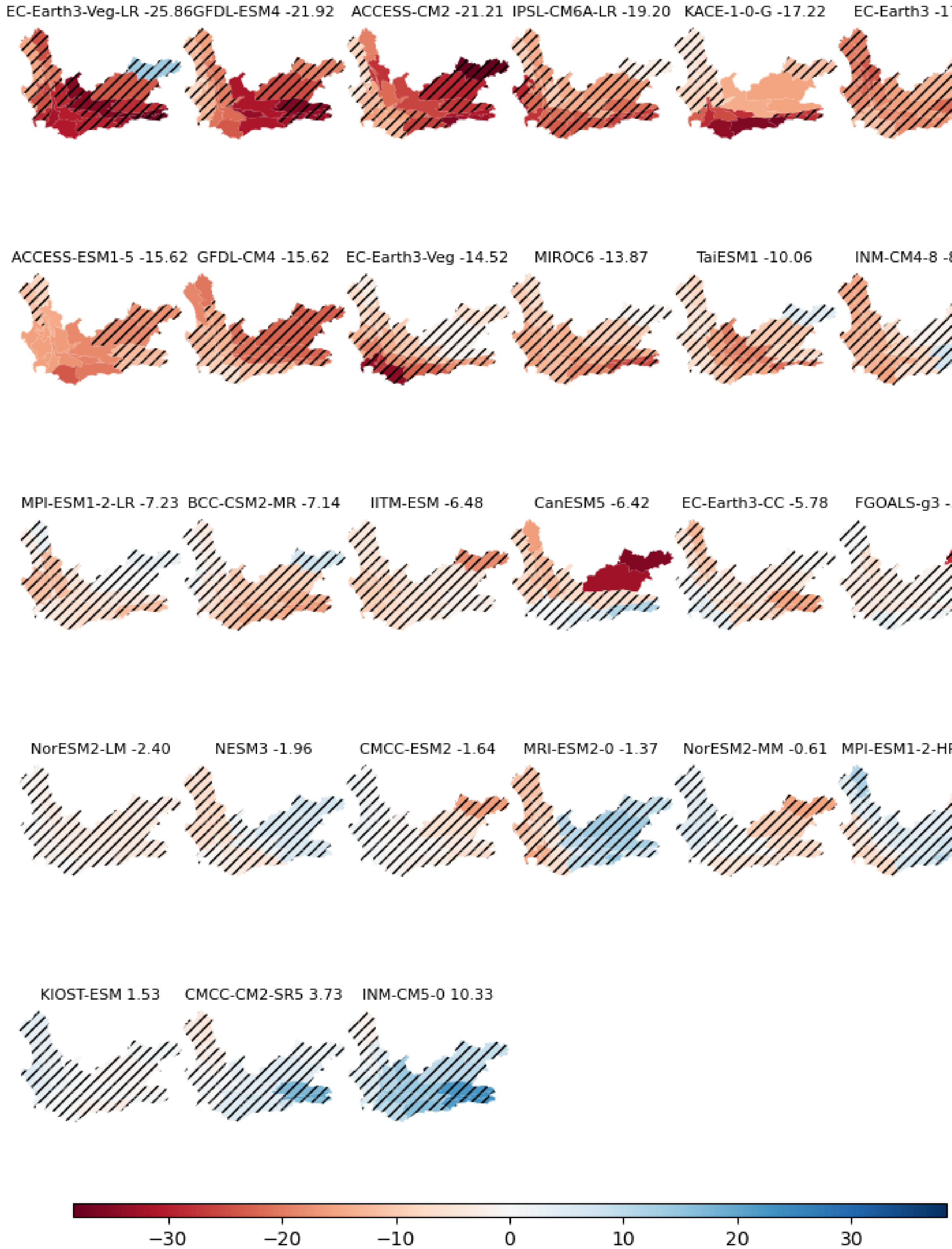

Figure 33: Projected changes in seasonal autumn (MAM) total rainfall (mm) across the SmartAgri zones derived from the CMIP6 model ensemble SSP2 4.5 pathway experiment for the period 2030-2060. Figure titles are the name of the model and the area average change in rainfall (mm). Diagonal hashing indicates trends that are not statistically significant with a p-value threshold of 0.05.

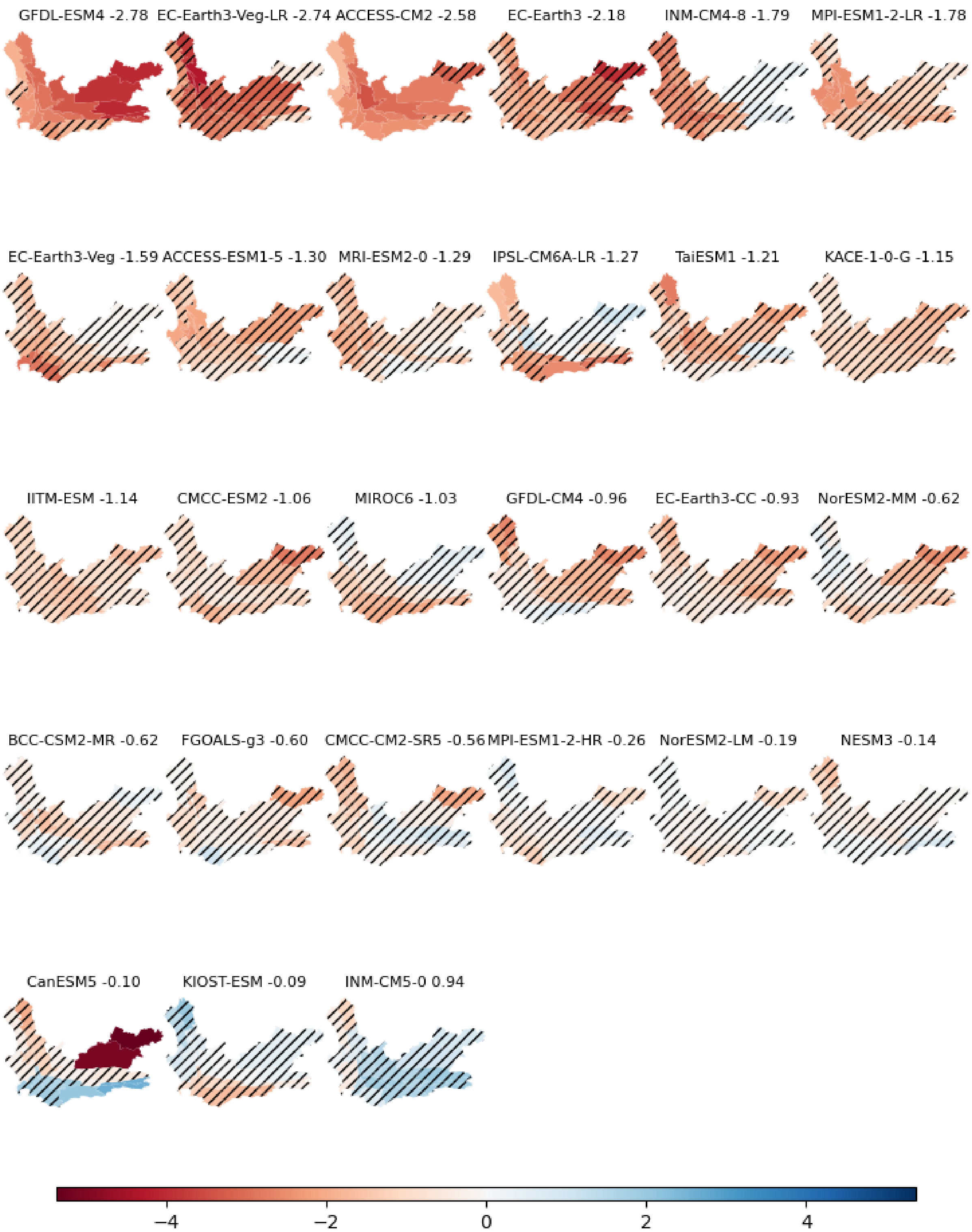

Figure 34: Projected changes in maximum 1 day daily rainfall (mm) for the MAM season across the SmartAgri zones derived from the CMIP6 model ensemble SSP2 4.5 pathway experiment for the period 2030-2060. Figure titles are the name of the model and the area average change in rainfall (mm). Diagonal hashing indicates trends that are not statistically significant with a p-value threshold of 0.05.

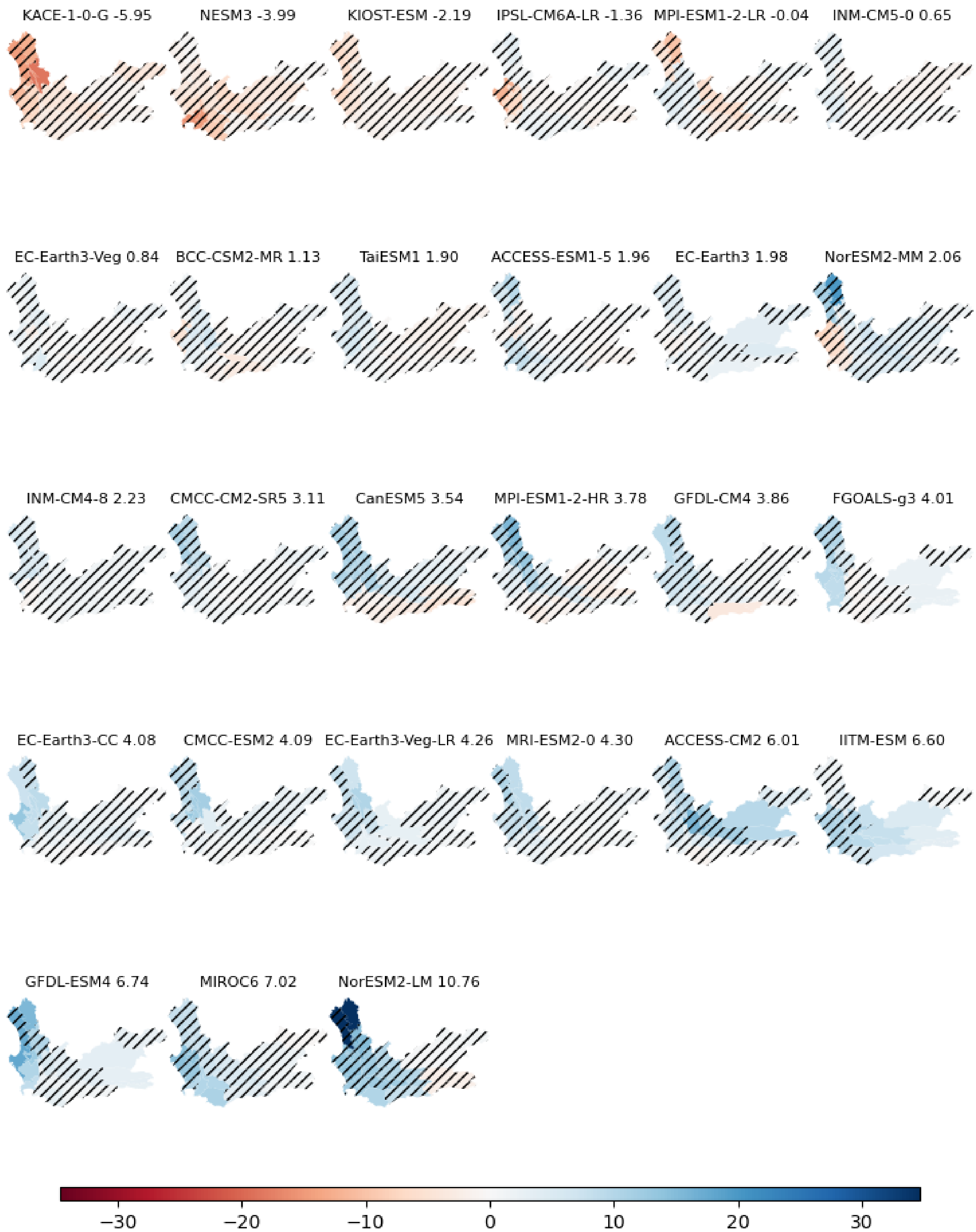

Figure 35: Projected changes in maximum consecutive dry days for the MAM season, across the SmartAgri zones derived from the CMIP6 model ensemble SSP2 4.5 pathway experiment for the period 2030-2060. Figure titles are the name of the model and the area average change in days. Diagonal hashing indicates trends that are not statistically significant with a p-value threshold of 0.05.

Projection archetypes

In order to simplify the application of the climate projections, four "archetype" models have been identified that broadly represent the range of projected changes in temperature and precipitation. These archetypes have been identified by plotting the joint distribution of projected changes in annual mean temperature and annual total precipitation over the province (Figure 36), as well as taking into account some of the spatial patterns of annual rainfall and temperature projections (Figures 37 and 38). To more clearly identify archetypes with large magnitude differences, the CMIP6 SSP5 8.5 emissions pathway was used, whereas the plots in the main part of the document are based on the more likely CMIP6 SSP2 4.5 emissions pathway.

The resultant four archetype models are:

Archetype model name	Provincial scale projection
MPI-ESM1-2-LR	Almost no rainfall change, low magnitude temperature increase (~1.2°C)
TaiESM1	High temperature increases (~2.4°C), large rainfall reduction
GFDL-CM4	Moderate temperature increases (~1.7°C), large rainfall reduction
EC-Earth3	Moderate temperature increases (~1.7°C), mixed spatial pattern of rainfall change (increases in Nelspoort region, decreases elsewhere). [Note, this pattern occurs in multiple models, hence identifying it as plausible archetype]

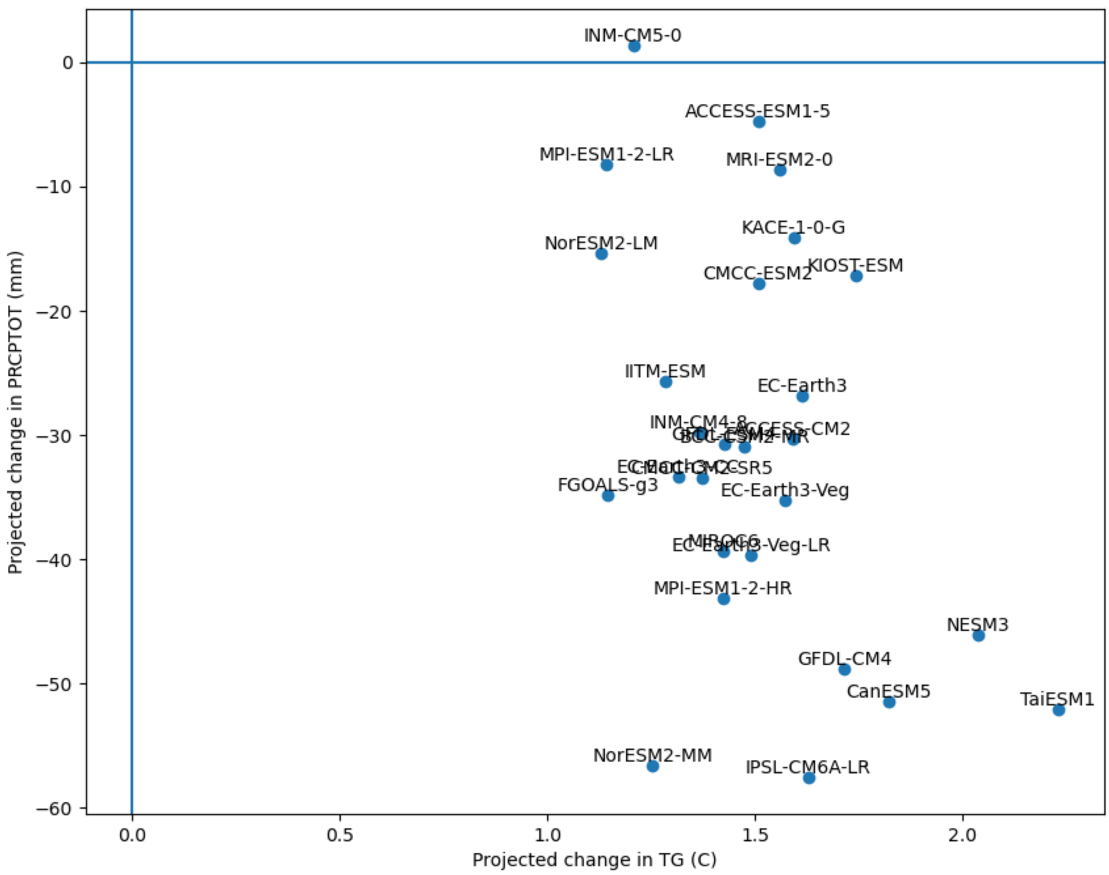

Figure 36: Joint distribution of projected changes in annual mean temperature (TG, °C) and rainfall (PRCPTOT, mm) across the Western Cape province for the period 2030-2060 based on the CMIP6 SSP5 8.5 emission pathway.

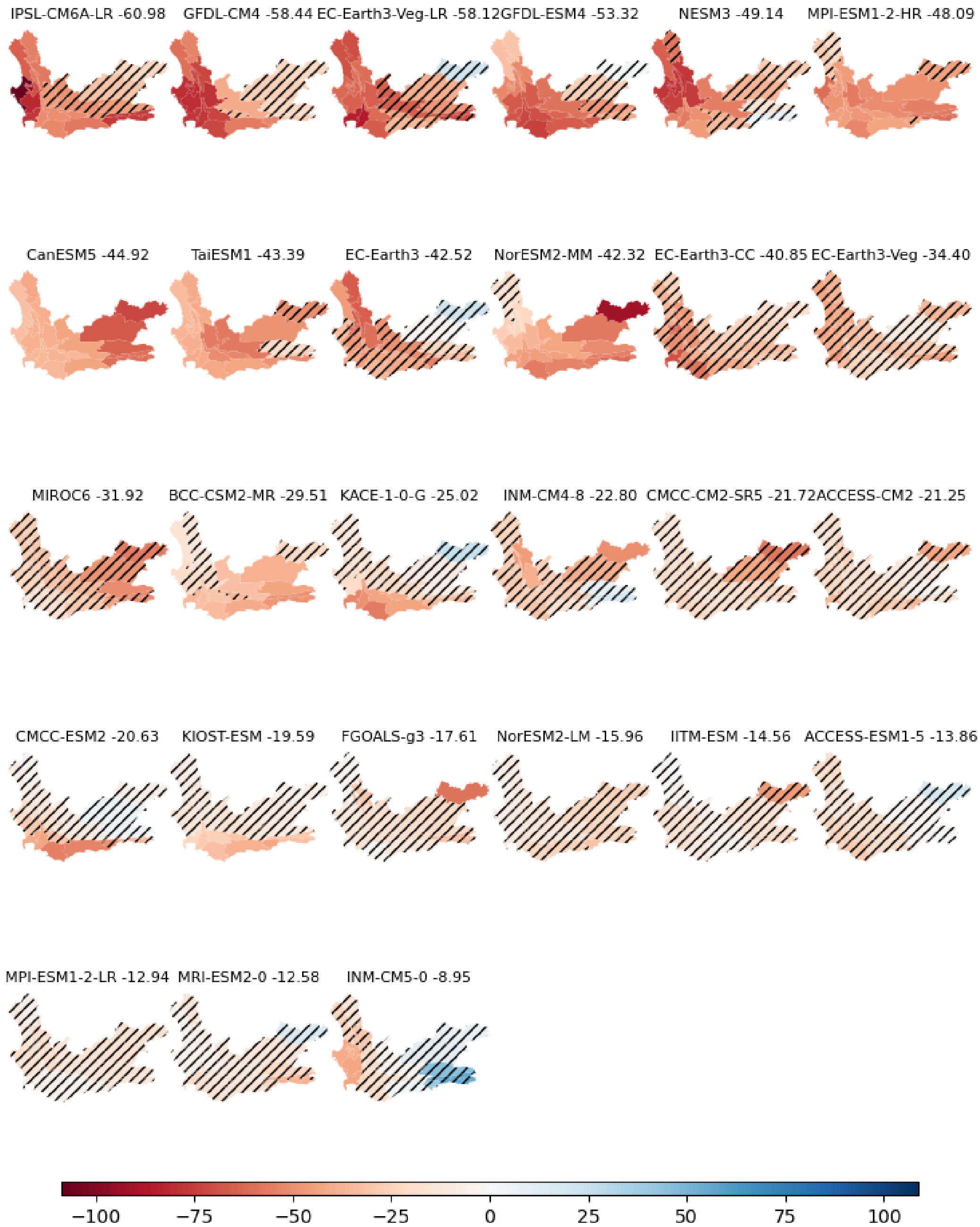

Figure 37: Projected changes in annual total rainfall (mm) across the SmartAgri zones derived from the CMIP6 model ensemble SSP5 8.5 pathway experiment for the period 2030-2060. Figure titles are the name of the model and the area average change in rainfall (mm). Diagonal hashing indicates trends that are not statistically significant with a p-value threshold of 0.05.

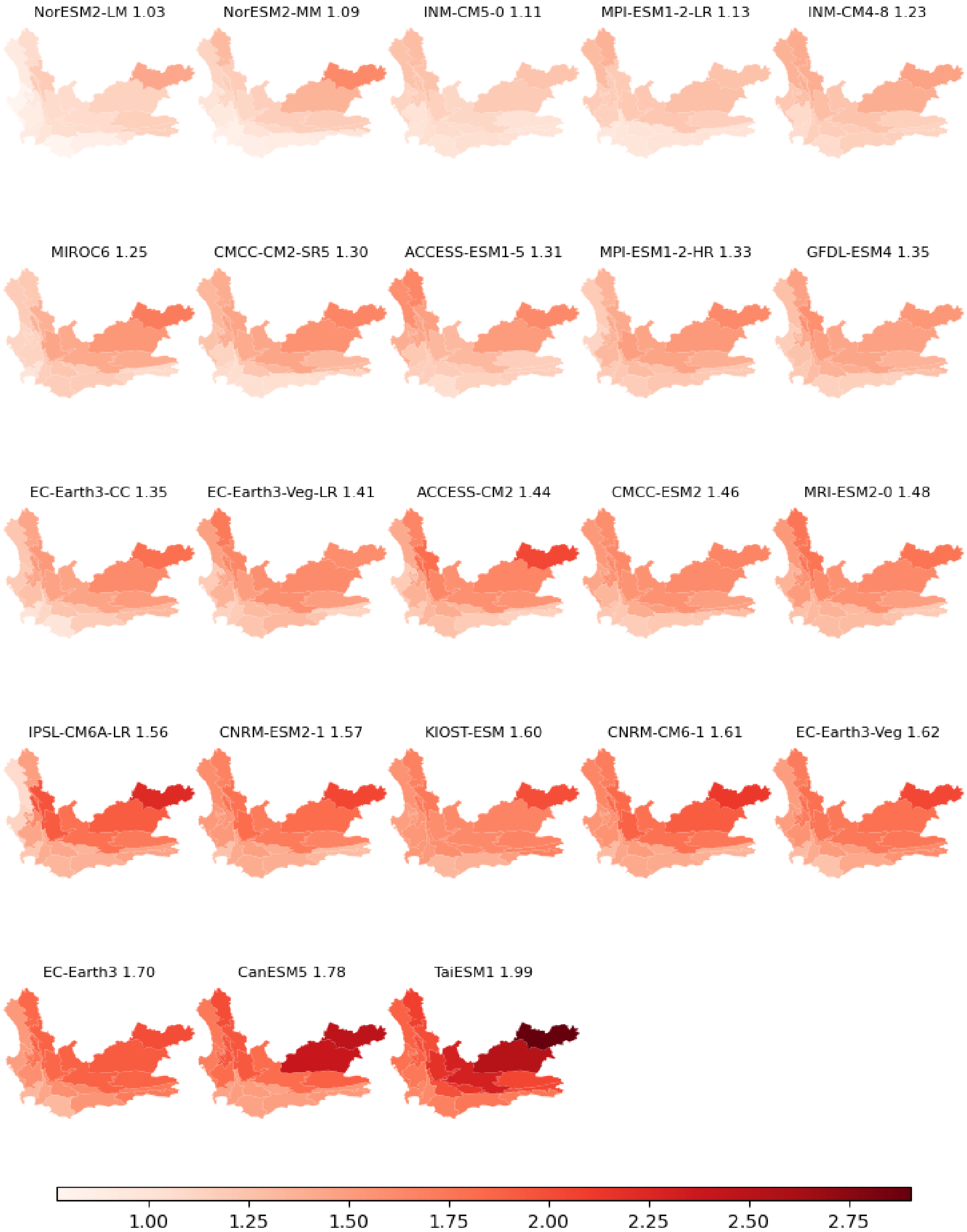

Figure 38: Projected changes in annual mean temperature (°C) across the SmartAgri zones derived from the CMIP6 model ensemble SSP5 8.5 pathway experiment for the period 2030-2060. Figure titles are the name of the model and the area average change in rainfall (°C). Diagonal hashing indicates trends that are not statistically significant with a p-value threshold of 0.05.

The archetype projected changes in annual rainfall and annual mean temperatures are presented in Figures 39 and 40, respectively, for SSP5 8.5 for the future period 2030-2060. Other variables and SSPs are available in the digital appendix (see Appendix A).

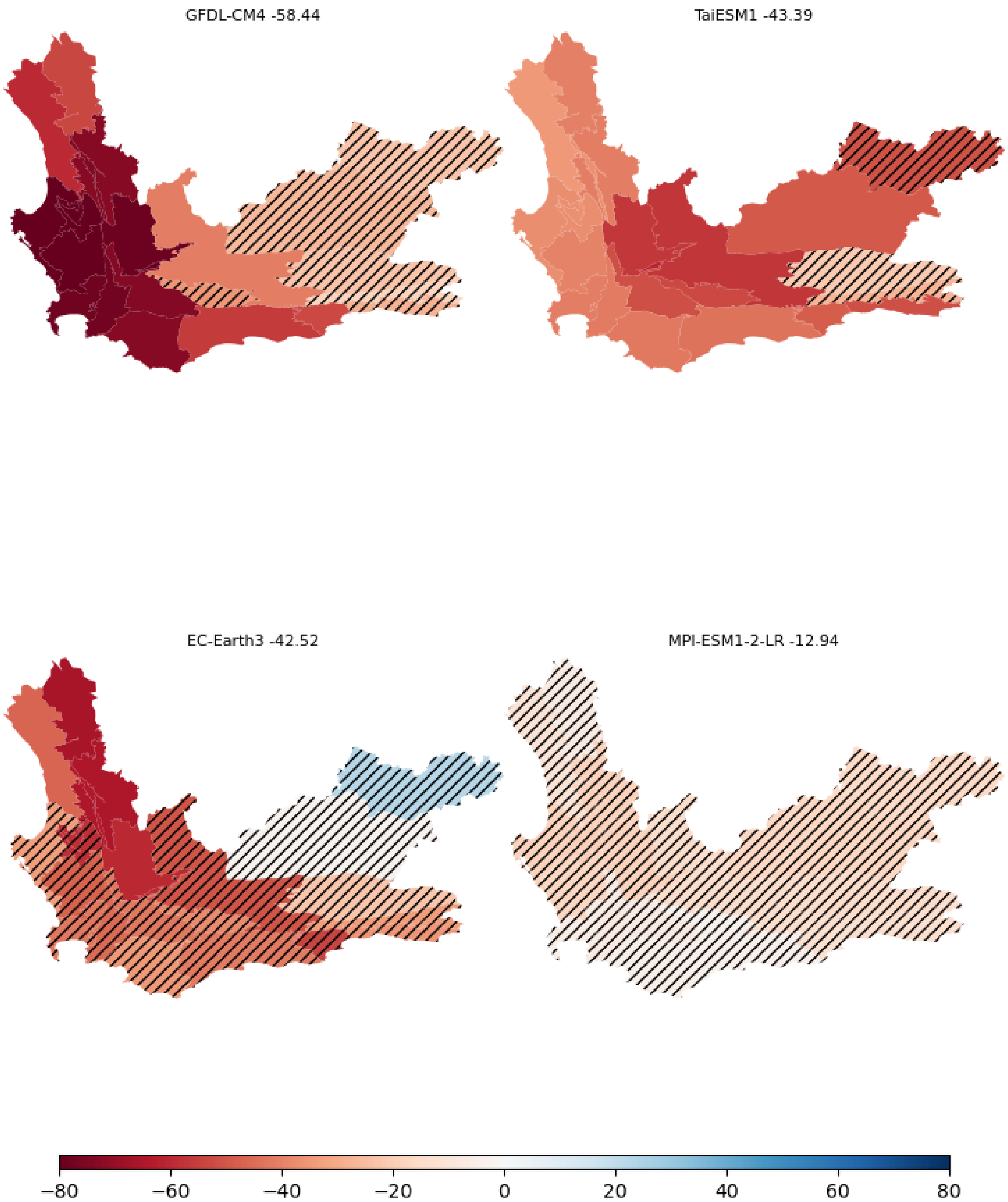

Figure 39: Projected changes in annual total rainfall (mm) across the SmartAgri zones derived from the CMIP6 model ensemble SSP5 8.5 pathway experiment for the period 2030-2060 for the 4 archetype models. Figure titles are the name of the model and the area average change in rainfall (mm). Diagonal hashing indicates trends that are not statistically significant with a p-value threshold of 0.05.

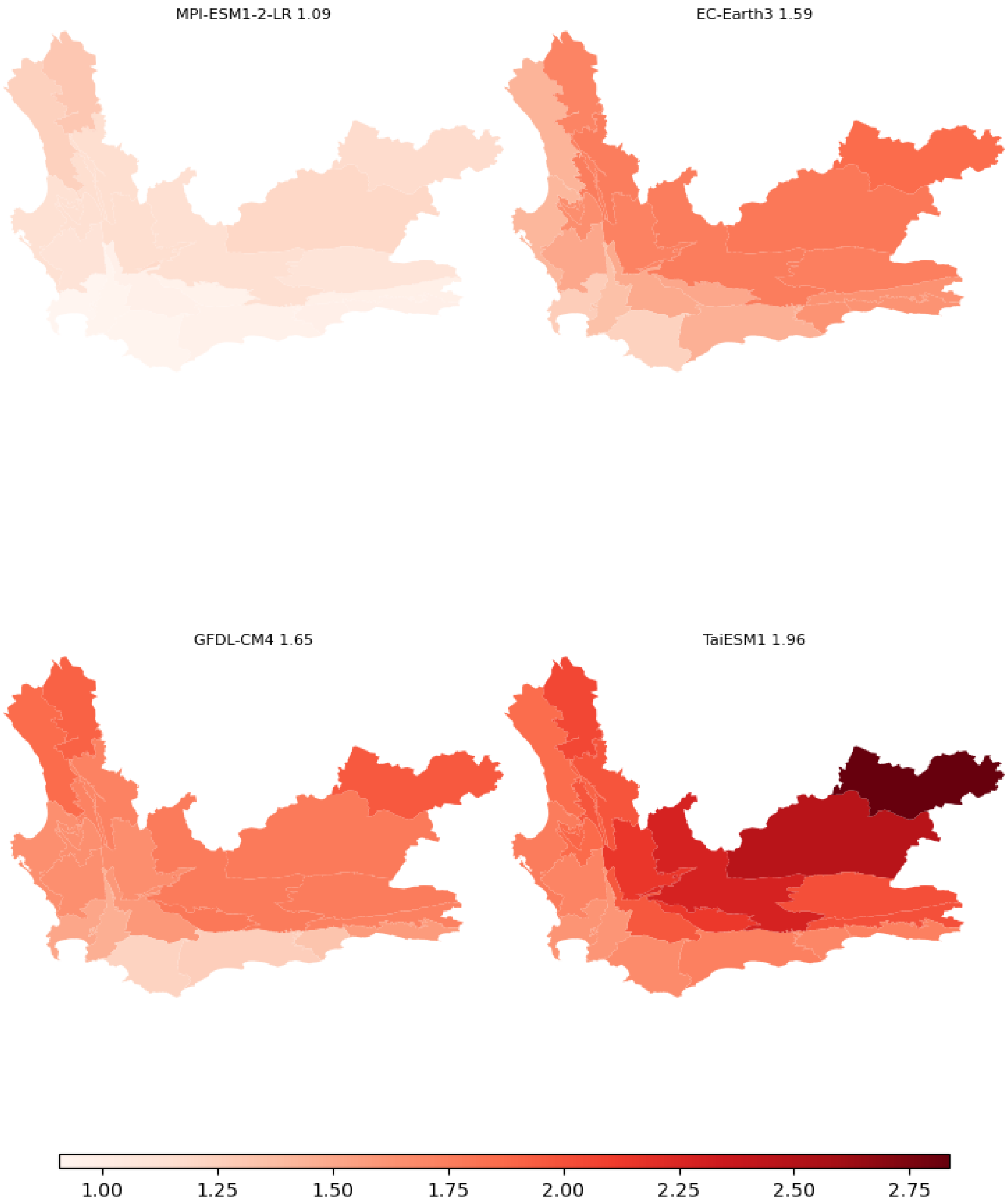

Figure 40: Projected changes in annual mean temperature (°C) across the SmartAgri zones derived from the CMIP6 model ensemble SSP5 8.5 pathway experiment for the period 2030-2060 for the 4 archetype models. Figure titles are the name of the model and the area average change in temperature (°C). Diagonal hashing indicates trends that are not statistically significant with a p-value threshold of 0.05.

The archetypes identified are useful in providing a smaller sample of the full ensemble that roughly represent the same range of plausible projected changes. However, it must be noted that archetypes are a compromise and by no means should be assumed to be representative of the full range of plausible futures across all seasons, SmartAgri zones or indices. They are intended to be used as illustrative projected changes and/or to guide further analysis of impacts.

Evaporation indices

As the evaporation is very important for agriculture, an analysis of projected changes in evaporation has been attempted using Potential Evapotranspiration (PET). Whereas the PET presented in the observed climatology and trends section was derived using the Penman-Monteith approach, which includes direct changes in radiation and humidity (vapour pressure), projected changes in humidity, in particular, are very unreliable due to the simplicity of the representation of the land surface in climate models and the fact that, in areas of complex topography, it is not advisable to use changes in near surface humidity for estimating changes in evaporation.

Rather, a simpler approach to estimating PET was deployed. This approach is based on the Hargreaves-Samani formula (Hargreaves and Samani, 1982) and accounts for changes in both temperature and humidity by taking into consideration the max-min temperature differential (which is affected by air humidity). The adopted formula also includes the proxy estimate of change in radiation based on changes in rainfall (Droogers and Allen, 2002), under the assumption that rainfall is associated with cloudiness.

Figure 41 presents the projected changes in core summer (DJF) and core winter (JJA) mean annual PET based on this approach and the CMIP6 ensemble projections for the SSP2 4.5 scenario and the 2030-2060 future period. These are presented as plume plots across the clustered zones so that the PET estimation can be readily compared across multiple ensembles. Observed PET from CRU (as presented in the observations section above) is also included. The results show that there is strong agreement across all ensembles and generally there is agreement with the observed PET. The model ensembles appear to under-estimate recent observed changes in PET, particularly for the south-eastern coastal clustered zone (Mossel Bay to Outeniqua). As the observed PET uses the more complex Penman-Monteith approach, it may be that local changes in humidity are driving these differences. As this zone is strongly influenced by onshore moisture advection, this seems a reasonable conclusion.

The strong agreement between observed PET calculations and the multiple model ensembles suggests that, given the underlying assumptions, the calculations are robust. These results also clearly indicate that potential evapotranspiration is almost certainly going to continue to increase across all regions.

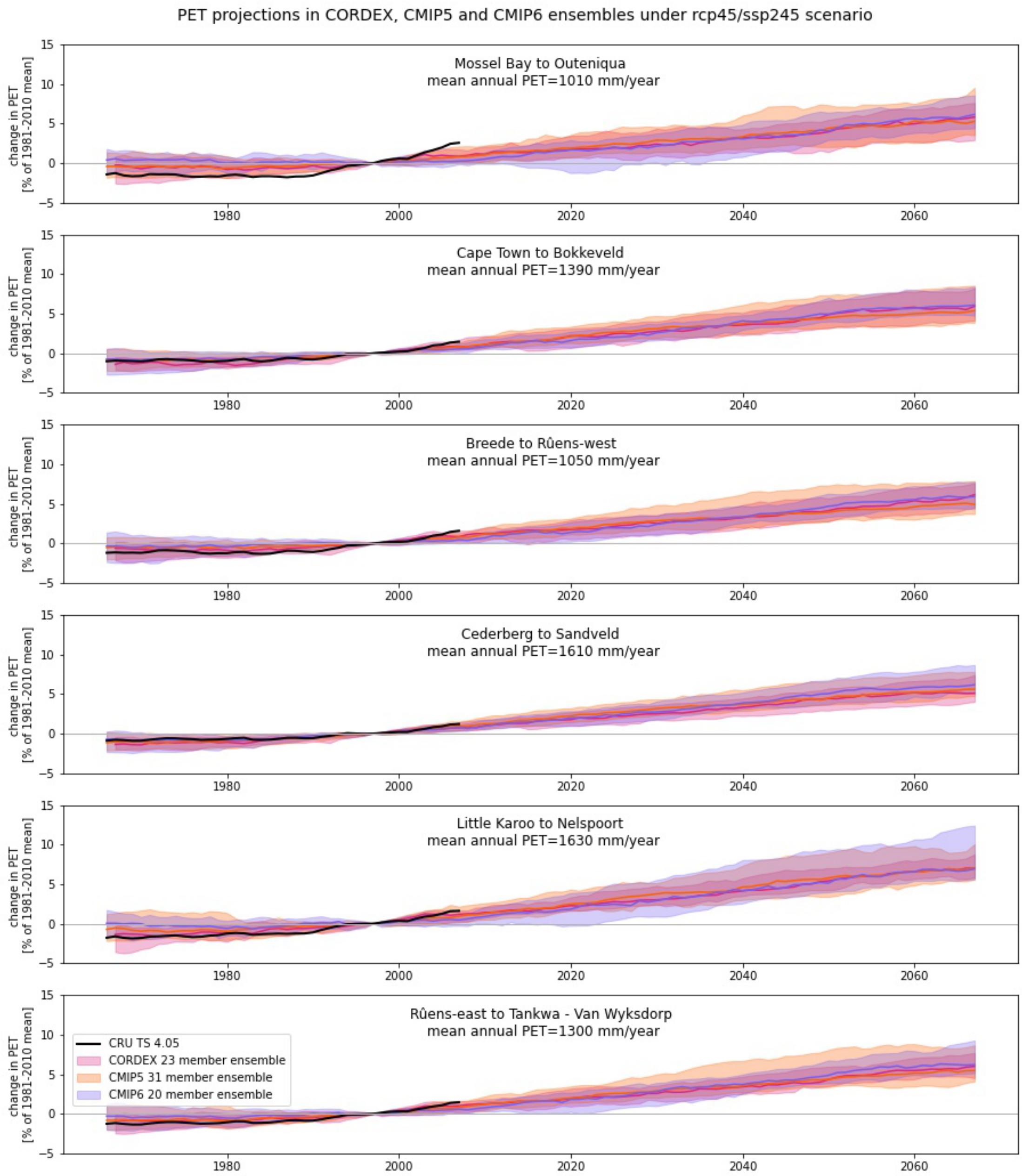

Figure 41: Plume plots of changes in mean annual Potential Evapotranspiration (PET) derived from CMIP5, CMIP6 and CORDEX model ensembles, and observed PET from the CRU TS4.05 dataset.

Projected changes in drought indices

Drought is a complex phenomenon and is often understood using different framings. Meteorological drought is focused on deficits in rainfall. Hydrological drought is focused on deficits in soil moisture and runoff. Socio-economic drought refers to the more complex aspects of drought as they impact the broadly-understood socio-economic system. Here, two very widely used drought indices are deployed. The first is the Standardised Precipitation Index (SPI, McKee et al., 1993) which is a drought index based only on rainfall deficit. The value of SPI is that rainfall deficits (or excess) are standardised relative to the baseline distribution and this allows us to compare across regions with varying baseline rainfall distributions. SPI is calculated over different accumulation periods typically ranging from one month through to as long as 36 months. These accumulation periods help unpack the time scales of droughts. Here, a 12-month accumulation period is applied, ending at the end of the year (December) to capture annual time scale rainfall deficits dominated by winter rainfall.

The second index uses a further development of SPI, called the Standardised Precipitation Evaporation Index (SPEI, Vicente-Serrano et al., 2010). This index calculates a moisture budget (precipitation minus potential evapotranspiration) and so comes closer to identifying hydrological drought.

To translate SPI and SPEI into values that are more meaningful than the original statistical z-scores, counts of the number of years in sets of ten years (decades) were calculated, where SPI or SPEI is lower than -1.0. An SPI or SPEI of less than -1.0 is only a moderate drought condition and would normally be expected to occur around two to three times per decade.

Figures 42 and 43 present an alternative set of plots that integrate CORDEX, CMIP5 and CMIP6 based projected changes in both SPI and SPEI. These plots are divided into 10-year segments extending from the past into the future. Each segment has three subplots that are violin plots representing the distribution of values from each ensemble (with “bulging” sections indicating a larger number of ensemble members projecting the given value).

What can clearly be seen is that the different model ensembles agree very well on the changes in both SPI and SPEI. From this it can be concluded that these projected changes are relatively robust. The projected changes in SPI are much weaker than the changes in SPEI, which is to be expected as changes in SPI do not include the effect of increasing temperatures.

The very clear message emerging from this analysis is that mild drought conditions under current or recent conditions are likely to be far more common in the future across all clustered zones, if the effects of increasing temperature on evaporation are included. The increase in such conditions in the south-eastern coastal zone (Mossel Bay to Outeniqua) is somewhat weaker than elsewhere. This increase in the frequency of droughts is, however, not limited to mild droughts only and extends to droughts of higher severity as manifested by frequency of drought years with SPEI12 < -2 (not shown).

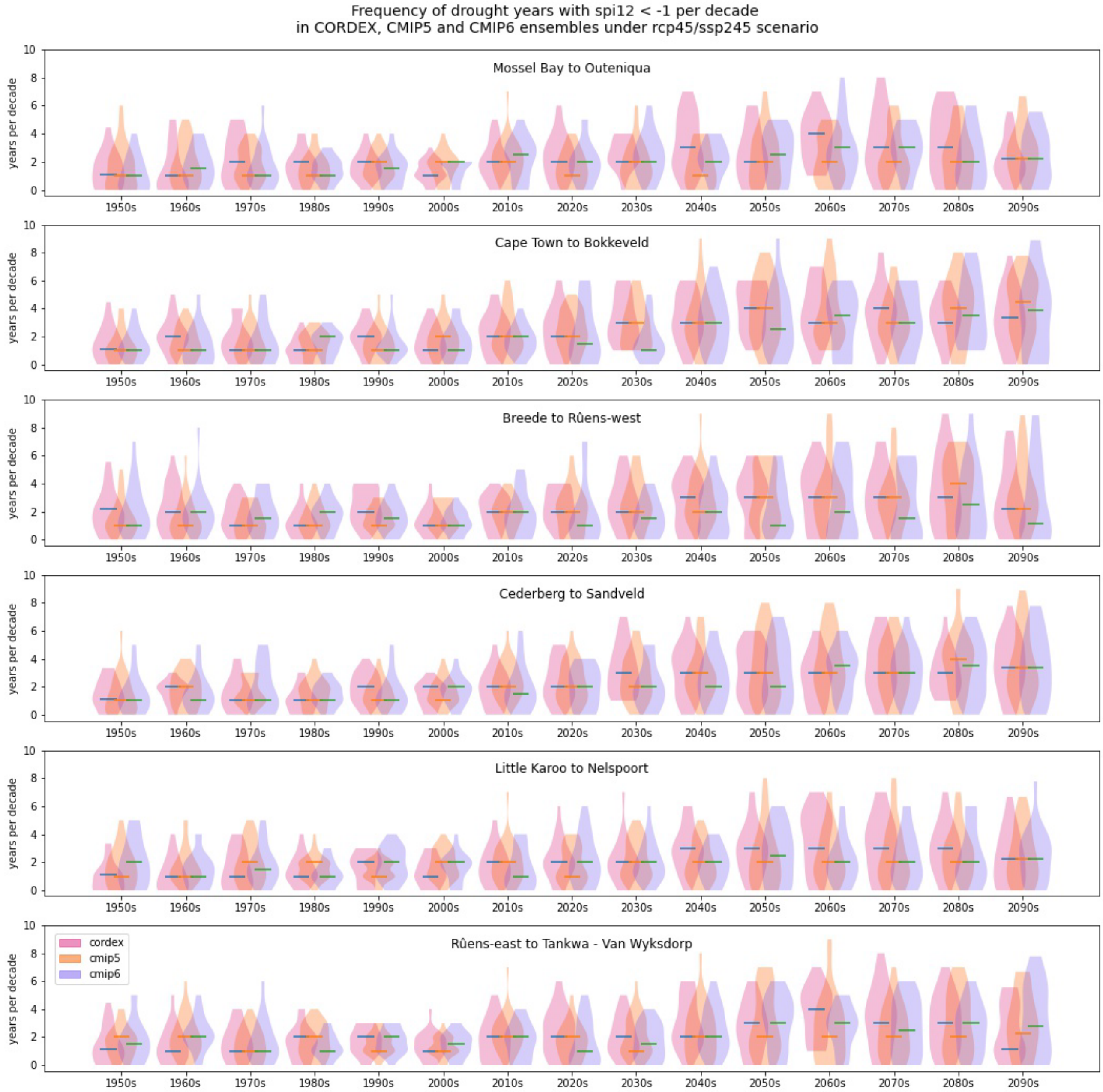

Figure 42: Plots of changes in years/decade with SPI < -1.0 across the six clustered SmartAgri zones. Each violin plot represents the ensemble distribution of projected changes for a particular ensemble (see the legend) for that particular 10-year period. Horizontal bar marks the median of the ensemble. Note that "violins" may appear truncated but reflect all data – the presented index (number of drought years per decade) takes only values between 0 and 10.

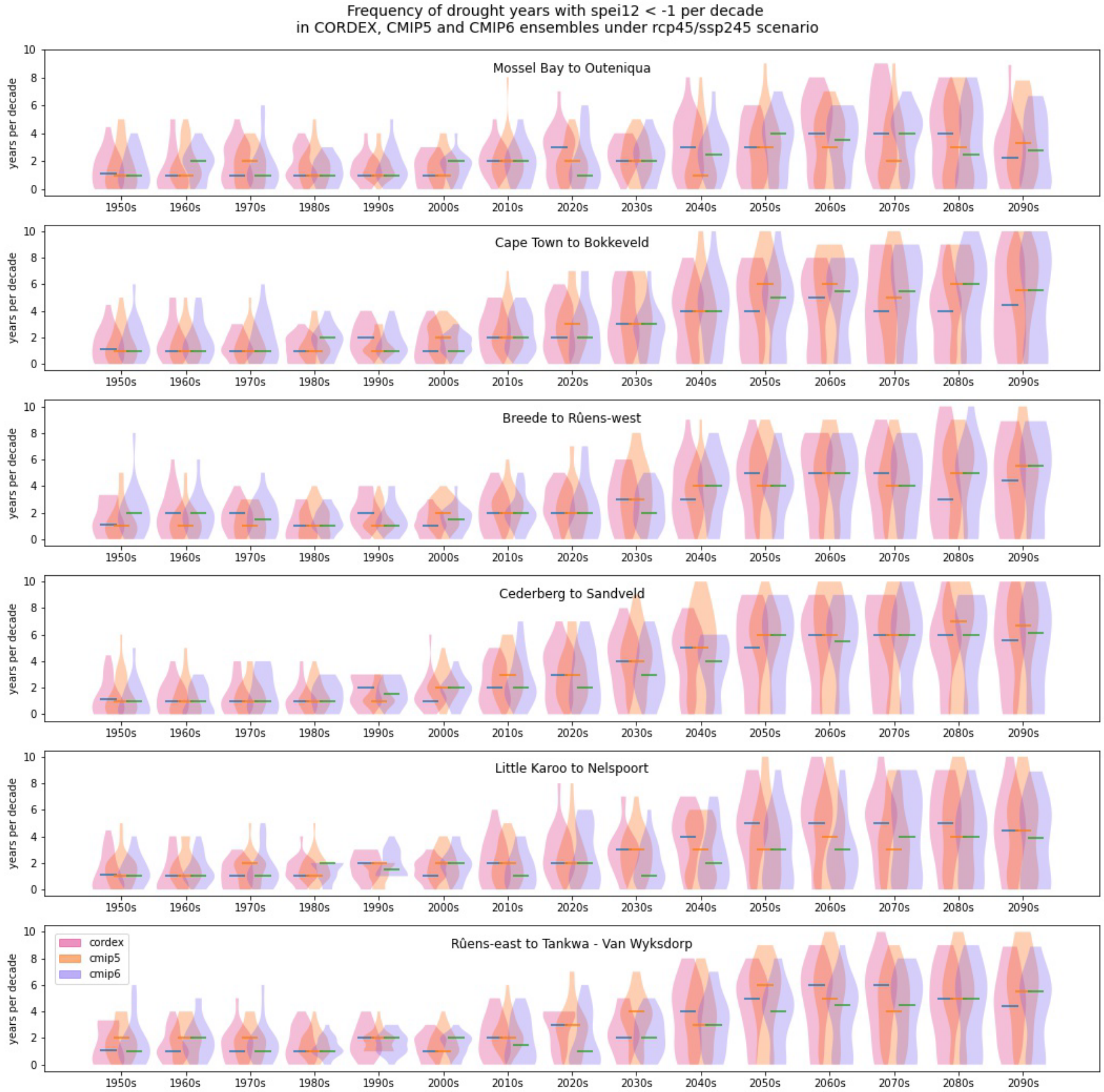

Figure 43: Plots of changes in years/decade with SPEI < -1.0 across the 6 clustered SmartAgri zones. Each violin plot represents the ensemble distribution of projected changes for a particular ensemble (see the legend) for that particular 10-year period. Horizontal bar marks the median of the ensemble. Note that "violins" may appear truncated but reflect all data – the presented index (number of drought years per decade) takes only values between 0 and 10.

Summary of climate change projections

An analysis of projected changes in climate, with respect to a number of agriculturally relevant climate indices, across the SmartAgri zones, is presented in this report. Selected results are included based on projections forced by the SSP2 4.5 shared socio-economic pathway, which represents a “middle of the road” global response to climate change (some level of mitigation). This pathway is insufficient to avoid 1.5°C global warming and shows some significant probability of exceeding 2°C global warming. While of course there is significant uncertainty associated with the global economic and political response, the SSP2 4.5 is a reasonable scenario to explore.

To summarise the key findings of the above analysis:

Temperature indices

- Temperatures are projected to increase significantly over the next 30 to 40 years and beyond, across all SmartAgri zones. Projected increases in mean temperature averaged over the whole province are of the order of 1°C to 1.8°C by 2060 compared to the recent past (1981-2010).
- Mean annual average daily temperature projections for some SmartAgri zones, most notably those further from the coast, are even higher, with some models projecting increases as high as 2°C (see Figure 25).
- Projected changes in mean daily minimum temperatures (night time temperature) are also strongly positive and in some inland zones (e.g. Nelspoort) they are even higher than the increases in maximum temperatures, reaching as high as 2.7°C (see Figure 26).
- Increases in temperature also result in an increase in the number of hot days. The projected increase in the number of days exceeding 30°C ranges from as few as five more days/year through to as many as 30 more days/year for inland zones (e.g. Nelspoort, see Figure 28).

Rainfall indices

- As expected, projected changes in rainfall related indices exhibit higher uncertainty, with some models projecting only minimal reductions in rainfall across the province and others projecting as much as a 20% reduction in annual rainfall averaged over the province (see Figure 24).
- Most SmartAgri zones show projections of decreasing rainfall in summer (DJF), though in many cases these changes are small enough that they pass the statistical significance test. This does not mean that drying is not likely, but rather that natural variability (variations from year to year) is high, and so there remains some probability that the projected changes are the result of natural variability rather than climate change.
- However, rainfall changes in some SmartAgri zones and some seasons are statistically significant and could be as large as a 40% reduction (e.g. Nelspoort in summer, see Figure 29).
- The Nelspoort and adjacent Koup zones exhibit the highest uncertainty in projected rainfall changes across all seasons, most likely as a result of their location between the mid-latitude winter rainfall dynamics and the subtropical summer rainfall dynamics. Rainfall in these zones will be very sensitive to how a model represents the transition between these two zones. Some models project increases in summer rainfall in these zones, while other project very strong decreases (see Figure 30). In winter these zones show fairly consistent drying projections, again with statistically significant strong drying projected by some models.

- Projected changes in the number of rainy days (more than 1 mm rainfall) also involves fairly high uncertainty across both summer (DJF) and autumn (MAM). However, the reduction in wet days does not appear to be as pronounced as the reduction in rainfall, with most zones showing statistically insignificant changes. These suggest that rainfall reductions are mostly associated with less rainfall per event rather than fewer events (see Figures 31 and 34).
- Similarly, projected changes in consecutive dry days, while on the whole indicating an increase in dry spell lengths, have weak statistical significant in most cases. However, some increases in dry spell duration are significant and as large as 20 days in summer (see Figure 32). It must be noted that in many cases the baseline maximum dry spell duration in these areas is large.

Evaporation and drought indices

- Projected changes in PET are consistently positive across all zones and across all models in all ensemble datasets, largely driven by consistent increases in temperature. These projections align well with analysed PET based on observations (see Figure 41).
- Projected changes in frequency of drought events as determined by SPI and SPEI threshold exceedance (SPI or SPEI < -1) indicate consistent increases in frequency of drought events towards the end of the century, with more rapid increases for SPEI based drought due to the inclusion of temperature driven evaporation (see Figure 43).
- For many of the clustered zones a 1-in-10 drought event under current conditions is projected to shift towards a 1-in-2 event (five events per decade) by mid-century when the effect of increasing temperature on evaporation is considered.

Concluding remarks

In conclusion, the results presented above, while encapsulating several persistent sources of uncertainty ranging from global socio-economic scenarios, through to modelling uncertainties and natural variability, paint a clear picture of negative impacts of climate change across the province, especially with respect to agriculture. Decreasing rainfall should be expected in most areas and even when rainfall decreases are not projected, or do not manifest, increasing temperatures will almost certainly bring significant water balance challenges to agriculture.

Ongoing monitoring of hydro-climate variables across the province is critical to further refining and understanding emerging trends, as well as improving our ability to simulate the regional climate and reduce some of the significant uncertainties.

7. References

Abba Omar, S., & Abiodun, B.J. 2020. Characteristics of cut-off lows during the 2015-2017 drought in the Western Cape, South Africa. *Atmospheric Research*, 235, 104772. https://doi.org/10.1016/J.ATMOSRES.2019.104772.

Almazroui, M., Saeed, F., Saeed, S., Nazrul Islam, M., Ismail, M., Klutse, N.A.B., et al. 2020. Projected change in temperature and precipitation over Africa from CMIP6. *Earth Systems and Environmental Sciences,* 4, 455–475.

Arblaster, J.M., Meehl, G.A., & Karoly, D.J. 2011. Future climate change in the Southern Hemisphere: Competing effects of ozone and greenhouse gases. *Geophysical Research Letters*, 38(2), L02701. https://doi.org/10.1029/2010GL045384.

Barnes, E.A., Barnes, N.W., & Polvani, L.M. 2014. Delayed Southern Hemisphere climate change induced by stratospheric ozone recovery, as projected by the CMIP5 Models. *Journal of Climate*, 27(2), 852–867.

Botai, C., Botai, J., de Wit, J., Ncongwane, K., & Adeola, A. 2017. Drought characteristics over the Western Cape Province, South Africa. *Water*, 9(11), 876.

Burls, N.J., Blamey, R.C., Cash, B.A., Swenson, E.T., Fahad, A. al, Bopape, M.-J.M., et al. 2019. The Cape Town "Day Zero" drought and Hadley cell expansion. *npj Climate and Atmospheric Science* 2, 27. https://doi:10.1038/s41612-019-0084-6.

Conradie, W.S., Wolski, P., & Hewitson, B.C. 2022. Spatial heterogeneity of 2015-2017 drought intensity in South Africa's winter rainfall zone. *Advances in Statistical Climatology, Meteorology and Oceanography*, 8, 63-81.

Doblas-Reyes, F.J., Sörensson, A.A., Almazroui, M., Dosio, A., Gutowski, W.J., Haarsma, R., Hamdi, R., Hewitson, B., Kwon, W.-T., Lamptey, B.L., Maraun, D., Stephenson, T.S., Takayabu, I., Terray, L., Turner, A., & Zuo, Z. 2021. Linking Global to Regional Climate Change. In Climate Change 2021: The Physical Science Basis. Contribution of Working Group I to the Sixth Assessment Report of the Intergovernmental Panel on Climate Change [Masson-Delmotte, V., P. Zhai, A. Pirani, S.L. Connors, C. Péan, S. Berger, N. Caud, Y. Chen, L. Goldfarb, M.I. Gomis, M. Huang, K. Leitzell, E. Lonnoy, J.B.R. Matthews, T.K. Maycock, T. Waterfield, O. Yelekçi, R. Yu, & B. Zhou (eds.)]. Cambridge University Press, 150pp. https://www.ipcc.ch/report/ar6/wg1/downloads/report/IPCC_AR6_WGI_Chapter10.pdf

Dosio, A., Jones, R.G., Jack, C., Lennard, C., Nikulin, G., & Hewitson, B. 2019. What can we know about future precipitation in Africa? Robustness, significance and added value of projections from a large ensemble of regional climate models. *Climate Dynamics*, *53*(9), 5833-5858.

Droogers, P., & Allen, R.G. 2002. Estimating reference evapotranspiration under inaccurate data conditions. *Irrigation and Drainage Systems*, 16(1), 33-45.

Engelbrecht, C.J., & Landman, W.A. 2016. Interannual variability of seasonal rainfall over the Cape south coast of South Africa and synoptic type association. *Climate Dynamics*, 47, 295–313.

Eyring, V., Bony, S., Meehl, G.A., Senior, C.A., Stevens, B., Stouffer, R.J., & Taylor, K.E. 2016. Overview of the Coupled Model Intercomparison Project Phase 6 (CMIP6) experimental design and organization. *Geoscientific Model Development*, 9(5), 1937-1958.

Favre, A., Hewitson, B., Lennard, C., Cerezo-Mota, R., & Tadross, M. 2013. Cut-off Lows in the South Africa region and their contribution to precipitation. *Climate Dynamics*, 2331–2351.

Funk, C., Peterson, P., Landsfeld, M., Pedreros, D., Verdin, J., Shukla, S., et al. 2015. The climate hazards infrared precipitation with stations—a new environmental record for monitoring extremes. *Scientific Data*, 2, 150066. https://doi.org/10.1038/sdata.2015.66.

Fyfe, J.C., Gillett, N.P., & Marshall, G.J. 2012. Human influence on extratropical Southern Hemisphere summer precipitation. *Geophysical Research Letters*, 39(23), L23711. https://doi.org/10.1029/2012GL054199.

Giorgi, F., Jones, C., & Asrar, G.R. 2009. Addressing climate information needs at the regional level: the CORDEX framework. *World Meteorological Organization (WMO) Bulletin*, 58(3), 175.

Hargreaves, G.H., & Samani, Z.A. 1982. Estimating potential evapotranspiration. *Journal of the irrigation and Drainage Division*, 108(3), 225-230.

Harris, I., Osborn, T.J., Jones, P., & Lister, D. 2020. Version 4 of the CRU TS monthly high-resolution gridded multivariate climate dataset. *Scientific Data*, 7, 109. https://doi.org/10.1038/s41597-020-0453-3.

Hart, N.C.G., Reason, C.J.C., & Fauchereau, N. 2013. Cloud bands over southern Africa: seasonality, contribution to rainfall variability and modulation by the MJO. *Climate Dynamics,* 41, 1199–1212.

Hersbach, H., Bell, B., Berrisford, P., Hirahara, S., Horányi, A., Muñoz-Sabater, J., et al. 2020. The ERA5 global reanalysis. *Quarterly Journal of the Royal Meteorological Society*, 146(730), 1999-2049.

IPCC 2018. Global Warming of 1.5°C. An IPCC Special Report on the impacts of global warming of 1.5°C above pre-industrial levels and related global greenhouse gas emission pathways, in the context of strengthening the global response to the threat of climate change, sustainable development and efforts to eradicate poverty [Masson-Delmotte, V., P. Zhai, H.-O. Pörtner, D. Roberts, J. Skea, P.R. Shukla, A. Pirani, W. Moufouma-Okia, C. Péan, R. Pidcock, S. Connors, J.B.R. Matthews, Y. Chen, X. Zhou, M.I. Gomis, E. Lonnoy, T. Maycock, M. Tignor, and T. Waterfield (eds.)]. Cambridge University Press, 630 pp.

Jury, M.R., & Levey, K. 1993. The climatology and characteristics of drought in the eastern Cape of South Africa. *International Journal of Climatology*, 13(6), 629–641.

Kam, J., Min, S.-K., Wolski, P., & Kug, J.-S. 2021. CMIP6 Model-Based Assessment of Anthropogenic Influence on the Long Sustained Western Cape Drought over 2015–19. *Bulletin of the American Meteorological Society*, 102(1), S45–S50. https://doi.org/10.1175/BAMS-D-20-0159.1.

Kendon, E.J., Stratton, R.A., Tucker, S., Marsham, J.H., Berthou, S., Rowell, D.P., & Senior, C.A. 2019. Enhanced future changes in wet and dry extremes over Africa at convection-permitting scale. *Nature Communications*, 10(1), 1-14.

Kruger, A.C., & Nxumalo, M. 2017. Surface temperature trends from homogenized time series in South Africa: 1931--2015. *International Journal of Climatology,* 37, 2364–2377.

Landman, W.A., & Beraki, A. 2012. Multi-model forecast skill for mid-summer rainfall over southern Africa. *International Journal of Climatology*, 32(2), 303–314.

L'Heureux, M.L., & Thompson, D.W.J. 2006. Observed relationships between the El-Niño-Southern oscillation and the extratropical zonal-mean circulation. *Journal of Climate*, 19(1), 276–287.

Lim, E.-P., Hendon, H.H., Arblaster, J.M., Delage, F., Nguyen, H., Min, S.-K., et al. 2016. The impact of the Southern Annular Mode on future changes in Southern Hemisphere rainfall. *Geophysical Research Letters,* 43, 7160–7167.

MacKellar, N.C., New, M.G., & Jack, C. 2014. Climate trends in South Africa Observed and modelled trends in rainfall and temperature for South Africa: 1960 – 2010. *South African Journal of Science*, 110(7), 1–13.

Mahlalela, P.T., Blamey, R.C., & Reason, C.J.C. 2019. Mechanisms behind early winter rainfall variability in the southwestern Cape, South Africa. *Climate Dynamics,* 53, 21–39.

Maúre, G., Pinto, I., Ndebele-Murisa, M., Muthige, M., Lennard, C., Nikulin, G., et al. 2018. The southern African climate under 1.5 °C and 2 °C of global warming as simulated by CORDEX regional climate models. *Environmental Research Letters*, 13, 065002. https://doi:10.1088/1748-9326/aab190.

Mbokodo, I., Bopape, M.-J., Chikoore, H., Engelbrecht, F., & Nethengwe, N. 2020. Heatwaves in the future warmer climate of South Africa. *Atmosphere (Basel),* 11, 712.

McKee, T.B., Doesken, J.J., & Kleist, J. 1993. Analysis of Standardized Precipitation Index (SPI) data for drought assessment. *Water*, 26, 1-72.

Muñoz-Sabater, J., Dutra, E., Agustí-Panareda, A., Albergel, C., Arduini, G., Balsamo, G., Boussetta, S., Choulga, M., Harrigan, S., Hersbach, H., Martens, B., Miralles, D.G., Piles, M., Rodríguez-Fernández, N.J., Zsoter, E., Buontempo, C., & Thépaut, J.-N. 2021. ERA5-Land: A state-of-the-art global reanalysis dataset for land applications, *Earth System Science Data,* 13, 4349–4383.

Naik, M., & Abiodun, B.J. 2020. Projected changes in drought characteristics over the Western Cape, South Africa. *Meteorological Applications,* 27, 1–14.

Odoulami, R.C., Wolski, P., & New, M. 2021. A SOM-based analysis of the drivers of the 2015–2017 Western Cape drought in South Africa. *International Journal of Climatology*, 41(S1), E1518–E1530. https://doi.org/10.1002/joc.6785.

O'Neill, B.C., Kriegler, E., Riahi, K., Ebi, K.L., Hallegatte, S., Carter, T.R., et al. 2014. A new scenario framework for climate change research: the concept of shared socioeconomic pathways. *Climatic Change*, *122*(3), 387-400.

Otto, F.E.L., Wolski, P., Lehner, F., Tebaldi, C., van Oldenborgh, G.J., Hogesteeger, S., et al. 2018. Anthropogenic influence on the drivers of the Western Cape drought 2015–2017. *Environmental Research Letters*, 13(12), 124010. https://doi.org/10.1088/1748-9326/aae9f9.

Philippon, N., Rouault, M., Richard, Y., & Favre, A. 2012. The influence of ENSO on winter rainfall in South Africa. *International Journal of Climatology,* 32, 2333–2347.

Pinto, I., Jack, C., & Hewitson, B. 2018. Process-based model evaluation and projections over southern Africa from Coordinated Regional Climate Downscaling Experiment and Coupled Model Intercomparison Project Phase 5 models. *International Journal of Climatology*, 38, 4251–4261.

Pinto, I., Jack, C., & Wolski, P. n.d. Assessment of warming using observed and modelled data over Southern Africa. In review.

Pinto, I., Lennard, C., Tadross, M., Hewitson, B., Dosio, A., Nikulin, G., et al. 2016. Evaluation and projections of extreme precipitation over southern Africa from two CORDEX models. *Climatic Change,* 135, 655–668.

Reason, C.J.C., & Jagadheesha, D. 2005. Relationships between South Atlantic SST variability and atmospheric circulation over the South African region during austral winter. *Journal of Climate,* 18, 3339–3355.

Reason, C.J.C., & Rouault, M. 2005. Links between the Antarctic Oscillation and winter rainfall over western South Africa. *Geophysical Research Letters,* 32, L07705. https://doi:10.1029/2005GL022419.

Rouault, M., White, S.A., Reason, C.J.C., Lutjeharms, J.R.E., & Jobard, I. 2002. Ocean-atmosphere interaction in the Agulhas Current region and a South African extreme weather event. *Weather and Forecasting*, 17(4), 655-669.

Schamm, K., Ziese, M., Becker, A., Finger, P., Meyer-Christoffer, A., Schneider, U., et al. 2014. Global gridded precipitation over land: a description of the new GPCC First Guess Daily product. *Earth System Science Data*, 6(1), 49-60.

Seager, R., Osborn, T.J., Kushnir, Y., Simpson, I.R., Nakamura, J., & Liu, H. 2019. Climate variability and change of Mediterranean-type climates. *Journal of Climate,* 32, 2887–2915.

Seneviratne, S.I., & Hauser, M. 2020. Regional climate sensitivity of climate extremes in CMIP6 versus CMIP5 multimodel ensembles. *Earth's Future,* 8, e2019EF001474. https://doi:10.1029/2019EF001474.

Sousa, P.M., Blamey, R.C., Reason, C.J.C., Ramos, A.M., & Trigo, R.M. 2018. The 'Day Zero' Cape Town drought and the poleward migration of moisture corridors. *Environmental Research Letters,* 13, 124025.

Taylor, K.E., Stouffer, R.J., & Meehl, G.A. 2012. An overview of CMIP5 and the experiment design. *Bulletin of the American Meteorological Society*, 93(4), 485-498.

Thompson, D.W.J., Solomon, S., Kushner, P.J., England, M.H., Grise, K.M., & Karoly, D.J. 2011. Signatures of the Antarctic ozone hole in Southern Hemisphere surface climate change. *Nature Geoscience*, 4(11), 741–749.

Tyson, P.D., & Preston-White, R.A. 2000. The weather and climate of southern Africa. Cape Town: Oxford University Press.

Ukkola, A.M., De Kauwe, M.G., Roderick, M.L., Abramowitz, G., & Pitman, A.J. 2020. Robust future changes in meteorological drought in CMIP6 projections despite uncertainty in precipitation. *Geophysical Research Letters,* 47, e2020GL087820. https://doi:10.1029/2020GL087820.

Van Vuuren, D.P., Edmonds, J., Kainuma, M., Riahi, K., Thomson, A., Hibbard, K., et al. 2011. The representative concentration pathways: an overview. *Climatic Change*, 109(1), 5-31.

Vicente-Serrano, S.M., Beguería, S., & López-Moreno, J.I. 2010. A multiscalar drought index sensitive to global warming: the standardized precipitation evapotranspiration index. *Journal of Climate*, 23(7), 1696-1718.

Vogel, M.M., Hauser, M., & Seneviratne, S. I. 2020. Projected changes in hot, dry and wet extreme events' clusters in CMIP6 multi-model ensemble. *Environmental Research Letters,* 15, 94021. https://doi:10.1088/1748-9326/ab90a7.

Weldon, D., & Reason, C.J.C. 2014. Variability of rainfall characteristics over the South Coast region of South Africa. *Theoretical and Applied Climatology*, 115, 177– 185.

Wolski, P. 2018. How severe is Cape Town's "Day Zero" drought? *Significance,* 15, 24–27.

Wolski, P., Conradie, S., Jack, C., & Tadross, M. 2021. Spatio-temporal patterns of rainfall trends and the 2015–2017 drought over the winter rainfall region of South Africa. *International Journal of Climatology,* 41, E1303–E1319. https://doi:10.1002/joc.6768.

APPENDIX A: LIST OF MAPS AVAILABLE IN DIGITAL APPENDIX

Given the large number of plots available they have been made available as a separate ZIP file with a clear structure that allows specific plots to be readily located. The ZIP file directory structure is described below.

The “observations_and_trends” directory includes directories for all the observed datasets (CHIRPS, CRU, ERA5-Land and GPCC). Within each of these there are two subdirectories (climatologies and trends). Within each of these are the plots for all of the available indices. Note: CHIRPS and GPCC are daily rainfall datasets and therefore do not contain any temperature indices. CRU is a monthly dataset and therefore only provides indices that can be calculated from monthly data.

The “climate_change_projections” directory includes three subdirectories for the different types of plots. The “cmip6_multi-panel_plots” directory includes two subdirectories for each of the two future experiments (ssp245 and ssp585). Each of these contain plots showing the future change (or anomaly) projected for the different climate indices. Each plot contains subplots for each of the 28 CMIP6 models. There are also plots showing just the four “archetype” models. The “pet_spei” and “plumeplot” directories include subdirectories for each of the two future experiments (rcp45-ssp245 and rcp85-ssp585). The plots use data from CMIP5, CORDEX and CMIP6 and present the data for the six larger zones rather than the 23 SmartAgri zones.

- observations_and_trends
    - CHIRPS-2.0-0p05
        - climatologies
        - trends
    - CRU_TS-4.05
        - climatologies
        - trends
    - ERA5-Land
        - climatologies
        - trends
    - GPCC-FDD-2020
        - climatologies
        - trends

- climate_change_projections
    - cmip6_multi-panel_plots
        - ssp245
        - ssp585
    - pet_spei
        - rcp45_ssp245
        - rcp85_ssp585
    - plumeplots
        - rcp45_ssp245
        - rcp85_ssp585